(12)

AD A123708

AUTOMATIC SEISMIC SIGNAL PROCESSING

FINAL TECHNICAL REPORT

Contract F08606-80-C-0021

DTIC FILE COPY

ENSCO, INC.®

83 01 14 013

SAS-FR-81-04
4 February 1982

AUTOMATIC SEISMIC SIGNAL PROCESSING

FINAL TECHNICAL REPORT

Contract F08606-80-C-0021

PREPARED BY
ILKKA NOPONEN, ROBERT SAX AND STEVEN HIGGINS

PREPARED FOR
AIR FORCE TECHNICAL APPLICATIONS CENTER
VELA SEISMOLOGICAL CENTER
ALEXANDRIA, VIRGINIA 22314

ENSCO, INC.
SIGNAL ANALYSIS SYSTEMS DIVISION
813 NORTH ROYAL STREET
ALEXANDRIA, VIRGINIA 22314

UNCLASSIFIED

SECURITY CLASSIFICATION OF THIS PAGE (When Data Entered)

REPORT DOCUMENTATION PAGE	READ INSTRUCTIONS BEFORE COMPLETING FORM
1. REPORT NUMBER	2. GOVT ACCESSION NO. A123708 / 3. RECIPIENT'S CATALOG NUMBER
4. TITLE (and Subtitle) FINAL TECHNICAL REPORT ROUTINE AUTOMATIC SEISMIC ANALYSIS PACKAGE	5. TYPE OF REPORT & PERIOD COVERED TECHNICAL
	6. PERFORMING ORG. REPORT NUMBER SAS-FR-81-04
7. AUTHOR(s) ILKKA NOPONEN, ROBERT SAX AND STEVEN HIGGINS	8. CONTRACT OR GRANT NUMBER(s) F08606-80-C-0021
9. PERFORMING ORGANIZATION NAME AND ADDRESS ENSCO, Inc. SAS DIVISION ALEXANDRIA, VA 22314	10. PROGRAM ELEMENT, PROJECT, TASK AREA & WORK UNIT NUMBERS V/0704/B/PMP
11. CONTROLLING OFFICE NAME AND ADDRESS ADVANCED RESEARCH PROJECTS AGENCY NUCLEAR MONITORING RESEARCH OFFICE ARLINGTON, VA 22209	12. REPORT DATE 4 February 1982
	13. NUMBER OF PAGES
14. MONITORING AGENCY NAME & ADDRESS (if different from Controlling Office) AIR FORCE TECHNICAL APPLICATIONS CENTER VELA SEISMOLOGICAL CENTER ALEXANDRIA, VA 22314	15. SECURITY CLASS. (of this report) UNCLASSIFIED
	15a. DECLASSIFICATION/DOWNGRADING SCHEDULE

16. DISTRIBUTION STATEMENT (of this Report)

17. DISTRIBUTION STATEMENT (of the abstract entered in Block 20, if different from Report)

18. SUPPLEMENTARY NOTES

ARPA ORDER NO. 2551

19. KEY WORDS (Continue on reverse side if necessary and identify by block number)

Automatic seismic processors
Post-detection processing
Regional network coherent beamforming
Three-component polarization filtering
Automatic timing of signals
Automatic event location

20. ABSTRACT (Continue on reverse side if necessary and identify by block number)

We examined the feasibility of a post-detector as part of an automated seismic data processing system. The post-detector consisted of two parts. One is a three-component processor to determine the wave propagation, direction and distance of the signal. The other, a coherent beamforming process applied to a regional network of sensors to locate events within targeted seismically active areas of interest. Our results indicated

DD FORM 1 JAN 73 1473 EDITION OF 1 NOV 63 IS OBSOLETE

UNCLASSIFIED

20. ABSTRACT (Continued)

that three-component processing is approximately equivalent to a medium sized array in obtaining initial locations for automatic event association of detected signal. Significant detection gains were also observed, but not yet evaluated. Coherent beamforming of a regional network of sensors effectively detected and located small events in a targeted seismic region at teleseismic distance from the regional network. This was feasible, however, only in seismically active regions where well-located master events could be used to time align the signals. A grid of master events separated 5 to 10 degrees apart are needed to calibrate such a selected area of interest. Events could be detected and located which were otherwise insufficiently visible for conventional hypocenter locations. These arrival time-calibrated locations were usually accurate to 25 km and were for the most part uncontaminated by false side-lobe locations or by ambient false alarms. These preliminary results indicate that post-detection processing is sufficiently feasible to be tested on regional networks of three-component data, ideally situated at regional or teleseismic distance from targeted areas of interest.

This research was supported by the Advanced Research Projects Agency of the Department of Defense and was monitored by AFTAC/VSC, Patrick Air Force Base, FL 32925, under Contract Number F08606-80-C-0021.

AFTAC Project Number:	V/0704/B/PMP
Project Title:	Routine Automatic Seismic Analysis Package
ARPA Order Number:	4199
Name of Contractor:	ENSCO, Inc.
Contract Number:	F08606-80-C-0021
Effective Date of Contract:	10 June 1980
Contract Expiration Date:	15 February 1982
Project Manager:	Gregory B. Young (703) 548-8666

SUMMARY

Our research indicated that automatic detection and event association can be significantly improved by post-detection data processing. The post-detection analysis evaluated included three-component data, coherent beamforming of regional network data, and envelope and phase analysis of three-component data. The three-component processing was used to identify propagation phases such as P-waves and Rayleigh waves, to estimate the direction of seismic signals with a precision equivalent to that of a 10 to 15 km aperture seismic array, and to estimate distance with sufficient precision to reliably separate teleseismic, regional, local and core phase signals. By using master seismic events to time align other events within 5 to 10 degrees from such master events, it is feasible to use regional networks of seismic sensors to detect small events and accurately locate them with an accuracy of 25 km. This procedure was demonstrated as feasible in detecting and accurately locating small teleseismic events otherwise invisible on regional networks of linear dimension 1000 km located approximately 60 degrees from the source region scanned by the processor. False alarm side-lobe detections were negligible. An accurate timing algorithm was developed and demonstrated. This timing detector algorithm times the start time of signals and their envelope peaks. It was designed to measure the size and dominant period of the signal peak as well as its duration.

It is recommended that this preliminary feasibility demonstration of an automatic post-detection processor be optimized by determining the following parameters:

- Optimum pre-filter design parameters,
- Optimum station calibration by determining the shear velocity tensor which results in the most accurate direction estimations and distance estimations,
- Apply optimum site equalization parameters which improve regional network beamforming detections and locations.

Upon optimizing the post-detection processor, real-time operation of the post-detector needs to be demonstrated by applying it to a three-component regional network. Performance of the three-component regional network should be gauged in terms of its capability of detecting and locating events from selected areas of interest. Such areas of interest should be selected to be at either teleseismic or regional distance from the regional network.

ACKNOWLEDGMENTS

The authors wish to thank Mrs. Rachel C. Tierney for her preparation of the manuscript, tables and the figures.

TABLE OF CONTENTS

LIST OF FIGURES

LIST OF FIGURES
(Continued)

LIST OF FIGURES
(Continued)

LIST OF TABLES

LIST OF TABLES
(Continued)

SECTION I
INTRODUCTION

The immediate objective of our Automatic Signal Measurement Research is to significantly improve the automatic detection, timing, and propagation phase identification of small seismic signals. These provide an indication of the wave direction and other wave propagation characteristics. The event association process is thus enhanced by immediately identifying teleseismic P waves and separating them from probable regional phases, surface or shear wave phases, possibly local event signals and core phases. This is expected to improve the initial front-end signal detection, signal association, and event location process. An initial event location should be significantly improved by avoiding obviously erroneous detection associations.

Coherent beamforming by small arrays has been proven a useful adjunct for event association. This research will investigate the feasibility of obtaining much more accurate locations within prespecified seismically active regions. That would be performed by coherent beamforming of large-aperture station networks. The Automatic Association (AA) process is expected to be significantly enhanced by readily locating events from known seismically active regions of interest and by locating the other remaining events by any of the presently implemented global association processes.

SECTION II
AUTOMATIC SIGNAL TIMING, MEASUREMENT AND CHARACTERIZATION

A. SECTION INTRODUCTION

This research is to determine if it is feasible to automate and utilize three-component software as a post-detector. Our objective is to identify the wave propagation mode, provide station-to-source azimuth and distance information. By providing this information, the front-end Automatic Detector/Automatic Associator (AD/AA) processes can operate more effectively at much higher detector false alarm rates. This should significantly increase the detection capability of the seismic network and also improve the location capability by providing automatically determined event location estimates.

Using SRO data, we tested a model of the Three-Component Post-Detection Analyzer (TPA) on regional and teleseismic short-period signals. So far, in all cases examined, we observed that three-component particle motion of regional and teleseismic P-waves could be used to determine event azimuths and incidence angles. These will reliably provide preliminary location information to the AD/AA from positively identified linearly polarized signals. This should enable the AD/AA to operate under much higher FAR conditions. We used our real-time Complex Time Series (CTS) software to compute cross-products between complex representations of seismograms. In this way, we reliably identified P-waves and measured the vector of their angle of incidence. Errors of only several degrees in direction were observed on all events examined so far. We had less success with plane polarized regional signals in that complex cross-products often indicated erratic particle motions of the shear wave and surface wave portion of the seismogram. This effect was also observed by Sutton et al, (1967) using real cross-products. Strong S-to-P conversions close to the receiver explained at least part of the erratic particle motion.

We developed software to provide the AA with information extracted from three-component seismic stations. Its purpose is to identify properly associated detections of seismic phases, e.g., P-waves, S-waves, and Rayleigh waves. The software is designed to run unattended, without operator interaction. But, it allows easy operator review of data for quality control, storage control, and hardcopy. The software is designed to be self-initializing and real-time.

It is called on each current set of new data points rather than on segmented records of data. This will make it very easy to interface with any automatic system such as Regional Event Location System (RELS). The manner in which an Automatic Post-Detector (AP) is inserted in such a system is illustrated in Figure II-1. Regional three-component networks adjacent to an Area of Interest (AI) would be utilized in the following manner. Independent detections of signals by three-component sensors trigger the AP. It provides an approximate event location using identified P-wave signals. By accurately timing three or more signals, this approximate location of the event is automatically improved. Resulting locations are expected to have error ellipses ranging from about 50 kilometers to several hundred kilometers depending on the distance of the event, complexity of the source, and signal-to-noise ratio of the detected signals. Such locations are refined and improved by AA integration of the AP data into the global network. In the case of small signals from an adjacent AI, the locations are validated and improved by beamforming of the regional network. This aspect of the AA will be covered in Section III.

Our main purpose in including an AP in the front-end of a real-time automatic seismic system is to facilitate the solution of problems limiting the performance of the AA process. These problems are described on Table II-1. The adverse effects of AA errors are summarized on Table II-2. The utility of an AP, in particular the processing of three-component data, is to provide preliminary event locations, to identify the wave propagation (separate body waves from surface waves), and utilize emergence angle information to separate local, regional, teleseismic and core phases. These goals are summarized on Table II-3, Table II-4, and Table II-5. The advantages expected from implementing an AP as part of an automatic seismic system is shown on Table II-6. An important part of our research was to design a real-time three-component processor. It was designed to be inserted into a system such as RELS. Its purpose was the determination of the capability of three-component processing as an integral part of a front-end automatic seismic processor. The architecture of the real-time three-component processor shall be discussed in sub-section C.

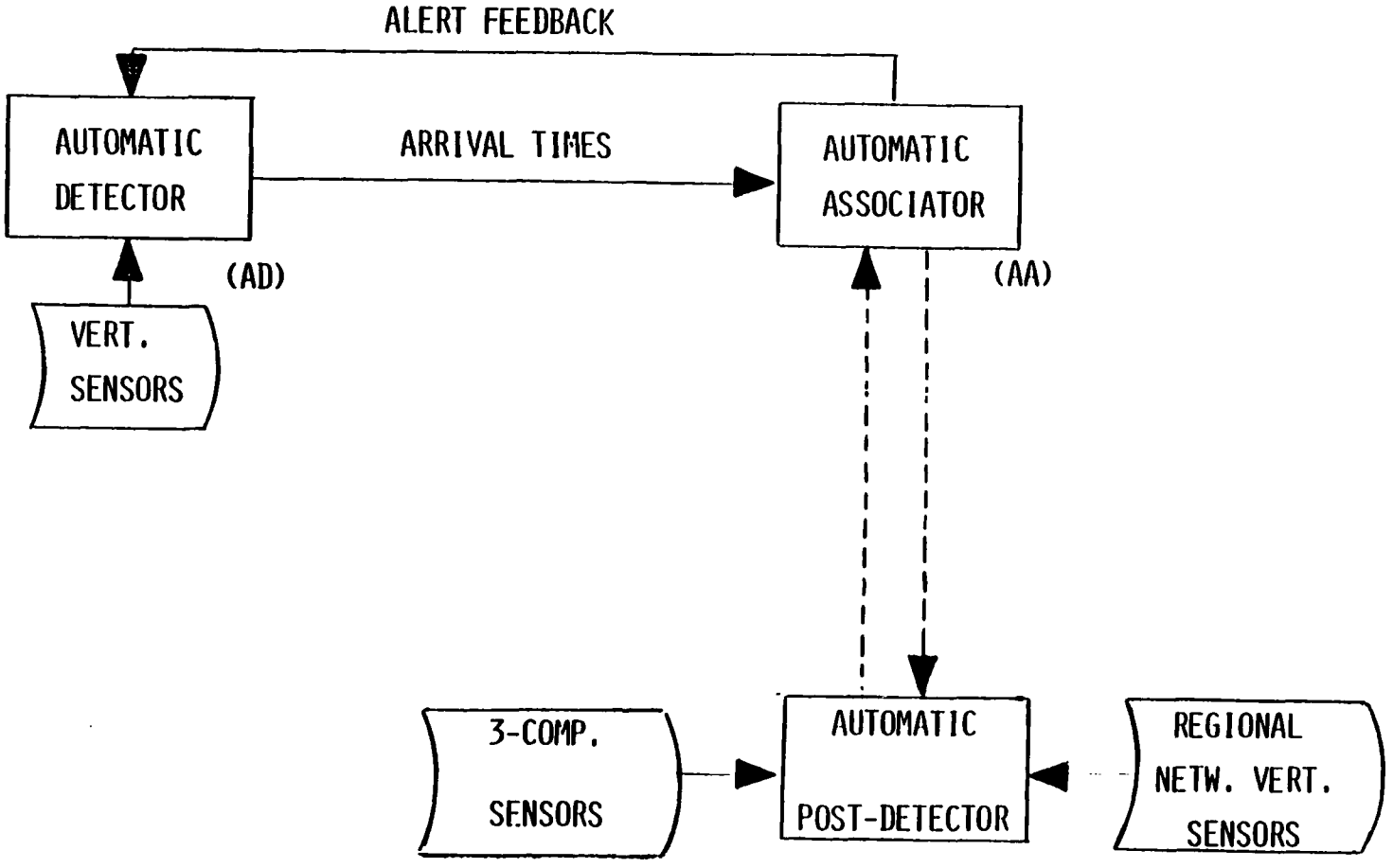

FIGURE 11-1

CONTEXT OF POST-DETECTION IN AN AUTOMATED SEISMIC NETWORK

AD/AA/AP

TABLE II-1

AA PROBLEMS LIMITING NETWORK PERFORMANCE

- FALSE ALARM ASSOCIATIONS
  - FALSE P-WAVE IDENTIFICATIONS
  - MIXED EVENTS
  - MIXED PHASES
  - MIXED LOCALS, REGIONALS, TELESEISMICS
- MISSED ASSOCIATIONS
  - LARGE EVENTS MASK SMALL EVENTS
  - FALSE ALARM INTERFERENCE
- LARGE TIMING ERROR
  - EMERGENT EVENTS
  - COMPLEX EVENTS

TABLE II-2

ADVERSE EFFECTS OF AA ERRORS

- MISSED EVENTS
- FALSE EVENTS
- LARGE LOCATION ERRORS
- WAVEFORM EXTRACTION ERRORS
  - FALSE SIGNALS
  - MISSED SIGNALS
- DEGRADED NETWORK CAPABILITY
  - REDUCED DET & LOC CAPABILITY
  - IMPAIRED EVENT IDENTIFICATION

TABLE II-3

OBJECTIVES OF POST-DETECTION PROCESSING

- IMPROVE AUTOMATIC DETECTION
  - IDENTIFY VALID SIGNALS
  - DESCRIBE PROPAGATION
- IMPROVE AUTOMATIC ASSOCIATION
  - EXTRACT DIRECTION AND DISTANCE RELATED INFORMATION
  - START PROCESS WITH MORE ACCURATE INITIAL LOCATION

TABLE II-4

IDENTIFY VALID SIGNALS BY POLARIZATION MEASUREMENTS

- TELESEISMIC P-WAVES
- REGIONAL P-WAVES
- REGIONAL SURFACE WAVES
- CORE PHASES
- LOCAL SIGNALS

TABLE II-5

OBTAIN LOCATION RELATED INFORMATION BY 3-COMPONENT PROCESSING

- DIRECTION OF REGIONAL SIGNALS
- DIRECTION AND DISTANCE OF TELESEISMIC P-WAVES
- DIRECTION OF CORE PHASES

TABLE II-6

ADVANTAGES OF IMPLEMENTING AN AP

- IMPROVED NETWORK PERFORMANCE
  - DET, LOC & DISCR CAPABILITY
  - OPTIMUM ASI & ASN OPERATION
- LOWER INSTALLATION COST
  - MINIMUM COST SENSOR DEPLOYMENT
  - MINIMUM STORAGE & RETRIEVAL REQ'S
- LOWER NETWORK OPERATING COST
  - LOWER MANNING REQ'S OF AUTOMATED OPERATION
  - MORE EFFECTIVE COMPUTER/MANNING TRADEOFF
- MORE EFFECTIVE SURVEILLANCE
  - FAST RELIABLE EVENT LOCATION & SIGNAL EXTRACTION
  - FAST RESPONSE EVENT IDENTIFICATION
  - MORE RELIABLE VERIFICATION OF POSS. EXPLN'S

B. TIME-DOMAIN DETERMINATION OF INSTANTANEOUS WAVEFORM ENVELOPE, PHASE AND FREQUENCY AND APPLICATION TO THREE-COMPONENT PROCESSING

Unger (1978) demonstrated the feasibility of applying instantaneous amplitude, phase and frequency measurements to automatically detect, time and identify seismic events. Unger's results demonstrated 81% to 94% detection of known signals at 7 to 20 false alarms per hour. The advantage of his detector was to provide accurate timing of signals with a standard deviation of 0.2 seconds in those cases where signals were detected. He cited some problems with the accurate detection of emergent signals, but nonetheless recommended the algorithm for accurate automatic timing of seismic signals. Unger's algorithm was used by Sax et. al. (1978) for the automatic timing of a large data base of signals for the Event Identification Experiment conducted at the Vela Seismic Center (VSC). As a result of that experience, some deficiencies were observed in timing. However, in most of those cases where signals were correctly detected the timing was very close to that which would be performed by a seismic analyst. An important part of our research was directed toward improving the performance of Unger's detector so that accurate timing of signals could be an integral part of an automated seismic system. Our strategy was to develop a real-time, reliable Hilbert-Transform algorithm which phase shifts real data 90 degrees. Thus real time-series data is converted to a complex time series facilitating measurement of the instantaneous envelope and frequency signals, and performing complex arithmetical transformations such as complex filtering including adaptive polarization filtering of three-component data. A real advantage is obtained from this approach in that such measurements are more stable and accurate than analogous operations on real data. Figure II-2, taken from Unger (1978), shows some of the effects of noise on signal timing. In designing our new real-time Hilbert-Transform algorithm, we concentrated on improving the accuracy and precision of instantaneous frequency measurements. The basic algorithm used is given as follows:

x_i - i^{th} data point,

w_i - i^{th} complex data point,

and $\Delta\Theta_i$ - change in phase angle from i-1 to i^{th} data point.

The complex data w_i is initially approximated as

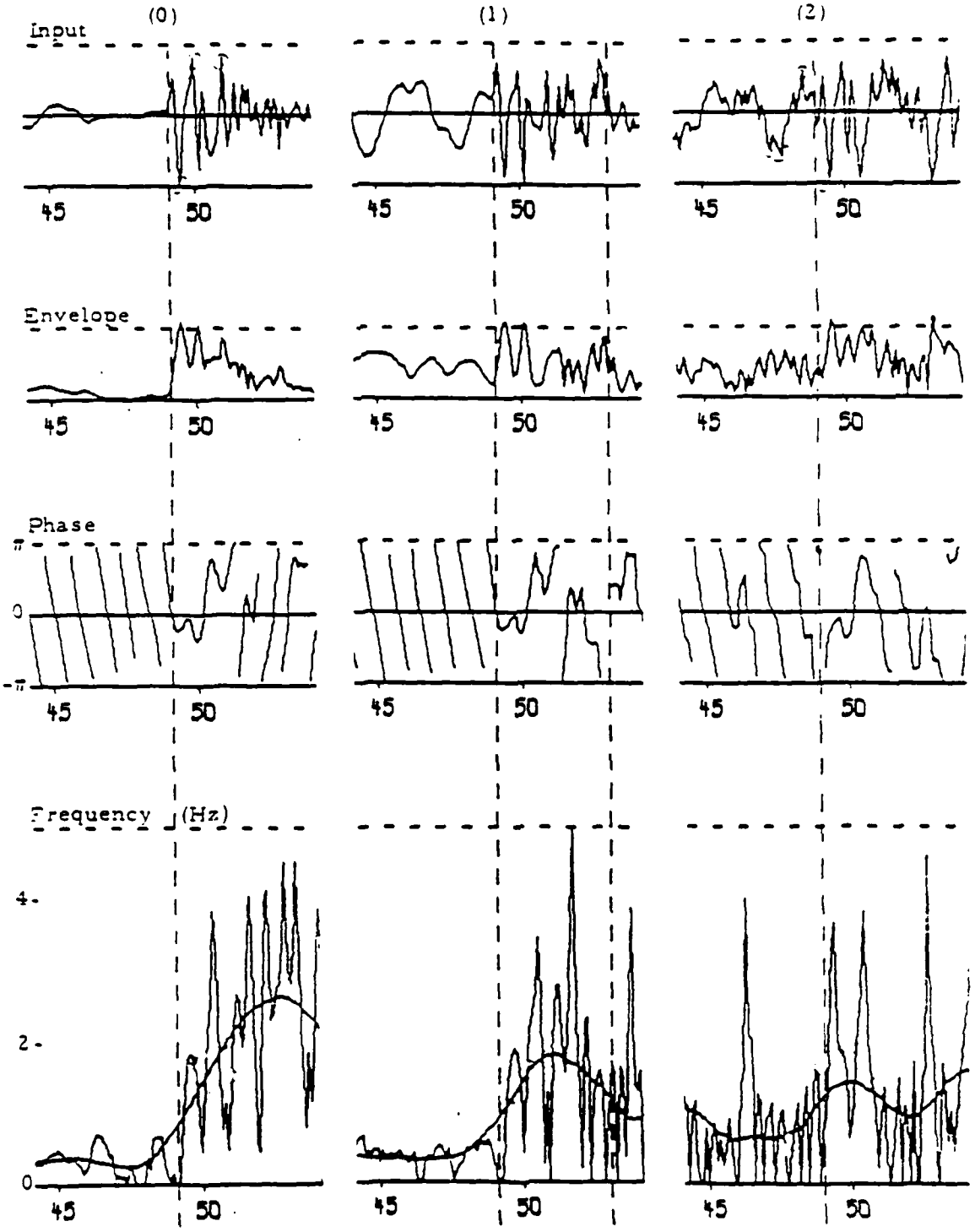

FIGURE II-2

EFFECTS OF NOISE ON SIGNAL TIMING

$$w_{i,j} = \left(\frac{x_i + x_{i-1}}{2} \right) + \frac{j}{-} \left(\frac{x_i - x_{i-1}}{\Delta\Theta_{i-1}} \right)$$

real part imaginary part

For j = 1. j iterations on each data point:

$$\Delta\Theta_i = (1-\mu)\ \Delta\Theta_i + \mu \left[(1-\beta)\ \Delta\Theta_{i-1} + \beta \left(\frac{w_{i,j}}{|w_{i,j}|} - \frac{w_{i-1}}{|w_{i-1}|} \right) \right]$$

Some optimum convergence rates for this algorithm are $\mu = .5$ and $\beta = .0625$. The program determines the number of point iterations j to attain 1% accuracy in the determination of the normalized frequency parameter. Examples of the quality of this algorithm are shown on Figure II-3 and Figure II-4. The algorithm makes possible precision measurements of envelope, frequency, complex-cepstrum, complex adaptive filtering, fixed filters and other real-time time series manipulations.

In this particular research, we concentrated on applying complex time series analysis to the problem of detecting and accurately timing signals; and of determining their propagation type, direction and distance. Figure II-5 shows a teleseismic P-wave event. The raw data traces; vertical, north-south and east-west components; are shown on the bottom three traces. The top trace is the bandpass filtered vertical component. This same event is shown on an expanded time scale plot on Figure II-6. The top three traces are the vertical, north-south and east-west components of ground motion. The bottom three traces of Figure II-6 are envelope power-scaled seismograms obtained by complex time series manipulation. The equations are shown on the seismogram plots, where Z, N, and E are the complex seismograms with real parts shown on the top three traces. The processed traces illustrate that all three components of the signal can be seen with clarity and can be readily detected, timed and measured as an automatic process. Compared to the top three bandpass filtered data, the processed traces peak where the signal is clearly correlated. Cursory visual analysis of the filtered data would show the signal coming from the west whereas the processed trace shows it coming from the northwest, within about 8 degrees of the true azimuth.

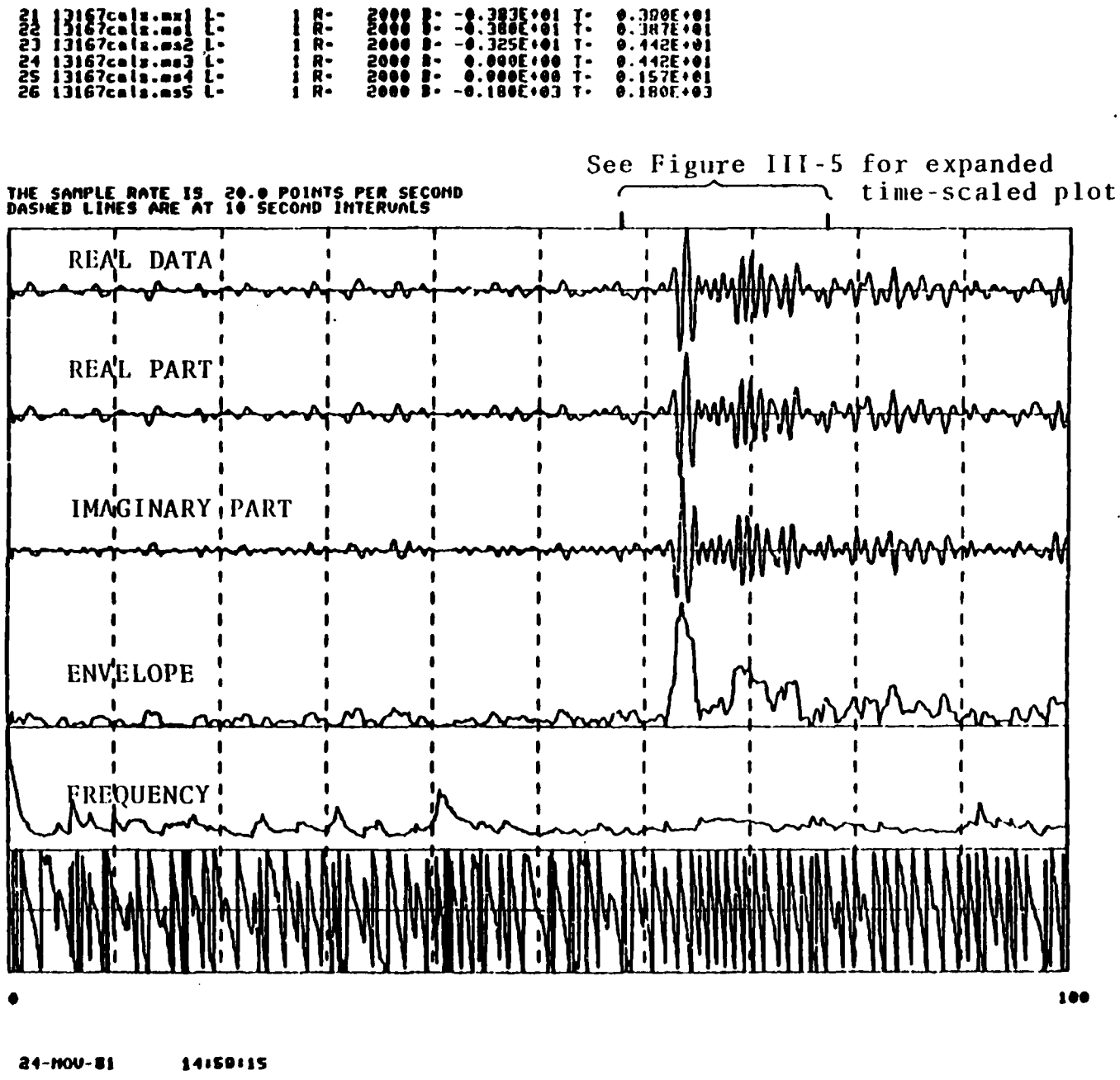

FIGURE II-3

EXAMPLE OF COMPLEX TIME-SERIES ALGORITHM

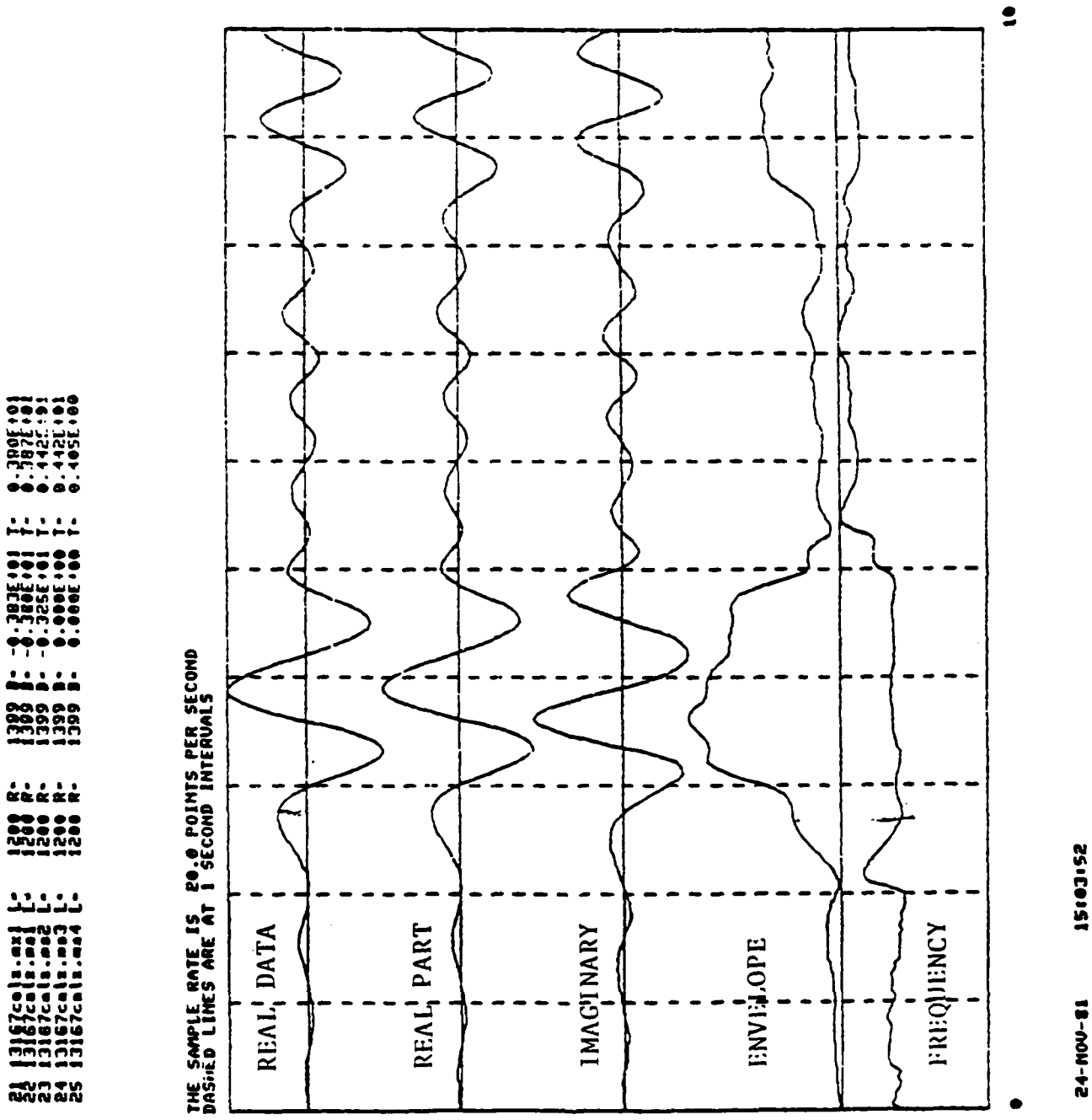

FIGURE II-4

EXPANDED TIME-SCALE PLOT OF COMPLEX TIME-SERIES

STATION ANMO, KAMCHATKA EVENT, M_B = 4.8, DIST 64°, DIR N 41° W

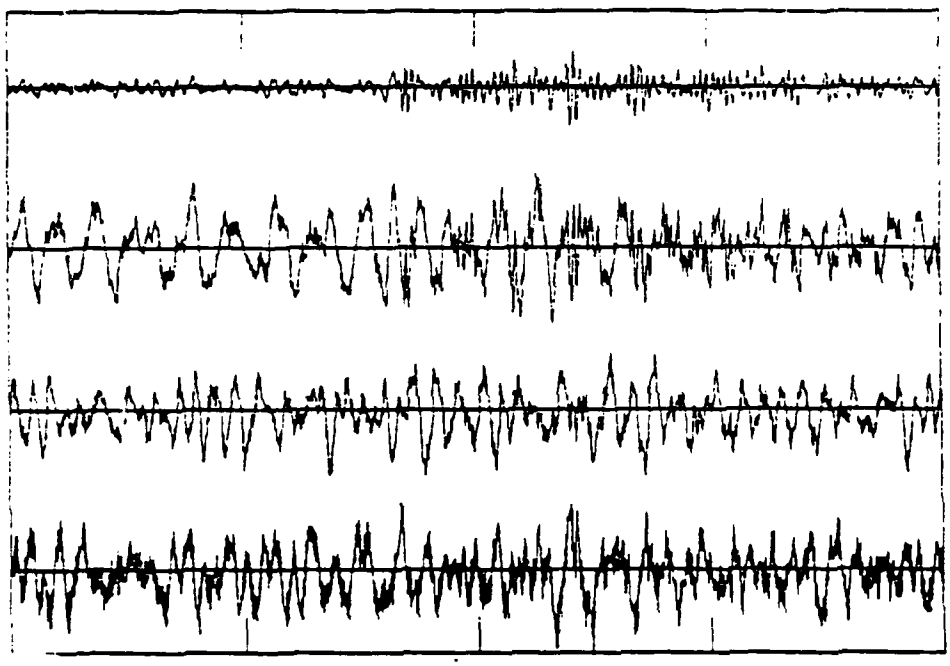

INPUT DATA TO THE POST-DETECTION PROCESS

FIGURE II-5

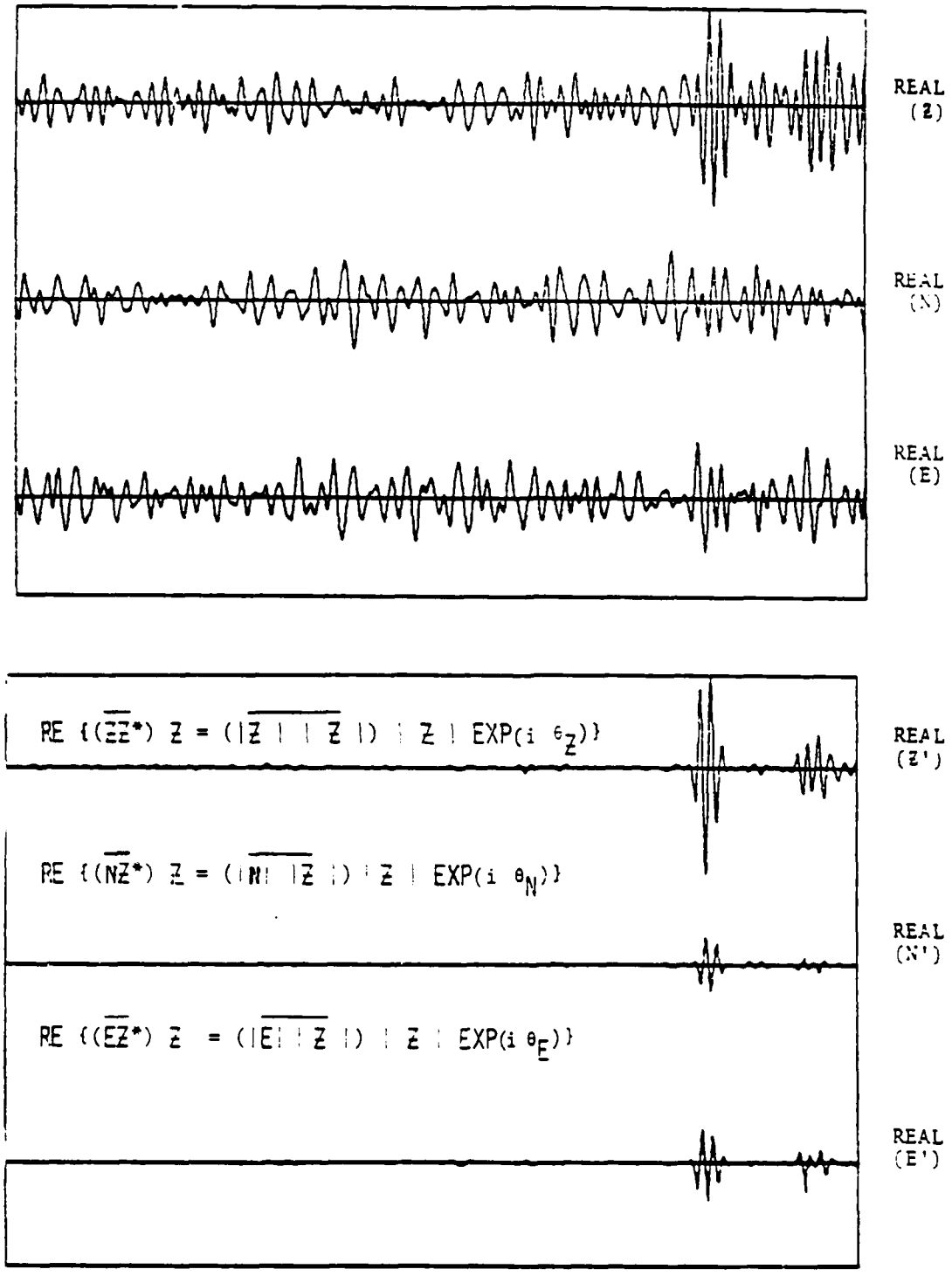

EXRACTION OF POLARIZED DATA COHERENT WITH Z

FIGURE II-6

Note on Figure II-6, that estimates of the processed horizontal components involve cross-power products of the horizontal and vertical components. Figure II-7 show the real and imaginary parts of these averaged cross-power products. Since the real parts are much larger than the imaginary parts, the signal is identified as a P-wave. If the imaginary part were dominant, the signal would have been identified as a Rayleigh wave or as an internally reflected shear wave. The direction determined from these cross-products was 5 degrees west of the time azimuth. In an attempt to improve detection and propagation measurements, the cross-products were multiplied by a real gain factor G_x, where x refers to the component Z, N or E. The first term of G_x is a radiation pattern factor which passes components which are either zero or 180 degrees phase angle with respect to the vertical component; or ninety or two hundred seventy degrees: the first, passing P-waves; the second, passing Rayleigh waves. The second term is a Gaussian function of the difference of the log-frequency of the vertical and horizontal components. This is a signal coherence term which passes frequency matched components with a gain of one and frequency miss-matched components with a gain approaching zero. The effectiveness of these components depend heavily on the accuracy of the complex time series algorithm described previously and illustrated on Figure II-3. One disadvantage of using cross-product components to determine directions and apparent emergency angles is the distortion caused by small phase shifts between the vertical and horizontal components. One way of circumventing this is to use absolute values of the complex cross-products. This is shown on Figure II-7. Comparison of absolute values with the real and imaginary parts of the cross-products indicate that apparent correlated imaginary parts are probably due to small phase shift deviations between the radial and horizontal components of the P-waves. Using the absolute values to compute the apparent emergence angle yielded a ratio of 2.1 between the vertical, horizontal, and waves. This is closer to the expected value at the SRO station ANMO for this epicentral distance of 64 degrees. ANMO is a hard rock site, expected to have a shear velocity of 2.9 or possibly even higher. Referring back to Figure II-7 we see that the direction estimate obtained by using a polarization and coherence filter factor is within 3 degrees of the expected direction of propagation, N 41 degrees W. Thus these tests suggest that this type of filtering has some potential in improving detection and measurement of wave propagation characteristics. Further refinements and illustrations will be shown in later sections.

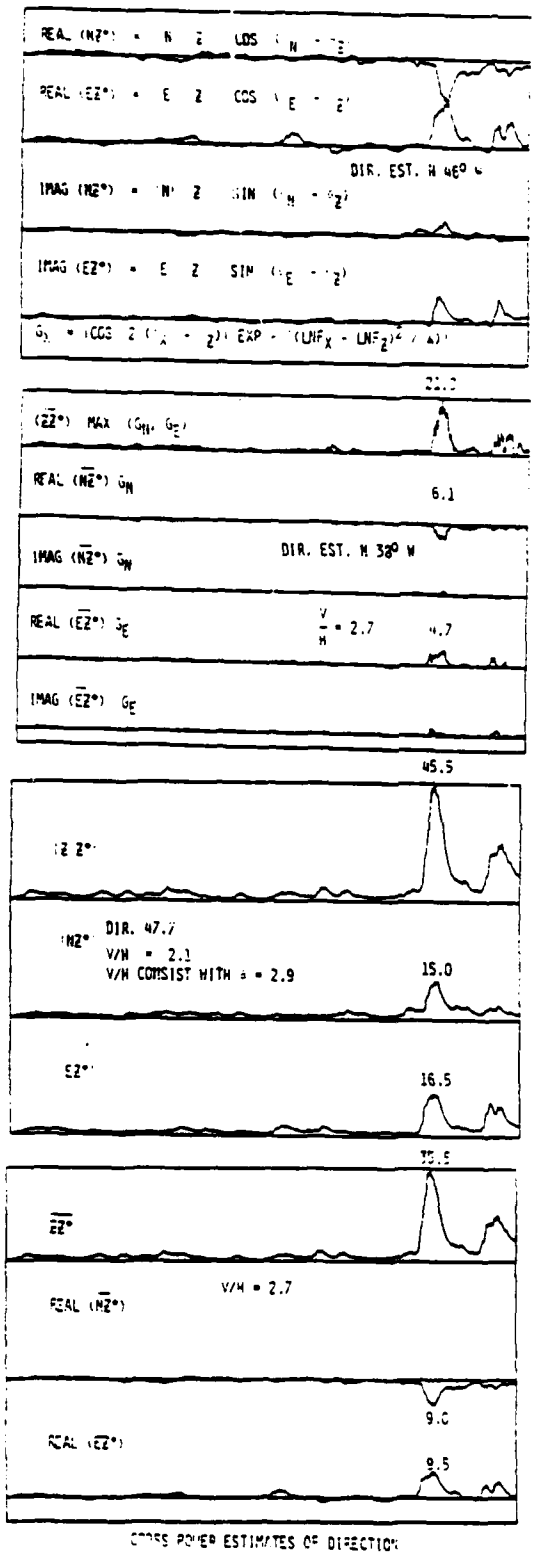

CROSS POWER ESTIMATES OF DIRECTION

FIGURE II-7

CROSS POWER PRODUCTS

C. AUTOMATIC TIMING OF DETECTED SIGNALS

The purpose of the automatic process which times signals is to provide the arrival time data of associated signals. It will use these times to locate the event. In order to locate the event accurately, the automatic timing must be at least as accurate and as reliable as that which would be performed by a seismic analyst. Since the automatic seismic system must correctly retrieve signal waveforms for event identification, the reliability of the system will depend on the reliability of the automatic algorithm used to time and extract signals for subsequent analysis. Thus, the function of automatically timing signals plays a key role in designing an automated seismic system. The automatic timing function fits into the software architecture of a three-component AP as shown on Figure II-8. At the front-end of the AP the three-component processor TPA applies polarization filters to the data to extract the three-component waveform of incident P-waves or Rayleigh waves. The output of the TPA is a state vector which describes the wave motion at each point of time. The element of this state vector used to detect and time signals is among other possibilities the envelope of the polarization filtered vertical component ground motion. After the signal is timed and measured by the Automatic Signal Editor (ASE), the data is rolled in core until the signal is centered on a record of prescribed length and displayed with appropriate annotation describing the wave motion in detail. In this sub-section, the procedures of ASE will be described and some examples will be shown.

Each envelope input to ASE is initially categorized as belonging to one of four possible states described as i_d = 0, 1, 2 or 3. At the start of a run, i_d is set equal to zero. The operation performed on the new envelope value, e, depend on the specified state. These are qualitatively described as follows:

- id = 0; pre-signal search for minimum envelope values preceding the signal to indicate the transition to the state id = 1.

- id = 1; pre-signal search for maximum values succeeding the last minimum to indicate the transition to id = 2 or back to id = 0 state.

- id = 2; post-signal search of peaks to find higher peaks, to move forward the start time estimate if an abrupt rise is observed, and to declare the end of the signal as indicated by the transition to id = 3.

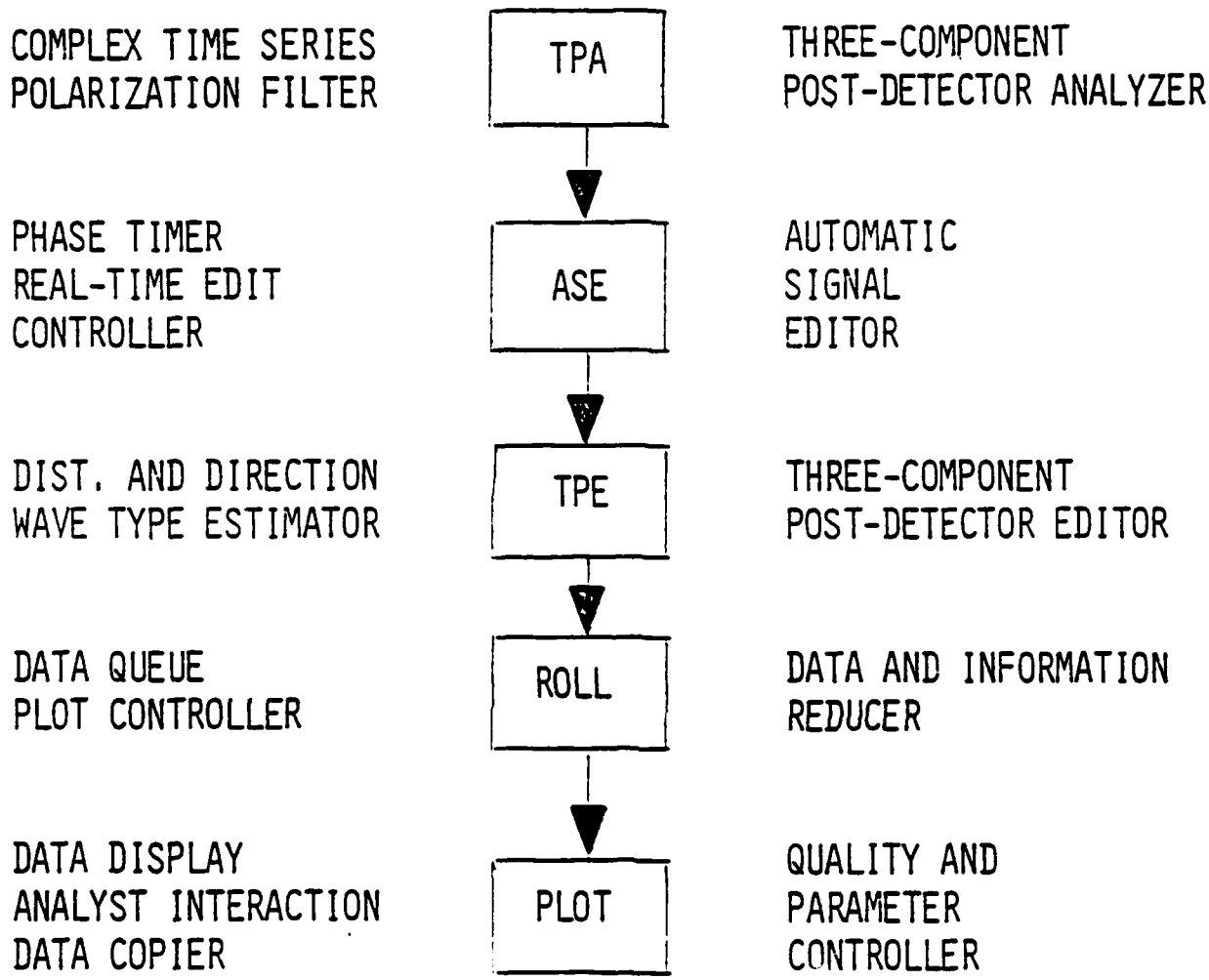

ARCHITECTURE OF REAL-TIME 3-COMPONENT POST-DETECTION PROCESSOR

FIGURE II-8

- id = 3; indicates to external processors that the detection of the signal is completed.

The automatic signal editor starts by searching for the start time of a significant envelope peak. This state is specified by id = 0. The operation is performed sequentially on each data point. The transition from one id state to another is abstractly described by

$$T\ (id_{i-1},\ id_i)$$

where T specifies the state of the preceding point with the first variable; and of the current point with the second variable. As previously stated id is either 0, 1, 2, or 3. The transitions, T, are determined by comparing detector envelope values e_i to preceding envelope values selected and stored from prior examinations of the data, e_1, e_2, ..., e_i. The state id = 0 signifies the search for a new bottom preceding a significant signal peak.

Continuation of the state id = 0, T (0, 0), is maintained if the envelope is not a minimum or if the minimum is greater than 7.5 times the average of preceding minimums. If this T (0, 0) test fails, the transition T (0, 1) occurs. On this transition, a new start time t_j and an alternative start time t'_j is specified. A test value, P_k, for testing for ascending peaks is initialized. The average value of detected minimums, $\overline{b_j}$, is updated.

On transition from state id = 0 to state id = 1, the Automatic Signal Editor (ASE) starts searching for signal peaks and also envelope minimums to alternatively time the start time of a signal. These operations are described logically as follows.

The purpose of the id = 1 state is to hold the start time for accurate timing of emergent and complex signals.

There are four conditions for maintaining the continuation of the state id = 1. These are designated as

$$T_1\ (1, 1),\ T_2\ (1, 1),\ T_3\ (1, 1) \text{ and } T_4\ (1, 1)$$

Under T_1 (1, 1) the id = 1 state is continued at values of the envelope which are not maximum or minimum values. The exception to this rule can occur on extremely large rise in the envelope. Spikes and glitches satisfying this condition are easily eliminated if insufficient duration can be considered a signal. This criteria must be set by the user.

An alternative continuation of the id = 1 state, T_2 (1, 1), occurs when minimum values of the envelope are less than ten times the average of preceding minimum envelope values. The purpose of this test is to prevent a sudden random rise of succeeding minimum envelope values from jamming the signal start time hold condition. This causes erroneously early timing of signals and false alarms. Failure of the T_2 (1, 1) test returns to the id = 0 state which advances the timing of the next apparent signal. A test is provided for the next peak following this release mechanism in order to assure that very large signal peaks are not overridden.

Two alternatives for continuation of the id = 1 state are provided upon encountering maximum values of the envelope. If the peak is larger than the preceding peak, the continuation transition T_3 (1, 1) is taken. The purpose of this test is to prevent late timing of emergent signals. A second continuation, T_4 (1, 1) is taken when the detection trough to peak z statistic is below the threshold or if the peak is significantly greater than the average of preceding peaks. If this latter test fails, the transition T_4 (1, 0) occurs to allow advancement of the start time of the next signal. This test is provided to avoid early timing and false alarms under complex noise condition such as coda. The failure of T_3 (1, 1), T_3 (1, 0), T_4 (1, 1) and T_4 (1, 0) results in the declaration of a significant signal peak as the transitions T_3 (1, 2) and T_4 (1, 2). These are considered normal transitions to the signal state. In these cases, a Z statistic test based on the difference between peak to average trough or on the peak to average trough ratio is used to declare a signal. In addition, a conditional test can detect signals as the sequence of transitions T_3 (1, 0), T_3 (0, 2). It is applied to avoid missing large signals preceded by an abrupt rise of envelope minimums. In that case, the ratio of the peak to preceding minimum must exceed the prescribed threshold. Finally, the transition T_3 (2, 3) indicates the final detection of a signal by sensing the end of the signal.

The declaration of state id = 3, is used to indicate to external automatic processes that a signal was detected; the time of its beginning, envelope peak occurrence, and duration was measured; and the magnitude of the peak measured.

D. TELESEISMIC EVENT LOCATION EXPERIMENT USING THREE-COMPONENT RECORDING

We attempted to determine approximate locations of a few tens of teleseismic events from three-component recordings of P-waves made at the Seismic Research Observatory in Bangui, Central African Republic (BCAO). In this experiment, complex cross-products of the vertical and horizontal components were used. Take Z(t), N(t) and E(t) to represent the complex seismograms recorded in vertical, N-S and E-W directions. The product of N and the complex conjugate of Z or Z* is

$$NZ^* = |N||Z| \left[\cos (\psi_N - \psi_Z) + i\sin (\psi_N - \psi_Z)\right]$$

where $\psi_N - \psi_Z$ is the phase difference between the vertical and N-S components. The real part of the above quantity gives the cross-power due to linearly polarized waves, imaginary part gives the cross-power due to elliptically polarized waves. The azimuth a of arriving P-wave is then

$$a = p - \tan^{-1}\left[\frac{\text{Re } (NZ^*)}{\text{Re } (EZ^*)}\right]$$

where $p = \pi/2$ for a positive denominator and $3\pi/2$ for a negative denominator.

The incidence angle of the P-waves can be estimated either as

$$i_1 = \tan^{-1} \frac{\text{Re } (ZZ^*)}{\sqrt{\text{Re } (NZ^*)^2 + \text{Re } (EZ^*)^2}}$$

or as

$$i_2 = \tan^{-1} \frac{|\ ZZ^*\ |}{\sqrt{|\ EZ^*\ |^2 + |\ NZ^*\ |^2}}$$

Presence of noise on the seismograms causes i_1 to be biased towards too small incidence angles, i_2 towards too large incidence angles. For signals with high SNR we observed $i_1 \simeq i_2$, for weak signals we used the average of i_1 and i_2 to estimate the (apparent) incidence angle i. Both a and i can be estimated continuously as functions of time. We chose to use the values of a (t) and i (t) measured from the first maximum of the signal envelope for locating the event. Since the contribution of scattered energy to the signal waveform increases with time, we preferred to use as early measurements as possible.

To verify that the arriving waves really are P-waves, we required the condition

$$[\mathrm{Re}\ (NZ^*)]^2 + [\mathrm{Re}\ (EZ^*)]^2 > [\mathrm{Im}\ (NZ^*)]^2 + [\mathrm{Im}\ (EZ^*)]^2$$

to be filled before making a measurement. In addition to the cross-products, we plotted out also the quantity

$$r = \frac{R - I}{R + I}$$

$$\text{where} \quad R = \sqrt{[\mathrm{Re}\ (NZ^*)]^2 + [\mathrm{Re}\ (EZ^*)]^2}$$

$$\text{and} \quad I = \sqrt{[\mathrm{Im}\ (NZ^*)]^2 + [\mathrm{Im}\ (EZ^*)]^2}$$

and found it to be a convenient indicator of the dominant polarization type. It ranges from -1 for pure elliptically polarized waves to +1 for pure linearly polarized waves.

We could also find whether the waves were predominantly linearly or elliptically polarized in the horizontal plane by computing the product NE^* and comparing its real and imaginary parts.

We band-pass filtered all input data with a pass-band centered at 1.0 Hz. Band-pass filtering improves signal-to-noise ratio and has no adversary side-effects to processing. On the contrary, the filtered seismogram resembles a harmonic wave with varying amplitude and frequency which is a natural input to a system that gives as output the envelope and frequency.

An example of determination of azimuth and angle of incidence is shown in Figure II-9. Errors in determining the azimuth and angle of incidence are plotted to Figures II-10 and II-11 as functions of true azimuth. The systematic, geophysical variation of these measurements are most apt to be correlated with event azimuth. The event azimuth primarily determines through what region of the Earth's upper mantle the seismic ray passes below the recording station. Velocity variations in the upper mantle below a station are the primary cause of the seismic ray direction anomalies observed at the station (Noponen, 1974 and Berteussen, et al., 1975). To create Figure II-11, we had to compute the expected (apparent) incidence angles from the tabulated wave slowness. In the absence of conspicuous layering, only the shear wave velocity in the top 6-12 km below the station determines the relationship between the apparent angle of incidence i and the wave slowness tabulated in seismological tables (Noponen, 1968).

It is obvious that regional corrections should be applied to the measured azimuths and incidence angles before they are used for location. The situation is quite analogous to locating events using an array station, and similar methods to calibrate locations as used e.g., at the NORSAR array can be used to improve location accuracy.

We plotted the BCAO location error vectors (for events with fair to good signal-to-noise ratio) into inverse velocity space. The plot is shown in Figure II-12, and when compared with the uncalibrated NORSAR full array location error vectors in Figure II-13 (Noponen, 1974) shows a qualitatively similar picture. The measurement error is apparently larger for the three-component BCAO station, as shown by the vectors radiating from the Algerian aftershock series in NW quadrant. This translates to a worse location capability after calibration. The average length of anomaly vectors is about 50% larger than at NORSAR.

Several of the measurements displayed in Figure II-10 and II-11 were made from seismograms having poor signal-to-noise ratios. We classified signals to four categories:

- Unmeasurable. No P-wave could be visually detected on any of the component close to the predicted arrival time.

- Poor. P-wave could be detected on the vertical trace, but amplitudes of the horizontal components were at time of detection lower than or comparable with the maximum noise amplitude seen on an about 20 seconds long noise record preceding the signal.

- Fair. P-wave could be detected simultaneously on all three component, and its amplitude was twice or more than the maximum noise amplitude seen before the signal.

- Good. Signal-to-noise ratios about ten on all components, or event magnitude larger than 5.0.

In Figures II-10 and II-11 records with "good" signals are distinguished by filled symbols. Records with poor or fair signals are denoted by open symbols. We show in Figures II-14, II-15 and II-16 examples of events with poor signal-to-noise ratio, from which apparently valid measurements could be made, judging on the agreement of their results with those from the other events.

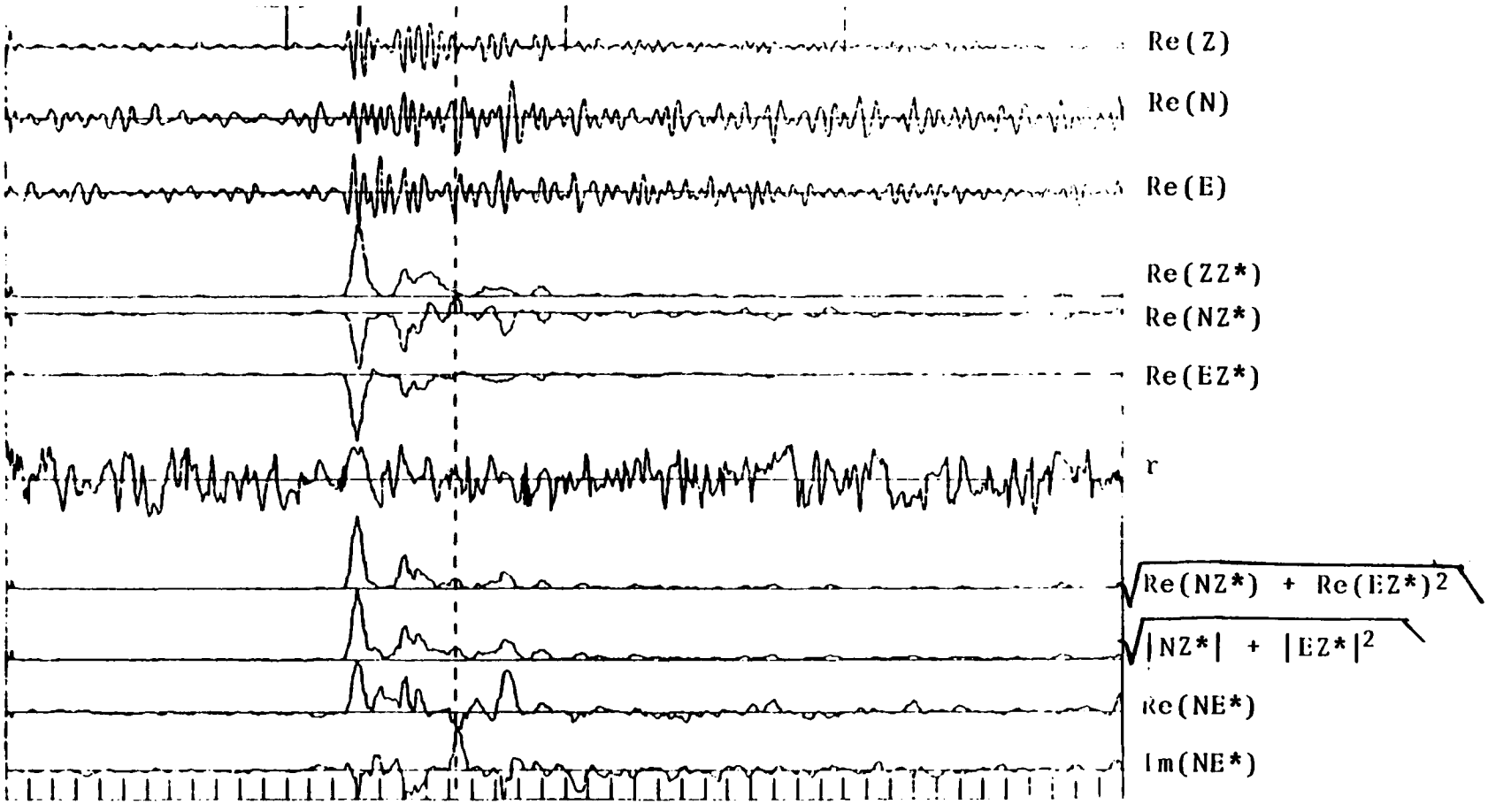

OUTPUT USED TO LOCATE A TELESEISMIC EVENT

An earthquake in NW quadrant from station BCAO. All traces have different gains. The trace notations are explained in text.

FIGURE II-9

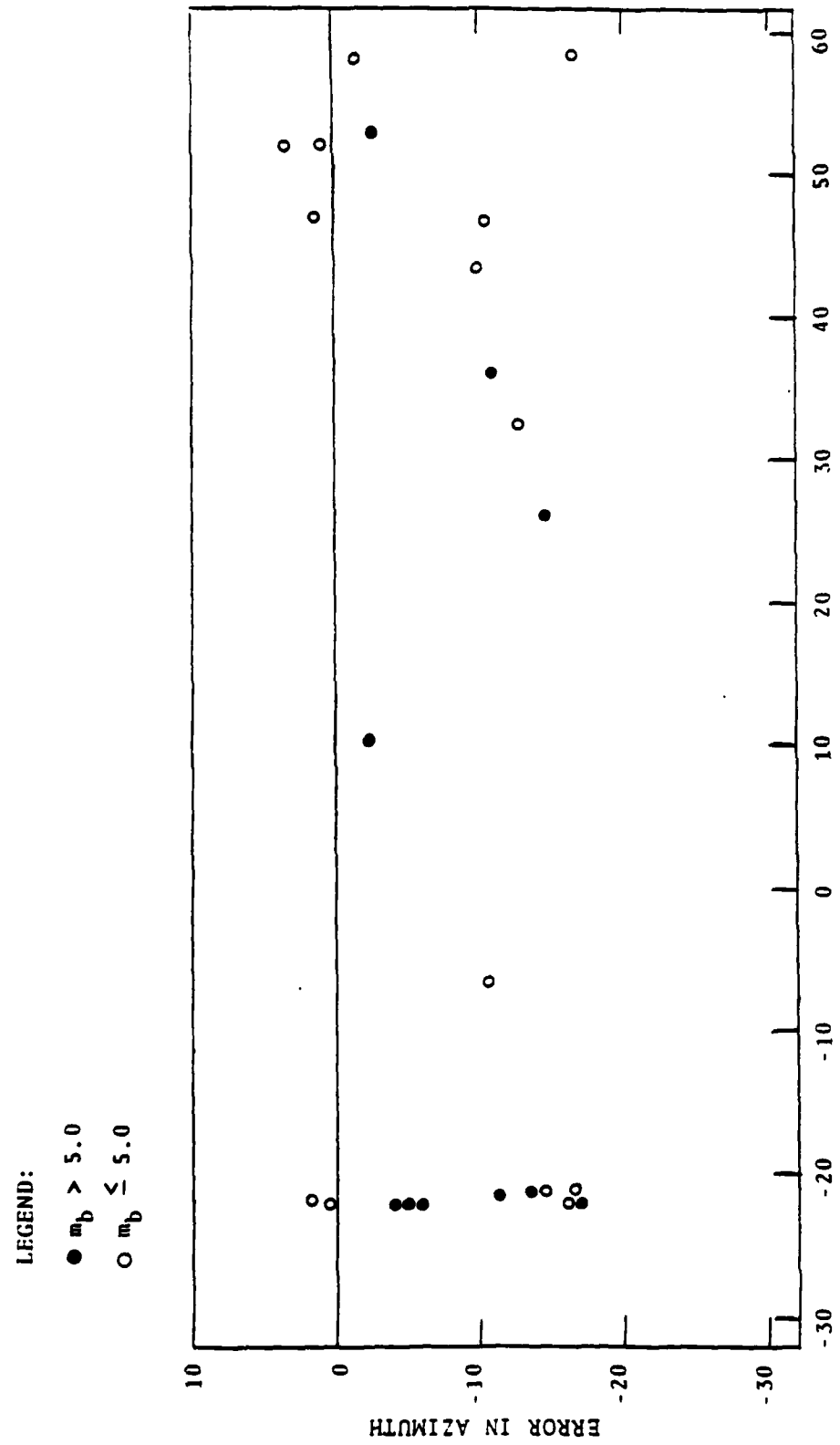

DIFFERENCES BETWEEN OBSERVED AND COMPUTED P-WAVES AZIMUTHS AT STATION BCAO

FIGURE II-10

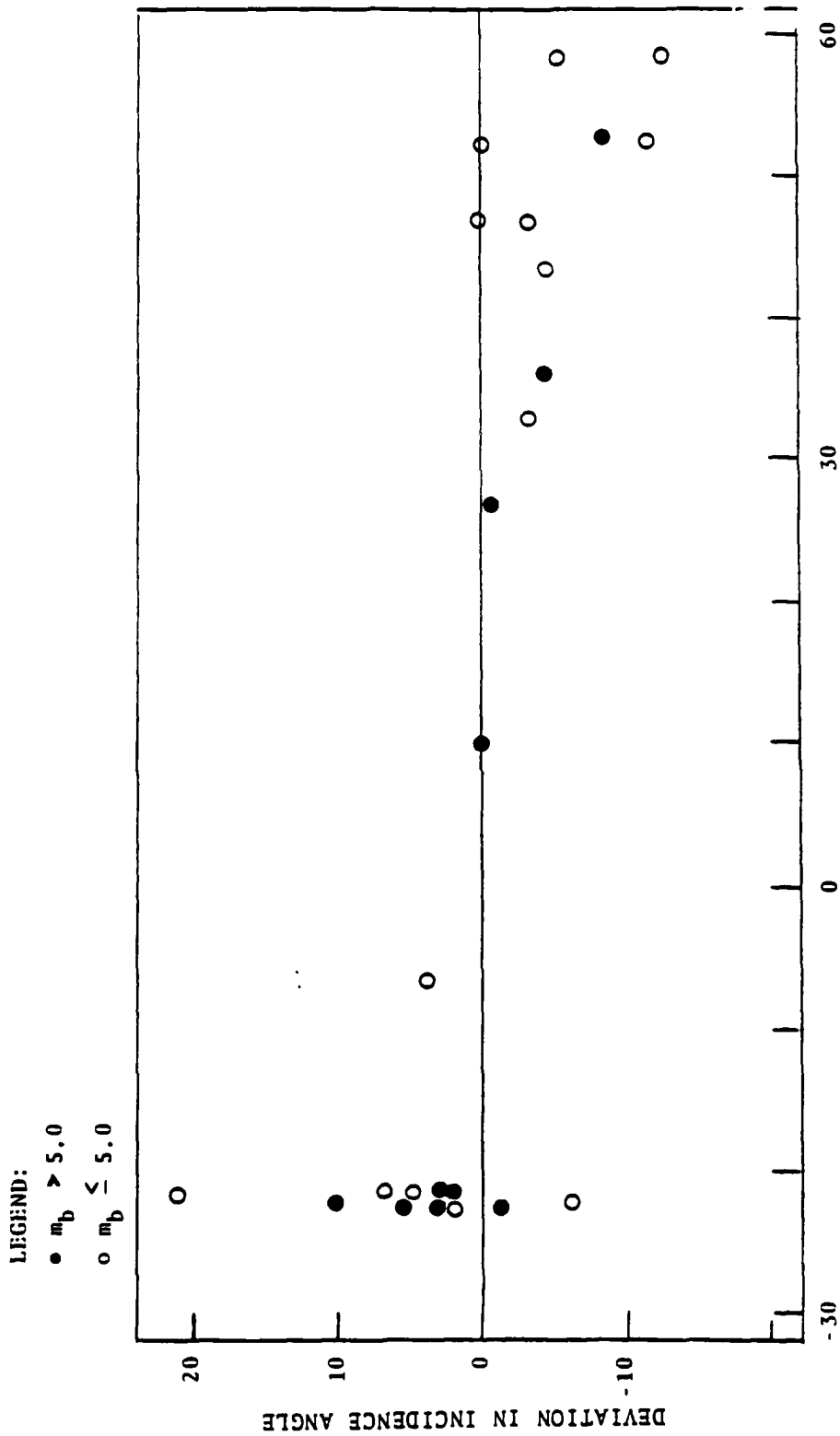

DIFFERENCES BETWEEN OBSERVED AND COMPUTED P-WAVE INCIDENCE ANGLES AT STATION BCAO, ASSUMING SHEAR WAVE VELOCITY UNDER THE STATION TO BE 3.5 KM/S

FIGURE II-11

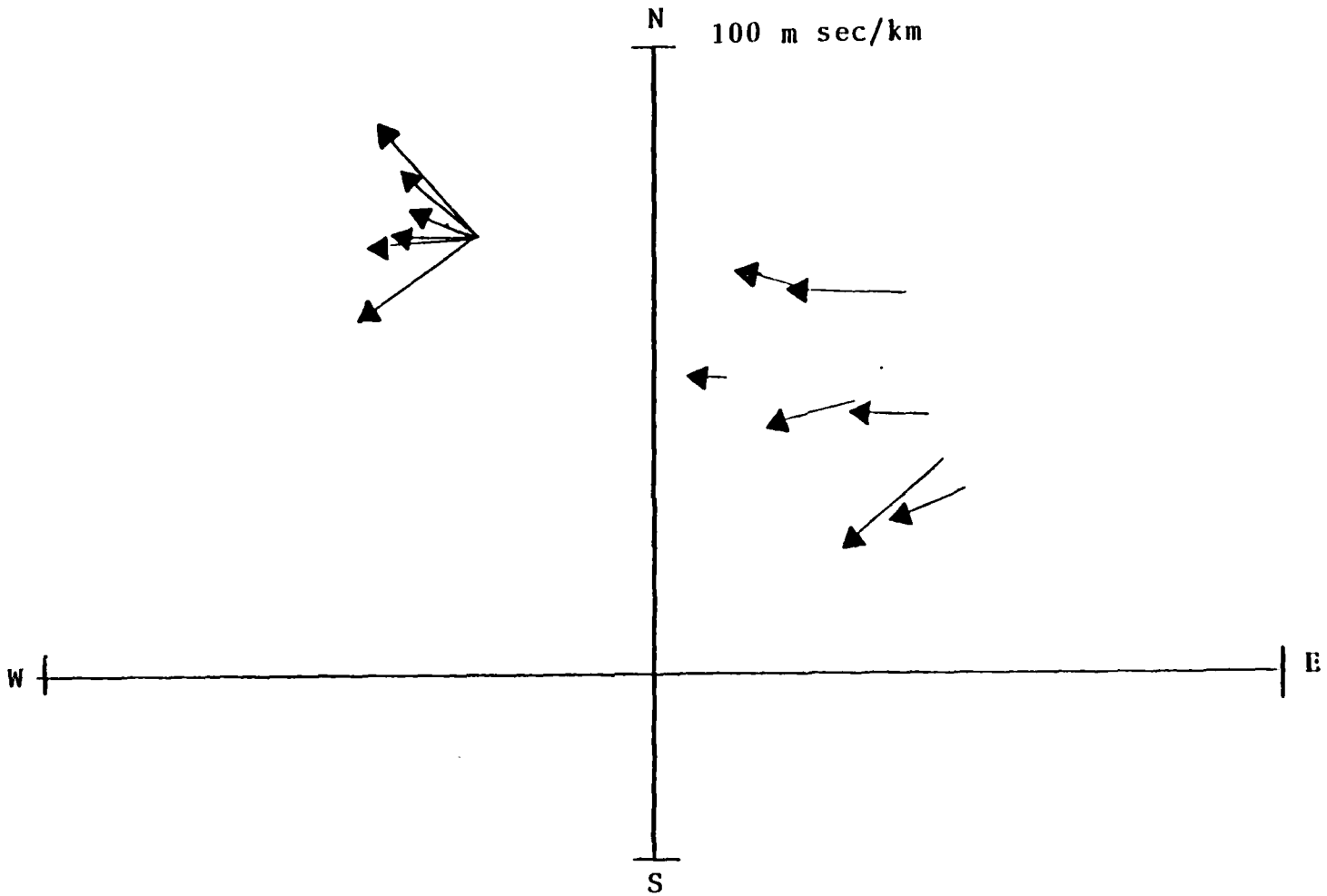

Slowness anomalies observed at BCAO three-component station. For explanation, see Figure II-13.

FIGURE II-12

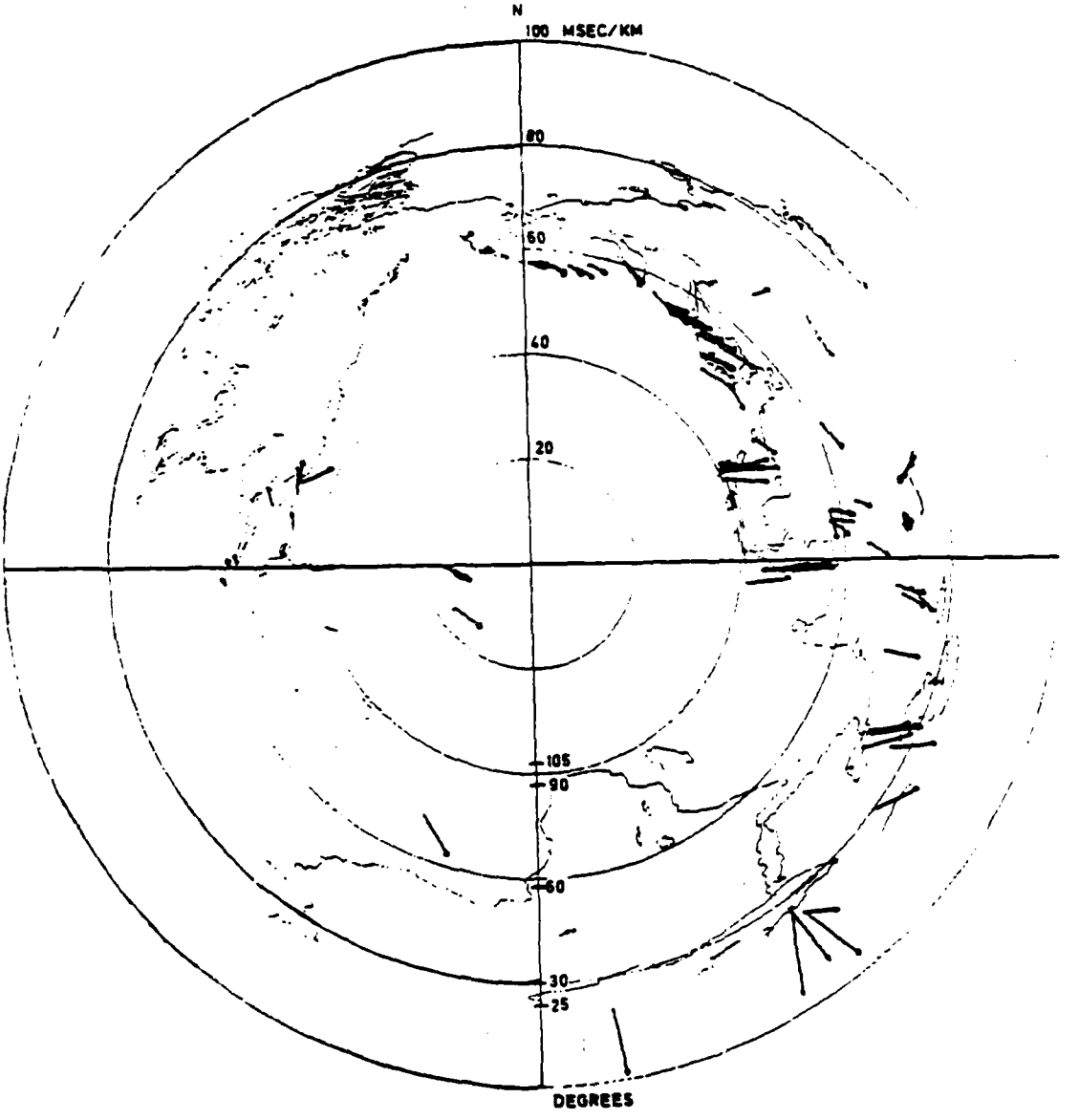

Slowness anomalies observed at NORSAR. Each observation is represented bv an arrow which starts from the slowness determined using the event location given bv NOAA and the 1968 P tables, and ends to the observed slowness.

FIGURE II-13

NORSAR LOCATION ERROR VECTORS PLOTTED IN INVERSE VELOCITY SPACE

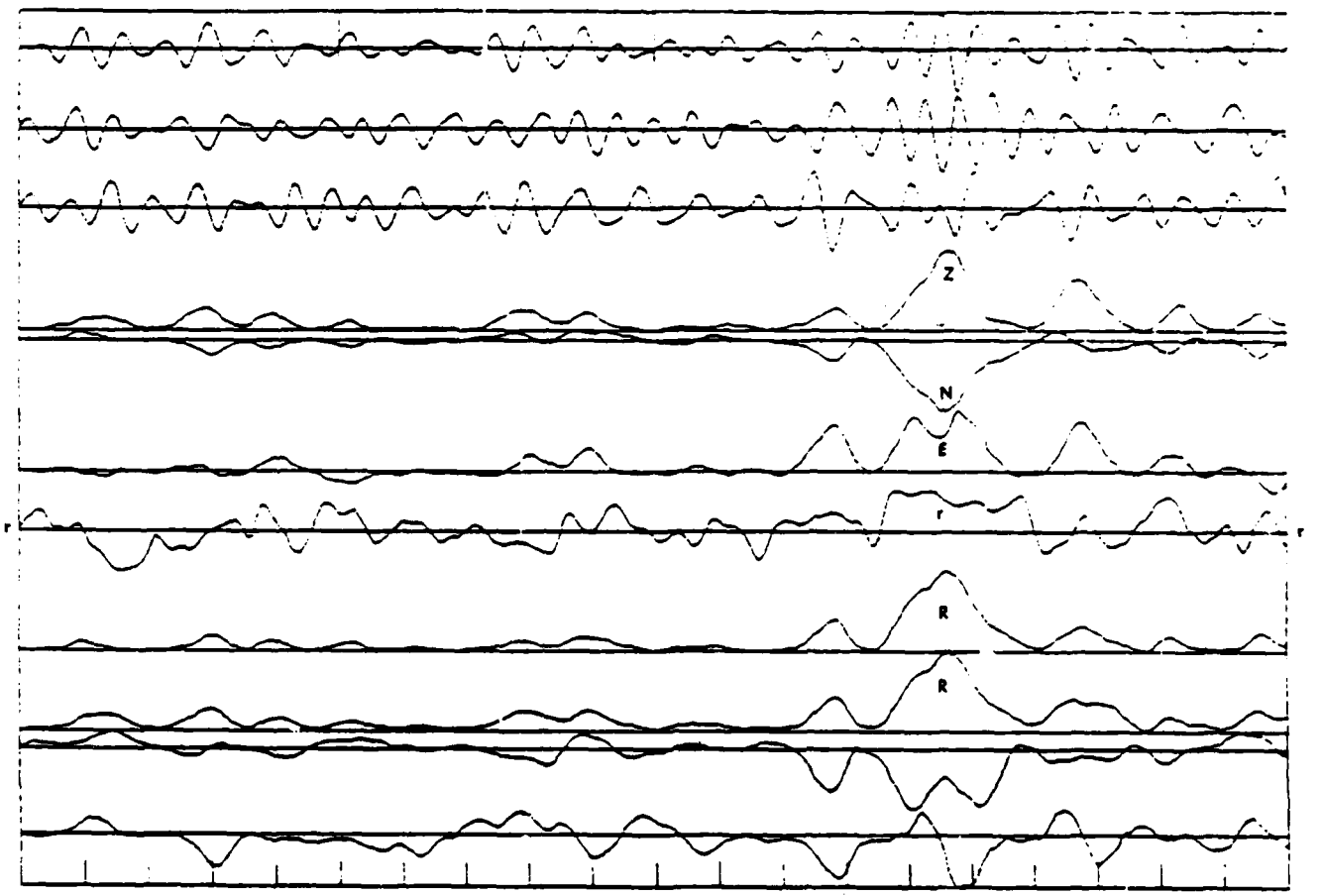

FIGURE II-14 (a)

EXTRACTION OF LOCATION INFORMATION FROM AN EVENT WITH POOR SNR

The azimuth is computed from amplitudes of N and E, the angle of incidence from Z and R. The decidedly positive r indicates P-waves. The measurements are included in Figures II-10 and II-11. (True azimuth -22 degrees). Event in Algeria, station BCAO. The traces are explained in Figure II-9.

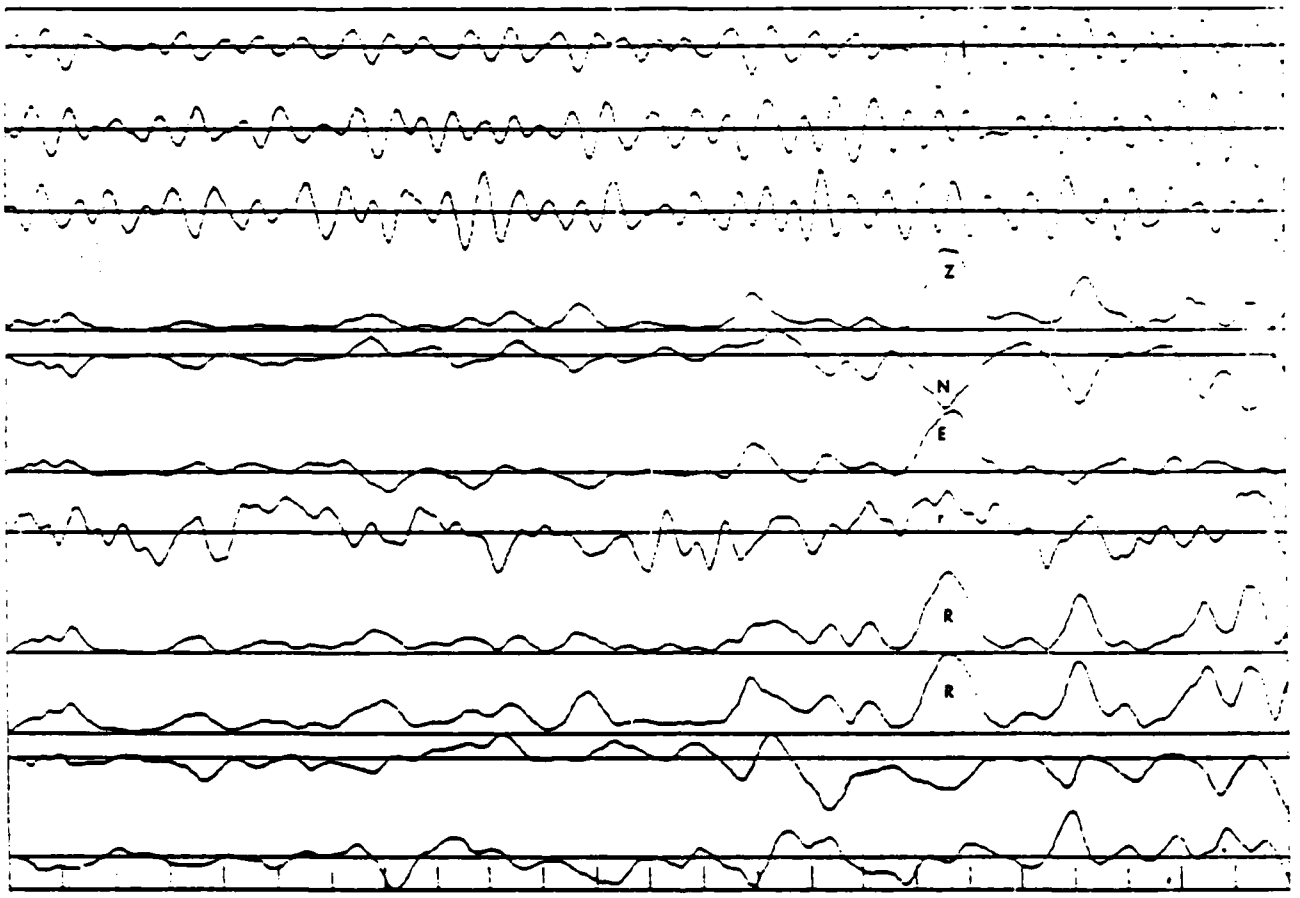

See Figure II-14(a) for description. Another event in Algeria.

FIGURE II-14 (b)

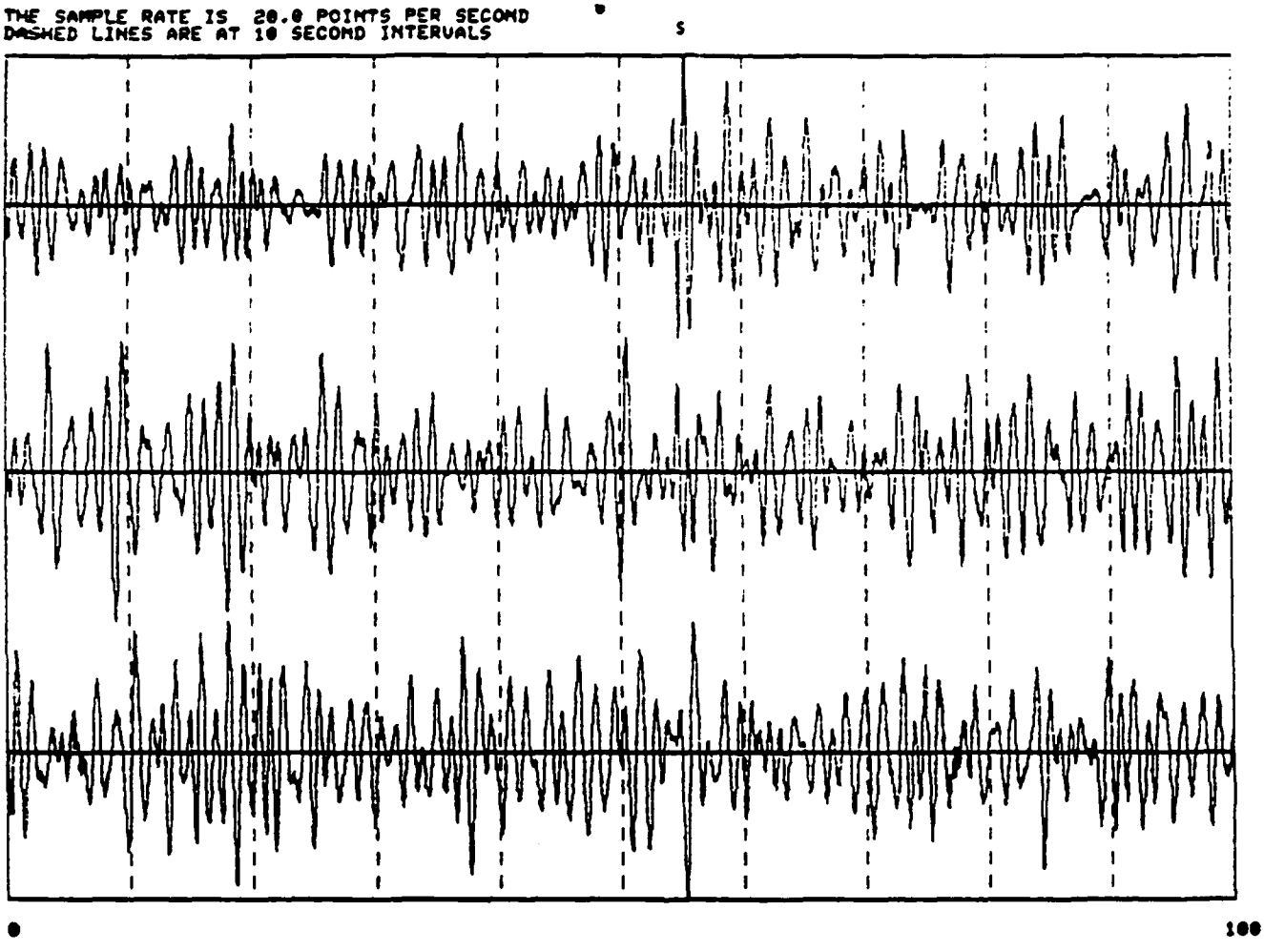

FIGURE II-15

AN EVENT WITH POOR SIGNAL-TO-NOISE RATIO

Measurements made from the records from an event in Central Asia (m_b = 4.2), station BCAO, are included in Figures II-10 and II-11 (true azimuth 52.2 degrees).

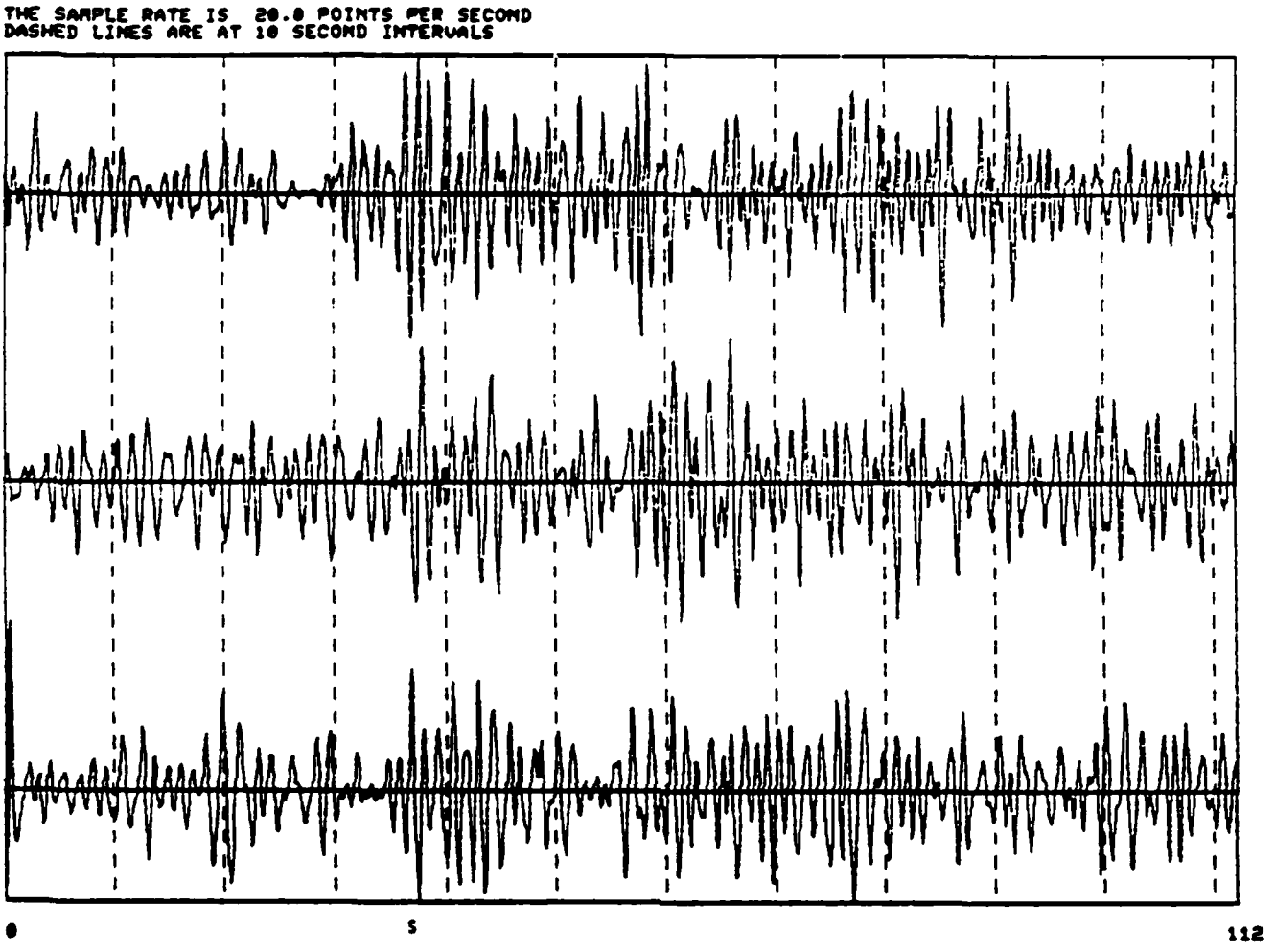

FIGURE II-16

AN EVENT WITH POOR TO FAIR SIGNAL-TO-NOISE RATIO

See the caption of Figure II-15. m_b = 4.3 and true azimuth 47.3 degrees.

E. CONCLUSIONS OF THE SECTION

We applied running phase and envelope measurements to determine azimuths and angles of incidence of teleseismic P-waves recorded at BCAO station (Central African Republic). Envelope ratios between running estimates of linearly polarized waves were used. Regional anomalies in azimuth and angle of incidence ("slowness anomalies") have to be corrected for before locating events using these measurements. Such calibration is already routinely done at array stations. Measurements made from an aftershock series give an estimate of calibrated location accuracy of the method, as the anomalies for all of the closely spaced events are equal. We computed the standard deviations of azimuth and angle of incidence deviations from the "true" values. These give the measurement errors apart from the geophysical anomaly. For events with good SNR, the R.M.S. azimuthal error was 4.8 degrees. The R.M.S. error in angle of incidence translates to an error of +- 13 degrees in distance, if that is computed. The average distance of events from the source is 39 degrees. The R.M.S. azimuthal error for all events, including those with poor SNR, is +- 6.6 degrees.

SECTION III
DETECTION AND LOCATION OF TELESEISMIC EVENTS USING ADAPTIVE AND NON-ADAPTIVE COHERENT BEAMFORMING OF REGIONAL-SIZE NETWORKS

A. SECTION INTRODUCTION

Adaptive and other methods of beamforming were applied to networks of seismic stations to both detect and locate small seismic events from some specific targeted source region. The station separations in the networks were a few hundred kilometers, and the network spatial extents were of the order of a thousand kilometers. Through extensive testing we arrived at an optimum coherent beamforming process to detect and locate such weak events, provided that the station network has been time and amplitude calibrated for the source region. Calibration can be done using well-located master events situated in the source region, with a spacing of about seven degrees. As master events are used for calibration, our approach bears some similarity to the variant of Joint Hypocentral Determination described by Dewey (1972). There are two important factors influencing performance: 1) the detection capability and 2) the validity and accuracy of location estimates. Signal-to-noise ratio improvement obviously improves detection of small events. Beam pattern sidelobe identification and reduction prevents multiple false alarm location of larger events. It is needed because we are covering only the target region, not the entire globe, with beams. Events from outside the target region cause false alarms and locations, if it is not recognized that though they cause the power output on the beams to rise, the signals are nonaligned (incoherent). We took both factors into account in designing a processor which reliably can detect small events from targeted teleseismic region. The processor is called coherent power-forming (CPF). To identify sidelobes, criteria of signal similarity were employed. These identify detections produced by dissimilar waveforms and on that basis suppress possible false alarm locations.

Location errors of the order of 25 km were observed for events within five degrees from a master event. The beamforming technique could locate events with signals so poorly visible that their timing accuracy is low and a joint epicenter location based on reading onsets has consequently a low accuracy.

The following methods to extract coherent signals are used or compared in this report:

- Conventional beamforming, which is a simple summation of

channels, after applying the time delays.

- Adaptive beamforming, in which after applying the time delays the channels are multichannel filtered as

$$y(t) = \sum_{ij} \sum a_{ij} \; x_{i-j}(t)$$

where $x_i(t)$ is the input value from channel i at time t and a_{ij} is a continually updated multichannel filter operator (j = 1, J spans the length J of the operator). The filter acts to minimize the output power. It is subject to Levin's constraint, which allows a wave propagating from the desired beam direction to pass through the array without being distorted during the power-minimization process (see e.g. Shen, 1979). Since in our case the background noise is uncorrelated between the widely separated sensors, improvement by the filtering is caused only through changes in the frequency contents of noise.

- Computation of semblance of the input channels. Semblance is a measure of signal similarity Neidell and Taner, 1971) and defined as

$$S_c = \frac{\overline{\left(\sum_i x_i \; (t) \right)^2}}{M \; \overline{\sum_i x_i^2 \; (t)}}$$

where x_i is the input sample at time t for channel i, and the cross-bar denotes moving average over successive samples in time. Values of semblance range from zero to one. The expected value for uncorrelated input is 1/M.

- Coherent input power, which is a new concept and shall be derived in a later section. It is computed as

$$P_c = \frac{P_b - P}{N - 1}$$

where P_b is the power of the conventional beam and P is the total input power, i.e.

$$P_b = (\Sigma x_i)^2 \quad \text{and} \quad P = \Sigma x_i^2$$

- The ratio of coherent energy to total input energy, or

$$r = \frac{P_c}{P}$$

This can be shown to be equivalent to the energy-normalized cross-correlation sum (Neidell and Taner, 1971), a multichannel coherence measure. We use here a noise-corrected version of r, or

$$r' = \frac{P_c}{STA(P) - LTA(P)}$$

which we call "signal coherency" and contains no bias due to noise. Obviously this can be evaluated only when input power is sufficiently above its long-term average (LTA).

As an example of the last two measures, assume that a spike is encountered on one of the input channels. P rises then sharply above its long-term average, the expected value of P_c remains zero (assuming input to be uncorrelated between to channels) and r' takes a low value, indicating "signal" coherency to be low.

B. SIGNAL COHERENCY ACROSS LARGE NETWORKS

To improve signal-to-noise ratio by coherent beamforming it is necessary to have some amount of signal coherency among the stations of the network. Even more important, signal coherency is necessary for locating the epicenter of the source. Locating relies on correctly aligned signals to display higher output power than incorrectly aligned signals. Coherent beamforming of completely incoherent signals is not possible.

Signal coherency among the stations of the Long Range Seismic Measurement (LRSM) network in continental United States was studied. Correlation coefficients between the P waveforms were computed, after aligning the waveforms at their first through. This method of alignment was chosen because the relative contribution of scattered and reflected waves is the smallest in the initial part of the waveform.

The P waveforms recorded at 14 LRSM stations from a moderately large (m_b = 5.6) deep earthquake at Kurile Islands. The P waveforms are shown in Figure III-1, aligned at their first troughs. The locations of these LRSM stations are shown in Figure III-2. Epicentral data and distances between the epicenter and the stations are shown in Table III-1.

As the signal coherency is expected to decrease with time along the waveform, the length of record extracted for correlation estimate influences the results. We chose to include four seconds of data to correlation estimates. Polarization (3-component) filtering indicated scattered, non-P type energy to dominate the BL-WV record after four seconds.

The computed correlation coefficients between pairs of stations are shown in Table III-2. The table indicates that pairs of stations close to each other in azimuth from the source have high correlation among their waveforms. The data is not sufficient to say how this is influenced by the tectonic structure of North America. We see a clear east-west difference in waveforms. however.

The correlation coefficients between pairs of stations are plotted against the distance between the stations constituting the pair in Figure III-3. This gives an estimate of how rapidly waveform correlation decreases with increasing distance between stations. Significant

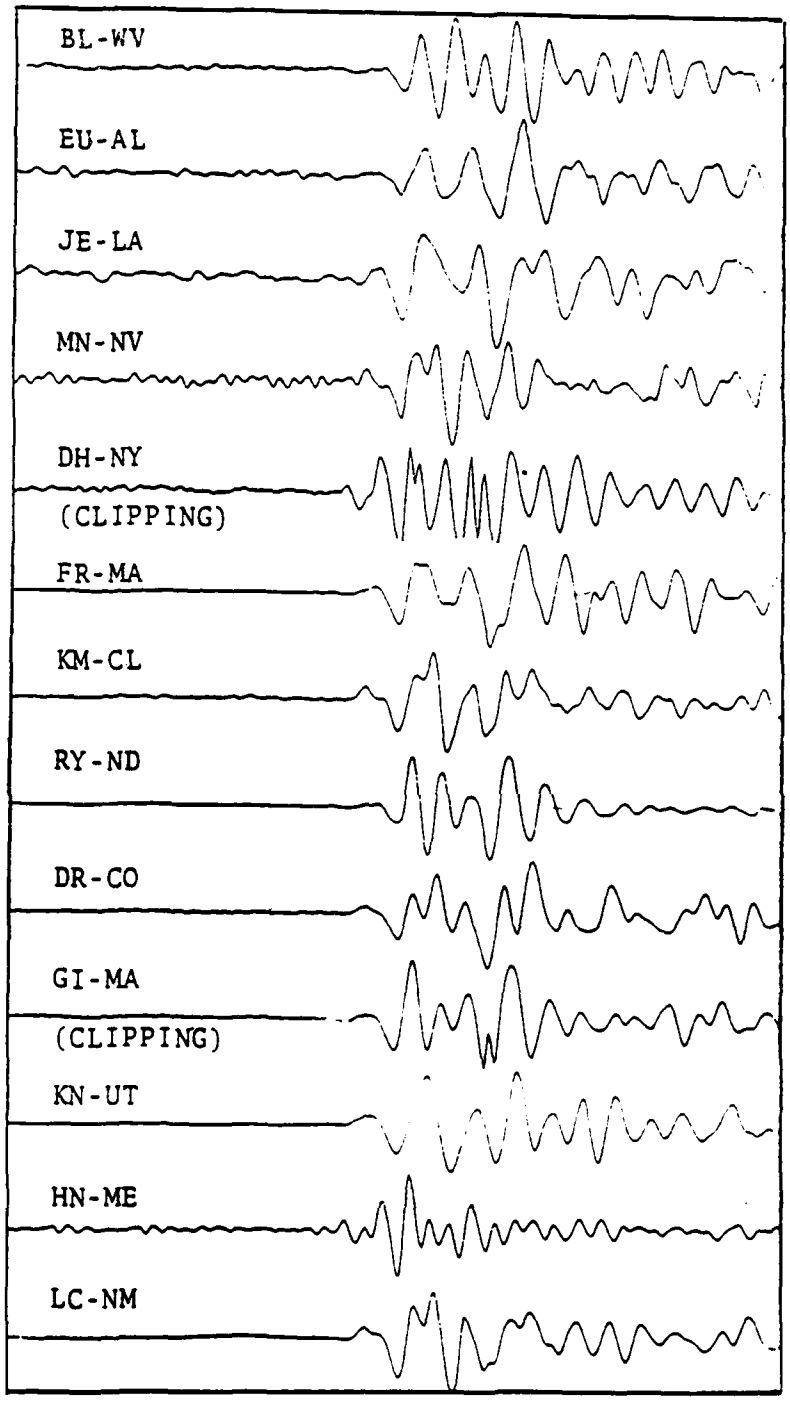

LENGTH OF RECORDS IS 15 SECONDS

FIGURE III-1

P-SIGNALS FROM KURILES EARTHQUAKE AT LRSM STATIONS

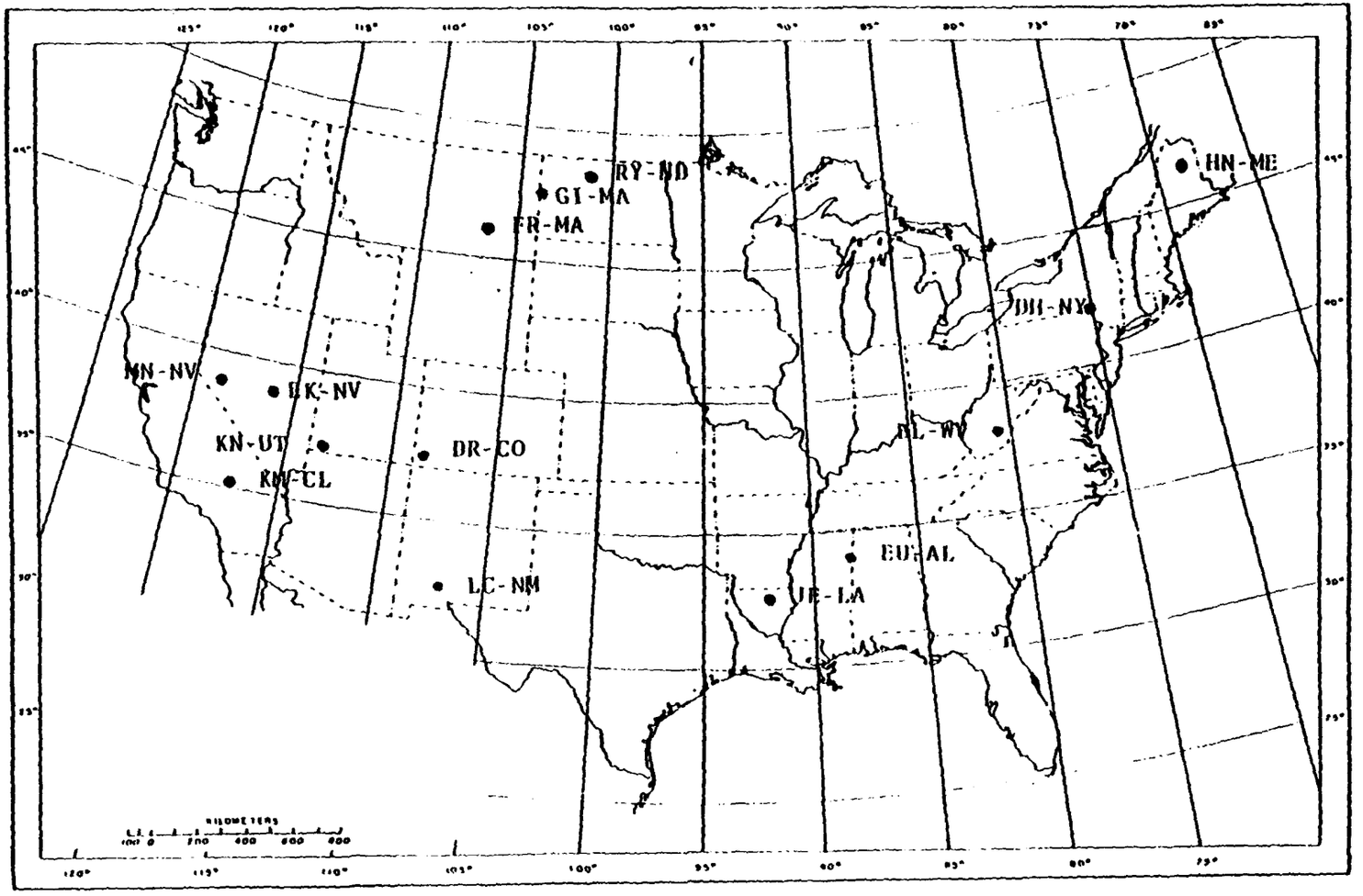

FIGURE III-2

LOCATIONS OF LRSM STATIONS RECORDING THE KURILES EARTHQUAKE IN MARCH 1964

TABLE III-1

DISTANCES TO STATIONS AND EPICENTRAL DATA OF THE KURILES EARTHQUAKE

DATE: 18 MARCH 1964
ORIGIN TIME: 04-37-26.9 UT
LOCATION: 52.5 N 153.6E
DEPTH: 440 km (284 km)
m_b: 5.6
REGION: NORTHWEST OF KURILE ISLANDS

NAME	LATIT.	LONGIT.	AZIMUTH	BACKAZ.	DIST.KM	DELTA
bl-bw	37.799	81.31Ø	41.47	329.27	8695.1	78.197
dh-ny	42.244	74.888	34.84	331.95	8534.5	76.753
dr-co	37.455	1Ø7.783	59.43	318.58	7341.1	65.ØZZ
ek-nv	39.2Ø9	115.71Ø	53.21	315.38	6726.8	6Ø.49E
eu-al	32.779	87.874	48.81	326.9Ø	8851.7	79.6ØE
fr-ma	46.1ØØ	1Ø6.44Ø	52.Ø6	316.14	671Ø.1	6Ø.346
gi-ma	47.193	1Ø4.219	49.92	316.7Ø	6739.4	6Ø.6ØE
hn-me	46.162	67.986	1e.46	335.21	839Ø.5	75.457
je-la	31.785	92.Ø15	52.34	325.37	8725.8	78.473
km-cl	34.881	117.257	67.63	316.56	6976.6	62.742
kn-ut	37.Ø23	112.827	63.Ø6	317.Ø8	7Ø76.9	63.644
lc-nm	32.4Ø2	1Ø6.599	62.18	32Ø.27	7838.2	7Ø.49Z
mn-nv	38.436	118.148	65.39	314.95	6638.3	59.7ØØ
ry-nd	48.Ø97	1Ø1.494	47.67	317.61	68Ø5.Ø	61.199

TABLE III-2

STATION	KM-CL	MN-NV	KN-UT	LC-NM	DR-CO	JE-LA	FR-MA	GI MA	EU-AL	RY-ND	BL-BW	HN-ME	DISTANCE
EU-AL	.27	.16	.54	.39	.02	.36	.75	.62	*	.24	.13	.06	80^0
JE-LA	.59								.36		.28	.05	78^0
BL-BW	-.22	-.14	-.09	-.20	-.01	.28	.02	.55	.13	.67	*	.49	78^0
HN-ME	-.18	-.02	-.20	-.04	.24	.05	.02	.41	.06	.58	.49	*	75^0
LC-NM	.87								.39		-.20	-.04	70^0
DR-CO	.67								.02		-.01	.24	66^0
KN-UT	.57								.54		-.09	-.20	64^0
KM-CL	*	.80	.57	.87	.67	.59	.41	.25	.27	.18	-.22	-.18	63^0
RY-ND	.18								.24		.67	.58	61^0
GI-MA	.25								.62		.55	.41	61^0
FR-MA	.41								.75		.02	.02	60^0
MN-NV	.80								.16		-.14	-.02	60^0
AZIMUTH	68^0	65^0	63^0	62^0	59^0	52^0	52^0	50^0	49^0	48^0	41^0	28^0	

WAVEFORM CORRELATION COEFFICIENTS BETWEEN PAIRS OF STATIONS

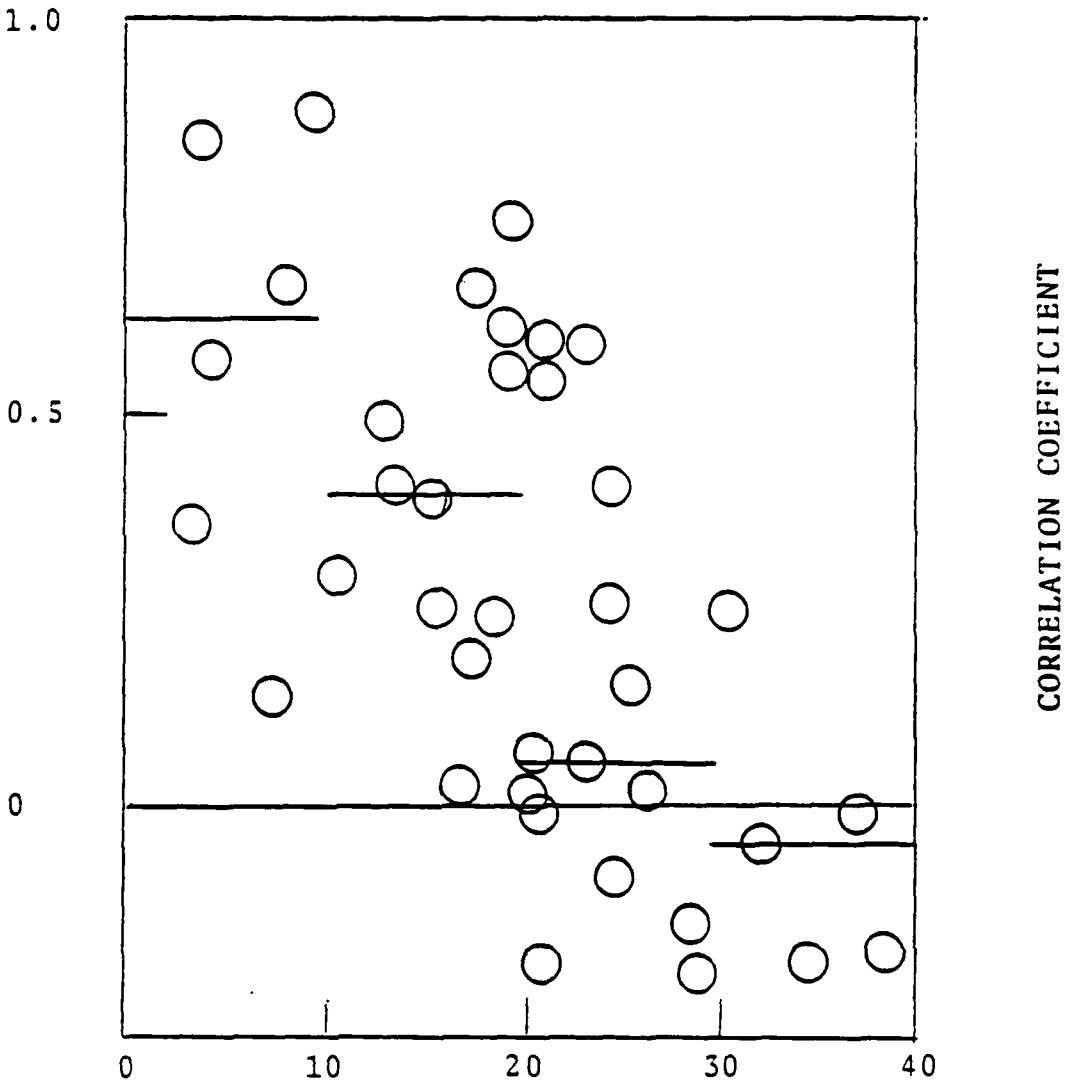

FIGURE III-3

CORRELATION COEFFICIENTS BETWEEN PAIRS OF STATIONS, PLOTTED AGAINST THE DISTANCES BETWEEN THE PAIR

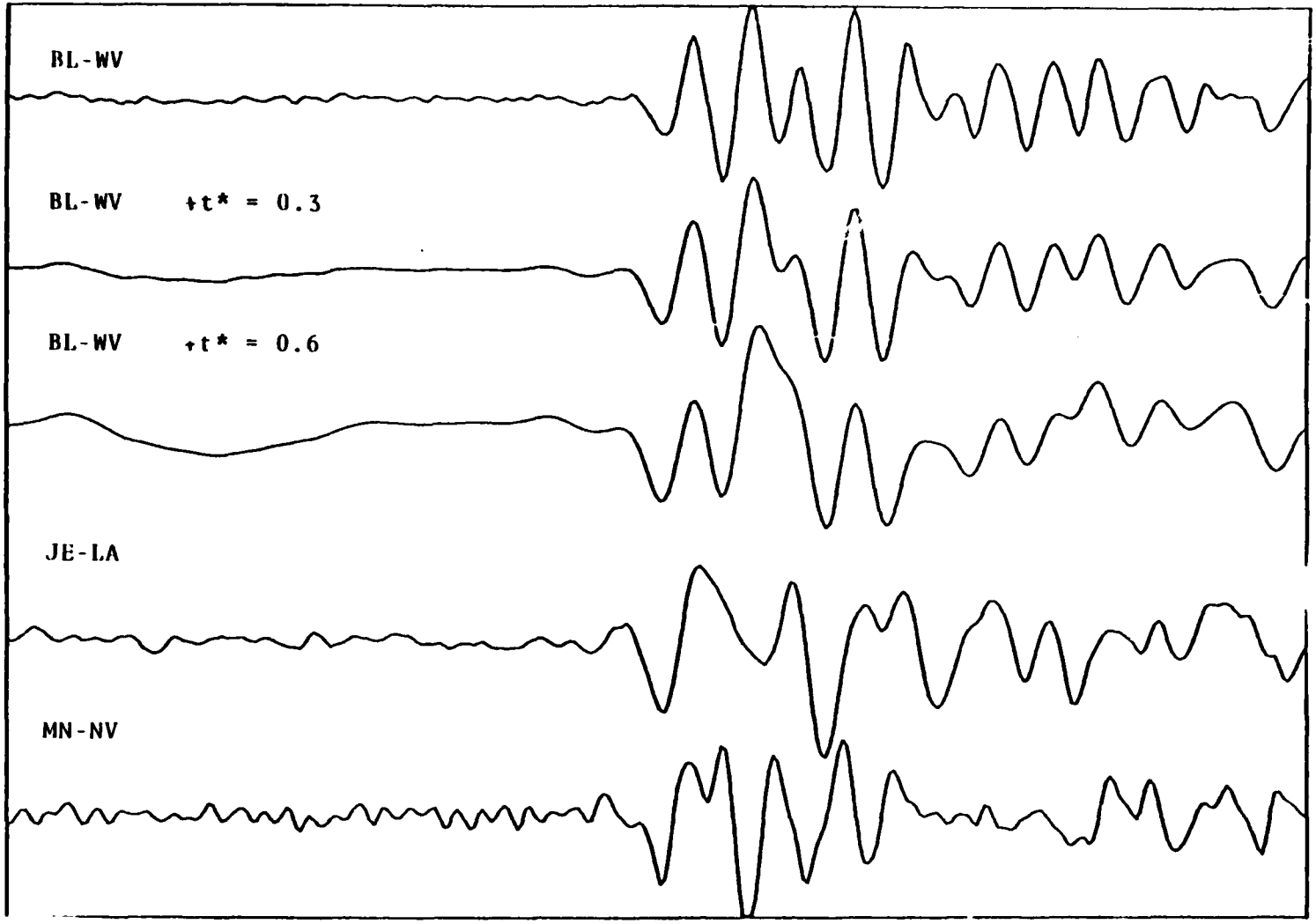

FIGURE III-4

ATTENUATED BL-WV RECORDS COMPARED WITH TWO WESTERN US LRSM RECORDS

correlation appears to persist out to distances of 20 degrees, and the waveforms are particularly well correlated across distances less than ten degrees.

Estimates for a difference in average anelastic absorption between the upper mantles below eastern and western United States have been given by various authors (for a review, see Der and McElfresh, 1977). We tried to attenuate the signal recorded at station BL-WV in eastern U.S. by a causal, constant-Q absorption operator. If the poor correlation between eastern and western U.S. stations were caused mainly by the suggested stronger absorption in western U.S. stations, attenuating the BL-WV signal should increase its correlation with the western U.S. stations. BL-WV seismograms attenuated by 0.3 and 0.6 t* units are compared in Figure III-4 with two western U.S. records. We could however, see no increase neither when attenuating the BL-WV for the expected teleseismic absorption difference ($\Delta t^* = 0.3$) or for double that amount. The results are shown in Figure III-5. We conclude that the loss of correlation with increasing station separation is not caused by the east-west wave absorption difference, and that applying attenuation corrections would not improve signal correlation between the stations.

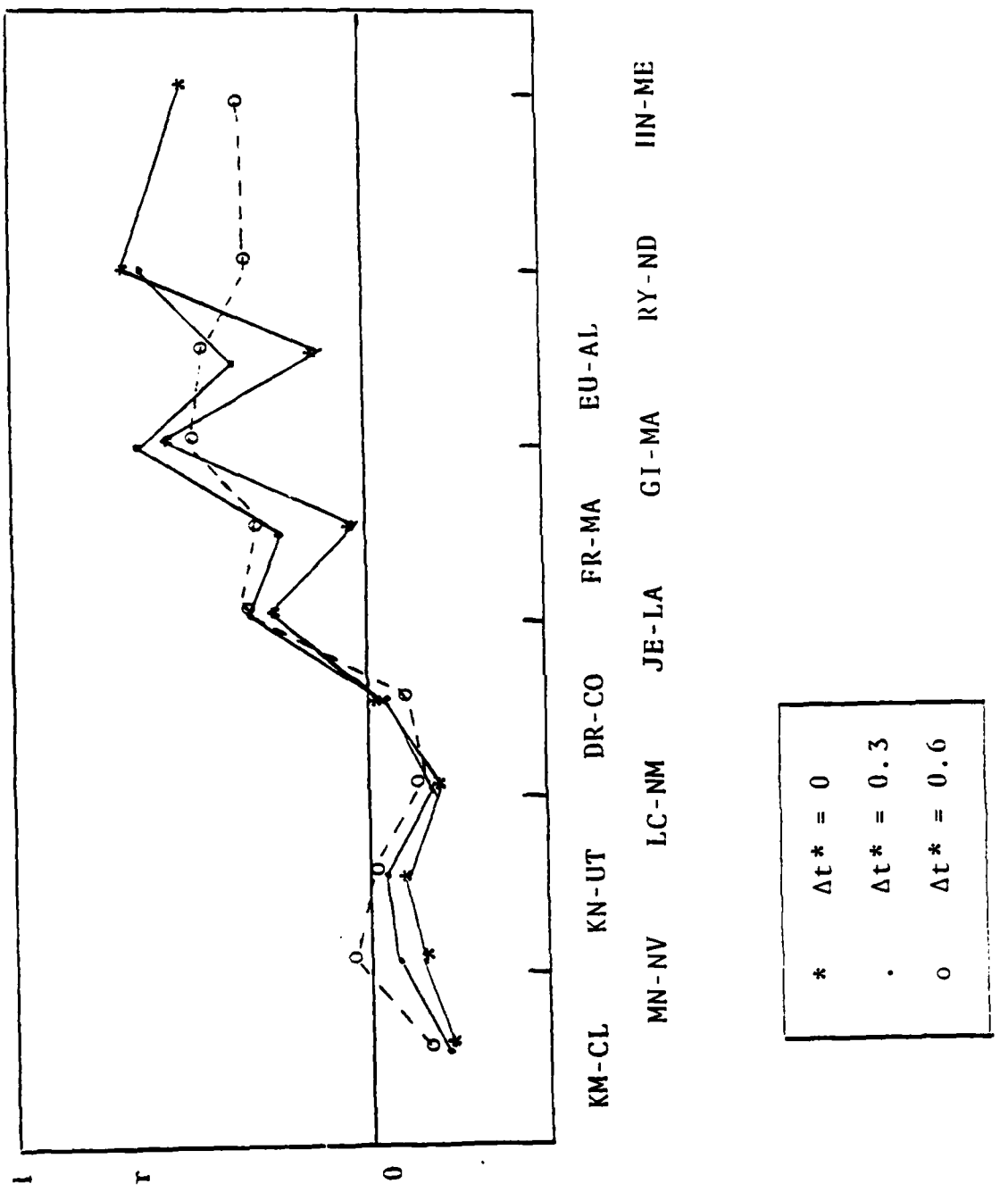

FIGURE III-5
CORRELATION OF ATTENUATED BL-WV RECORDS WITH OTHERS

C. IMPROVEMENT IN DETECTABILITY USING ADAPTIVE BEAMFORMING ALONE AND IN COMBINATION WITH SEMBLANCE COMPUTATION

Adaptive beamforming (multichannel filtering) was applied to records made at five LRSM stations in western United States. The network is shown in Figure III-6. The records where shown in Figure III-1 (stations DR-CO, KM-CL, KN-UT, LC-NM and MN-NV). We aligned the signals according to their first troughs. Using perfectly aligned signals simulates the beam with target point at the epicenter, with the assumption that the relative station times residuals are known and corrected for. We then added beams with different sets of lags to simulate beamforming to additional target points in the vicinity of the epicenter. The spatial response of the array suggests a beam spacing of 0.4 degrees (44 km). We then mixed in amplified noise taken from earlier parts of the recordings. Our goal is to find whether we can improve detectability from the $\sqrt{N}$ improvement offered by conventional beamforming, in the case of uncorrelated noise among the N channels.

In all, nineteen different beams were generated, corresponding to target points spaced 0.4 degrees apart on a line running in N-S direction and centered on the epicenter. In the first five experiments, we judged the results by the signal power to average noise power ratio (maximum short term average versus long term average or STA/LTA), and by the ratio of signal amplitude to the largest noise amplitude observed in the 30 seconds long noise record preceding the signal. These statistics are listed in Table III-3. The input data to the five experiments are shown in Appendix A. Output conventional and adaptive beams from the Experiments are shown in Figures III-7.

The results in Table III-3 indicate:

- Adaptive beamforming increases the STA/LTA (i.e. signal-to-noise) power ratio. It thus decreases average noise power relative to signal power.

- The ratio of signal amplitude to the maximum noise amplitude, observed on beam prior to signal arrival, is (for broad-band data) not larger for adaptive beams than for conventional beams. To reconcile this with the previous observation we conclude that noise variance increases in adaptive beamforming.

- The capability to locate, i.e. to produce the largest output power on the beam targeted to the epicenter, of the adaptive

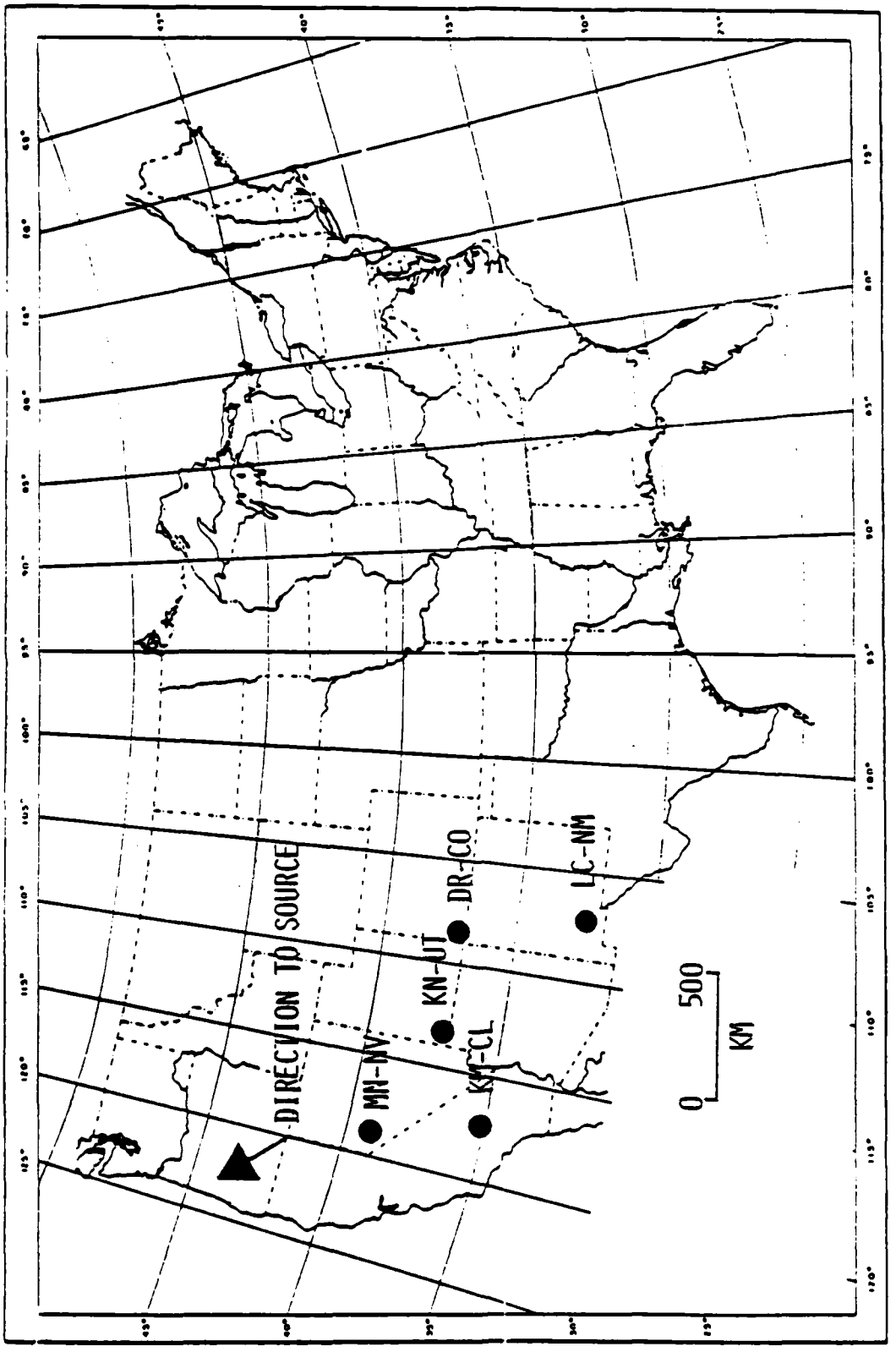

FIGURE III-6

STATIONS OF THE LRSM ARRAY IN WESTERN U.S.

TABLE III-3

SIGNAL-TO-NOISE RATIOS OF INPUT DATA AND OUTPUT BEAMS

	STA/LTA	S/N AMPL. RATIO	BEAM OF MAX. POWER*	COMMENTS
Experiment I: Input Data (Average)		2.5		
Conventional Beam	23.9	5.8	10	
Adaptively Filtered Beam	38.3	5.7	10	
Experiment II: Input Data		1.2		Lower input SNR than Exp. I
Conventional Beam	4.5	2.0	10	
Adaptive Beam		1.8	11	
Filtered Conv. Beam	4.0	1.4	8	(Output beams band-pass filtered, pass-band centered at 0.74 Hz)
Filtered Adap. Beam	9.7	2.4	10	
Experiment III: Input Data		1.1		As Exp. II, but input data band-pass filtered (pass-band centered at 0.74 Hz)
Conventional Beam	4.0	1.4	8	
Adaptive Beam	17.3	2.9	9	
Experiment IV: Input Data		1.7		Higher input SNR than Exp. II, different system response
Conventional Beam		2.5	10	
Adaptive Beam		2.3	10	
Conv. B. X Sembl.		3.3#	10	
Adap. B. X Sembl.		4.0#	10	
Experiment V: Input Data		1.8		As above, but input data band-pass filtered (pass-band centered at 1.0 Hz)
Conventional Beam	22.1	2.4#	10	
Adaptive Beam	41.3	2.9#	5	

*) Beam #10 is targeted to epicenter.
#) The largest noise amplitude found on all of the 19 beams is used to form the ratio.

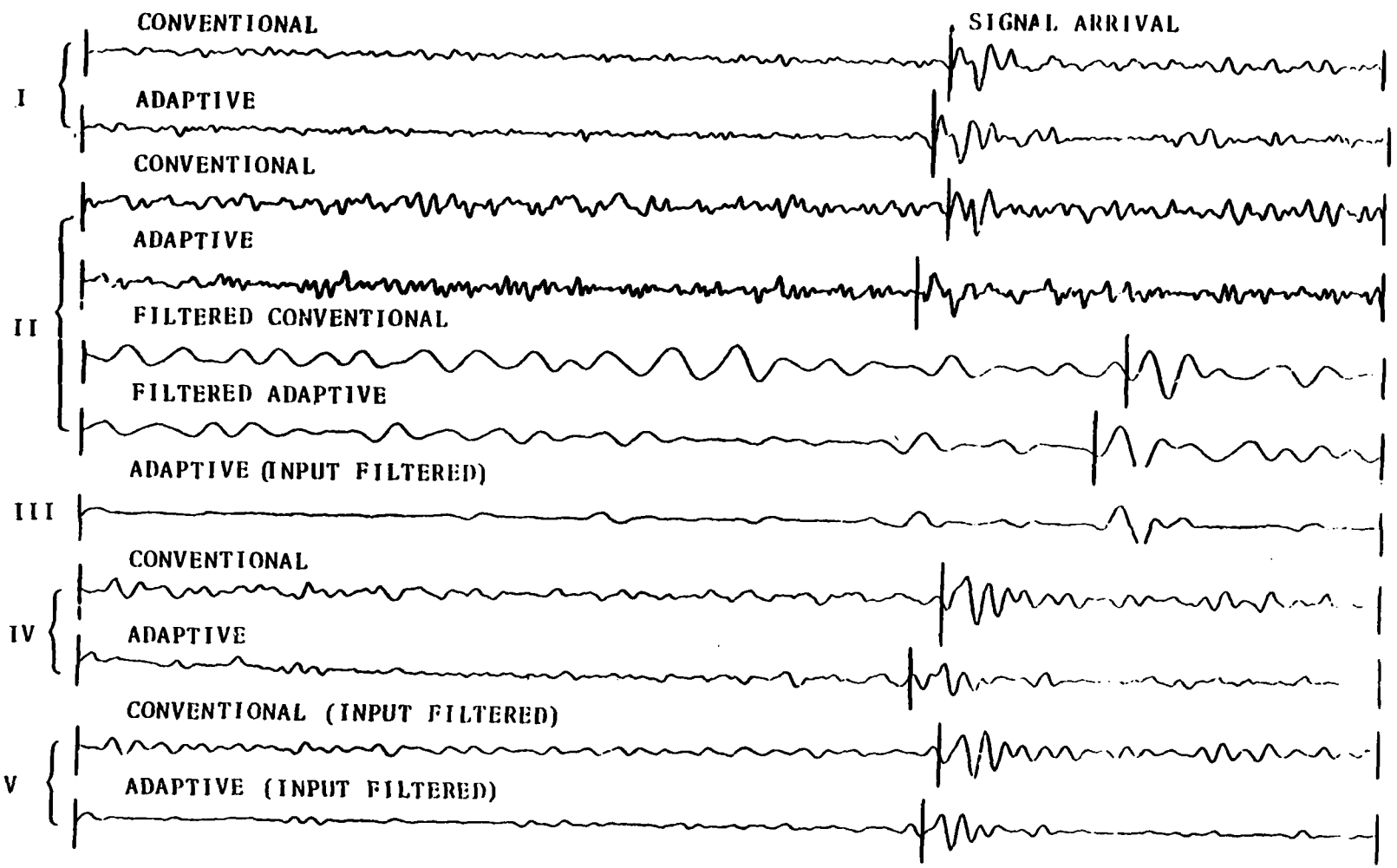

FIGURE III-7

OUTPUT FROM BEAMFORMING EXPERIMENTS

beam is not better than for the conventional beam.

- Adaptive beamforming of band-pass filtered data gave 2 to 6 dB larger signal-to-noise ratios than conventional beamforming of the same data, either filtered or unfiltered. The location capability was worsened, however.

The above results are not entirely unexpected. Frost (1972) states:

> "Noise voltages which are uncorrelated between taps may be partially rejected by the adaptive array in two ways. As in a conventional nonadaptive array, such noises are eliminated to the extent that signal voltages on the taps are added coherently at the array output, while uncorrelated noise voltages are added incoherently. Second, an adaptive array can reduce the weighting on any tap that may have a disproportionately large uncorrelated noise power."

As the noise is completely uncorrelated between the stations, situated hundreds of kilometers apart, we cannot make use of any spatial structure of noise to obtain noise rejection. However, after band-pass filtering the noise waveform is correlated between taps (samples) within each single channel. The multichannel filter minimizes output noise power by removing noise with temporal correlation, i.e., it whitens the noise. Bound by Levin's constraint, this adaptive frequency filtering does not influence the signal arriving from the look-direction. The adaptive beamformer thus treats the spectra of noise and of the look-direction signal differently.

We conclude that even in case of uncorrelated noise between the sensors, adaptive beamforming can give modest SNR improvement due to its special frequency filtering properties.

Since one of our conclusions above was that the variance of output noise is larger on the adaptive beams than on conventional beams, Z-statistics should be used to evaluate the improvement in detectability. The Z-statistic of some quantity is that quantity with the mean removed and its variance adjusted to one:

$$Z(x) = \frac{x - \mu(x)}{\sigma(x)}$$

We chose to use the logarithm of the moving average of power as x. Since we observed, as also Swindell and Snell (1977), that the distribution of x was slightly skewed, we used the median of x instead of average of x for $\mu(x)$, and computed $\sigma(x)$ using the positive deviations from median only. Use of median and only positive deviations gave better agreement in false alarm rates with the normal distribution, than use of average and both positive and negative deviations. We used Z-statistics in following beamforming experiments.

We also multiplied the output beams by semblance evaluated over a 1.5 seconds long window. This introduces further non-linearity to the output beams, but acts in favor of passing coherent inputs. It reduces side-lobes of signal, relative to the correctly aligned lobe.

We run some series of tests with different adaptation rates and band-pass filtering of output beams. The first series using Z-statistics is called Experiment VI, and results are summarized in Table III-4. Input data and output beams are shown in Appendix 1. We did not filter he input data, because we observed that it degrades location capability (signals resemble more sine waves, and side-lobes grow). We observed high adaptation rates combined with post-band-pass filtering, to give best results.

Even lower input signal-to-noise ratios are used in Experiment VII, where no detections can be made from the input data. The results are collected on Table III-5, where we also included results from using coherent power-forming in Experiment VII. The input data and output beams are shown in Appendix A. The following observations were made:

- Combination of adaptive beamforming and band-pass filtering of the beams improved the Z-statistic values of the output signals by varying amounts.

- Multiplication with semblance reduces significantly the side-lobes (see Appendix A).

- Coherent power-forming is equally good for detection as any of the other methods, and computationally much faster.

TABLE III-4 -- EXPERIMENT VI

	FILTERED				UNFILTERED			
	(1) Signal Z(x)	(2) Max. Noise Z(x)	(3) Signal /Noise Ratio	(4) Located to Beam	(1)	(2)	(3)	(4)
Input data:								
Chapter 1					3.1		1.1	
Chapter 2					6.3		1.7	
Chapter 3					5.1		2.1	
Chapter 4					<2.8		<1	
Chapter 5					<2.8		<1	
Conv. beam	4.8	2.6	1.4	#10	3.8	3.1	1.0	#10
Conv. beam x semblance	5.0	2.8	2.9	#10	4.6	2.8	1.7	#10
Adaptive beam x semblance	6.4	2.8	4.1	#10	4.4	2.4	2.4	#10

TABLE III-5 -- EXPERIMENT VII

	FILTERED				UNFILTERED			
	(1) Sign. Z	(2) Max. Noise Z	(3) Sign. Max. Noise	(4) Located to Beam	(1)	(2)	(3)	(4)
Input data:								
No detections Z < 2.8 at all Channels					<2.8			
Conv. beam	5.3	2.2	2.1	#9	4.1	2.6	1.2	#9
Conv. beam x semblance	5.0	2.6	2.5	#9	4.6	2.8	1.9	#9
Adaptive beam x semblance	5.0	2.6	3.0	#9	4.4	2.9	1.4	#9
Coherent power					5.7	3.0	---	#9

(3) is signal to maximum noise amplitude ratio.

D. COHERENT POWER - FORMING

In the previous chapter, our main consideration was detection of signals. In the following chapters of this section, we stress heavily the task of verifying that a detection really is from the targeted source region. In case of an array with sensor separations of hundreds of kilometers, noise is completely uncorrelated between the sensors, while the teleseismic P-signals are partially correlated. We want to extract only the coherent energy from the array input. Assuming the coherent energy (in some time window) to be C at each station, and the incoherent energy to be V_i at station i, we can write for the power on the conventional beam B, and for the total input power P (divided by number of channels N)

$$B = \frac{1}{N} \sum_i V_i + NC$$

$$P = \frac{1}{N} \sum_i V_i + C$$

Solving for the coherent power C we get

$$C = \frac{B - P}{N - 1}$$

and C/P, or the ratio of coherent to total power, is

$$r = \frac{C}{P} = \frac{B - P}{(N - 1)\ P}$$

The semblance coefficient s can be written

$$s = \frac{B}{NP}$$

and r can be written using s as

$$r = \frac{1}{N - 1} (Ns - 1)$$

which is equivalent to the energy-normalized cross-correlation sum (Neidell and Taner, 1971)

$$r = \frac{\sum_i \sum_{j \neq i} R_{ij}(0)}{(M - 1) \sum_i R_{ii}(0)}$$

where R_{ij} and R_{ii} are the waveform cross-correlation between stations i and j and the waveform auto-correlation at station i, respectively. As an example, coherent power and incoherent power (P - C) of the Experiment VII input are shown in Figure III-8 together with the corresponding conventional beam. The Z-statistics of the coherent power trace were listed in Table III-5.

The quantity r is of prime importance in classifying detections as aligned or incoherent. We use the noise corrected r described in section introduction. It is evaluated only when total power has risen one standard deviation above its mean. No detections are declared if this condition is not met.

In using coherent power-forming to locate events, we choose first the beam with the largest coherent power. It is immediately observed that even if none of our beams are correctly aimed to the epicenter, the increase of total signal energy due to an off-region event increases the variance of all coherent-power estimates. As the beam with the largest coherent power is chosen, an off-region event causes this power to exceed erratically the detection threshold set by e.g., a Z-statistic of long-term background noise. To avoid a false alarm, the ratio r is used to decide whether the arriving energy is mainly coherent or incoherent. A second threshold, that of r, has to be exceeded for a detection to be declared. The r threshold depends on the waveform similarity among the

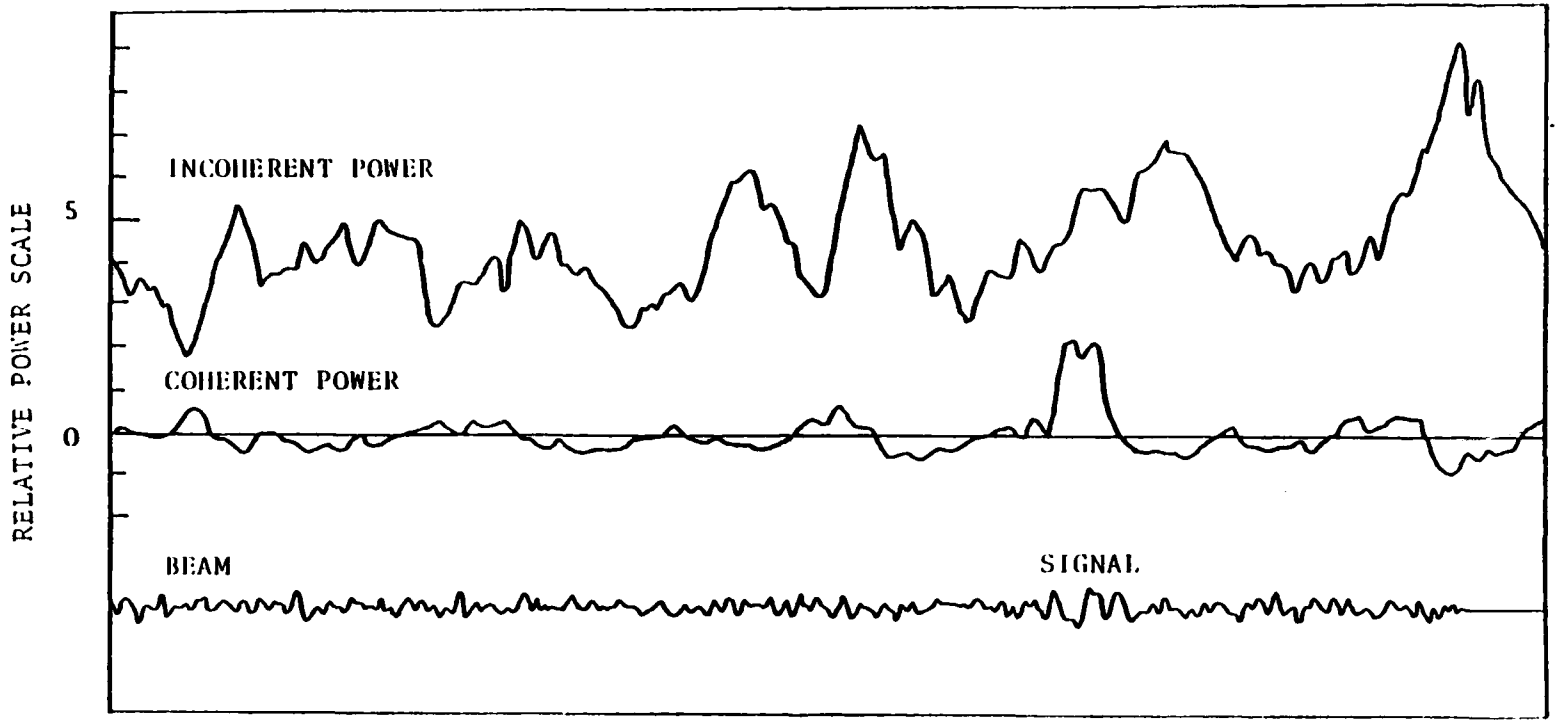

FIGURE III-8

INCOHERENT AND COHERENT POWERS AND THE CONVENTIONAL BEAM (AIMED TO EPICENTER) OF EXPERIMENT VII

different sensors, a geophysical parameter. For one particular network, we found r = 0.75 suitable.

We still encountered a few false alarms in testing, due to chance alignments of peaks and troughs of noise or coda with signals. Though this is in principle unavoidable, we could exclude virtually all false alarms by making a further condition that the relative amplitudes at the individual channels have to agree to some degree with those of the master event. To quantify this, we added the computation of semblance (see section introduction) among power values measured for the input channels. At one particular network, we found the semblance 0.75 to be a suitable threshold. Another possibility would have been simply to raise the threshold of r.

The G and r quantities can be formed in a computer fast enough to allow the creation of large number of beams in a reasonable time. To cover a region of a significant size many beams have to be formed, e.g. and array having the aperture 1000 km requires 500 beams to cover a target region with area 1000 x 1000 km. The adaptive beamformer which we used in the previous chapter is at least one order of magnitude slower than a coherent power-forming program.

TABLE III-6

MAXIMUM P-WAVE CROSS-CORRELATIONS AND THE CORRESPONDING TIME LAGS BETWEEN KN-UT AND SOME OTHER STATIONS

	MN-NV	DR-CO	LC-NM	KM-CL
LOW NOISE				
Lag (seconds)	-0.2	0.3	0.0	-0.1
Maximum Correlation	0.64	0.33	0.68	0.67
MODERATE NOISE ADDED				
Lag	0.2	-1.0	0.0	-1.0
Maximum Correlation	0.57	0.29	0.68	0.52

E. DETERMINATION OF BEAMFORMING DELAYS

The plane wave assumption in beamforming an array, or the assumption of applicability of tabulated travel times in beamforming a large network, breaks down when the array aperture/wave length ratio exceeds a certain limit. At a large array as, e.g., NORSAR, the time delays between the subarrays are adjusted by computing the cross-correlations between waveforms at each subarray and the reference subarray, and applying to each subarray the time correction determined by the lag of maximum correlation. In this study, we use instead large master events with high SNR's to map the station time corrections. These are stored in the beamforming program and applied in locating smaller events.

Use of master events should allow a better location accuracy than use of cross-correlation, because it gives Joint Epicenter Determinations. Further, as the waveform correlation is lower between widely separate stations than between sensors of an array, we may observe cycle-skipping using cross-correlations due to low correlation between the stations. As a test, we computed cross-correlations between KN-UT and the other western U.S. array stations (station locations in Figure III-6), using 4.0 seconds long sections of P-wave from the event listed in Table III-1. The maximum correlation and the time lag on which it occurs are shown in Table III-6. The lags are relative to alignment according to the first troughs. When a moderate amount of noise was mixed with the signals (SNR > 3), the lags of maximum correlation changed due to cycle-skipping. This result suggests that in this network, the correlation between the station waveforms is initially too weak to allow reliable time delay determination.

The quantities determined from a master event are the relative station residuals. The relative residual of station j with respect to station i is defined by

$$r_{ji} = (A_j - A_i) - (T_j - T_i)$$

where A's are observed arrival times, T's are tabulated travel times. After measuring the r_{ji} for a station network (i = 1, I) from a large event 1, we use them to align signals from another event k, at a distance X from 1. The errors S in alignment are

$$S = (r_{ji})_k - (r_{ji})_l$$

These errors should be small enough for the signals to add coherently in beamforming. We observed beam power to fall by 50% when the standard deviation of S increased from zero to 0.2 seconds, in case of the Kuriles event recorded at the western U.S. array.

Engdahl (1977) mapped the scatter S as a function of separation between stations j and i and between events k and l. This data came from a station network in Alaska. R.M.S. S values increase with both separations. Comparison with his results suggests that for station separations up to 1000 km the r.m.s. S values stay below 0.15 seconds, up to source separation 500 km. This suggests that the distance between the master event and the event to be located can be as large as 500 km, for a station network of the size of the western U.S. LRSM array.

F. AN EXPERIMENT TO DETECT AND LOCATE USING COHERENT POWER - FORMING

We attempted to locate a set of ten events in Central Asia, using a five-station network in Alaska. The maximum diameter of the station array is 739 km. The events occurred during the International Data Collecting Experiment, October 1-15, 1980. We used three master events, in the m_b range 5.2 to 5.9. These occurred during the same period. Time (and amplitude) corrections were interpolated between the masters so that they changed continuously from beam to beam. The determination of the corrections shall be discussed in the end of the section.

Figure III-9 shows the positions of two of the masters and nine of the events to be located. The other two events are situated further west. All events are listed in Table III-7. The results of the experiment are summarized in Table III-8. We tried to locate each event on three separate target regions, only one of which overlapped the true event site. Each region had dimensions 1822 x 1822 km. In all, 5043 beams were monitored in a time window about two minutes long and containing the signal onsets. No false alarms were encountered when aiming the beams to regions not overlapping the epicenters. The spacing of the masters is too sparse, and most of the events to be located fall outside the 500 km limit verified as acceptable in Chapter D. A considerably longer time period than two weeks is necessary to accumulate a sufficient number of master events.

A break-down of the results is shown in terms of event magnitude and distance from the nearest master in Figure III-10. It suggest that with a denser master spacing the score of locating accurately (now three out of ten) would be better.

A sample output from event two is shown in Table III-9. The beamformer proceeds along the traces forming the coherent power and total power for successive and overlapping segments 2.0 seconds long. For each segment, up to 3721 beams can be formed. The various thresholds were described in Chapter D. Plots of the input data for all events can be found in Appendix A. Though no false alarms from off-region events could be generated, the first side-lobes occasionally passed the coherence thresholds. They had regularly smaller power than the power from correct alignment, and could be excluded on that basis. The position of the side-lobes identified in Table III-8 are plotted in Figure III-11. The array response produces a regular pattern of side-lobes, which in our case typically has a lobe-to-lobe distance of 500 kilometers on the

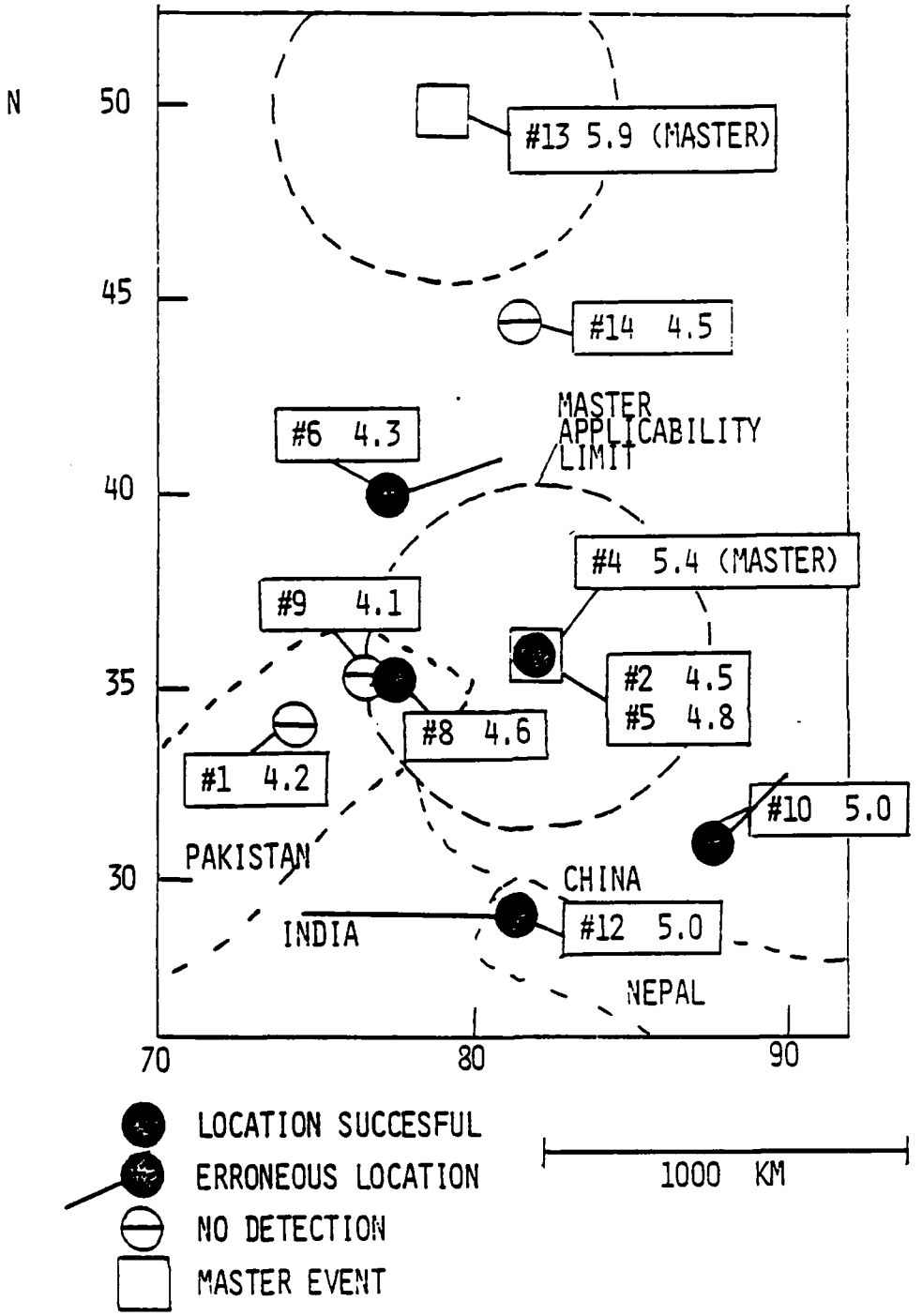

FIGURE III-9

EVENTS USED IN BEAMFORMING EXPERIMENT

TABLE III-7

EVENTS USED IN LOCATING EXPERIMENT

Masters are indicated by 'M'

No.	DATE	TIME	COORDINATES	DEPTH	m_b	REGION
1	80 Oct 05	10 47 18.4	34.650N 74.335E	33	4.2	SW Kashmir
2	80 Oct 06	22 58 59.3	35.670N 82.032E	33	4.5	Tibet
M4	80 Oct 07	09 32 08.5	35.598N 82.073E	33	5.4	Tibet
5	80 Oct 07	09 38 45.8	35.553N 82.005E	33	4.8	Tibet
6	80 Oct 07	22 49 35.4	40.003N 77.716E	33	4.3	Kirgiz-Sinkiang Border
M7	80 Oct 08	05 59 57.1	46.708N 48.215E	OG	5.2	SW Russia
8	80 Oct 08	07 14 41.0	35.181N 77.198E	33	4.6	E Kashmir
9	80 Oct 08	08 04 06.2	35.475N 76.958E	33	4.1	E Kashmir
10	80 Oct 08	16 19 57.6	31.354N 87.666E	33	5.0	Tibet
11	80 Oct 10	11 09 52.1	38.315N 45.770E	33	4.7	NW Iran-USSR Border RE
12	80 Oct 10	14 02 26.7	29.170N 81.208E	33	5.0	Nepal
M13	80 Oct 12	03 34 14.1	49.958N 79.085E	OG	5.9	E Kazakh SSR
14	80 Oct 12	16 03 36.3	44.239N 81.463E	44	4.5	N Sinkiang Prov.

TABLE III-8

RESULTS OF COHERENT BEAMFORMING EXPERIMENT

EVENT	m_B	DISTANCE FROM MASTER (KM)	
1	4.2	713	NO DETECTION
2	4.5	9	LOCATION WITHIN 19 KM FROM N.E.I.S. EPICENTER
5	4.8	8	LOCATION WITHIN 18 KM
6	4.3	621	LOCATION ERROR 313 KM
8	4.6	513	LOCATION WITHIN 45 KM
9	4.1		NO DETECTION
10	5.0	701	LOCATION ERROR 255 KM
11	4.7	954	REJECTED BY COHERENCY MEASURES
12	5.0	717	LOCATION ERROR 645 KM
14	4.5	661	REJECTED BY COHERENCY MEASURES

Events in the enclosed area accurately locatable.

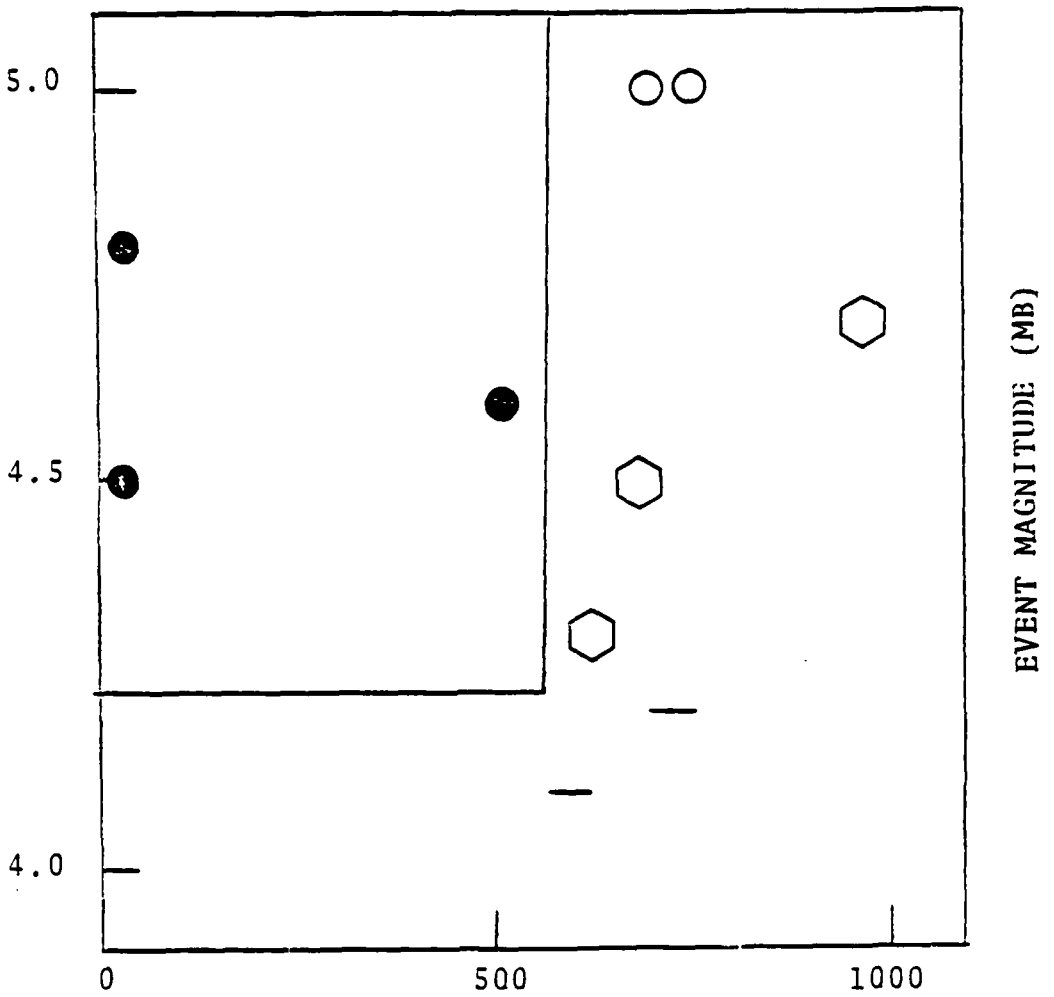

FIGURE III-10

LOCATION AND DETECTION STATISTICS

TABLE III-9

OUTPUT FROM COHERENT POWER-FORMING, EVENT TWO

```
    1      2       3      4      5      6     7      8
  99.10   841    2.51  0.000  0.253    0.2  2.37   2.55
 100.05   677    5.08  0.555  0.249    1.5  2.68   2.74
 100.65   637    5.06  0.374  0.246    2.3  2.68   2.81
 103.85   744    4.84  0.000  0.282    0.4  2.66   2.59
 104.60   703    7.19  0.551  0.254    2.2  2.83   2.80
 105.25   703    7.09  0.460  0.261    2.6  2.82   2.84
 104.50  1399    5.05  0.553  0.247    1.5  2.68   2.74
 101.70  1270    5.74  0.402  0.236    2.4  2.73   2.82
 105.10   150    5.13  0.401  0.283    2.1  2.68   2.80
 105.75   150    5.67  0.441  0.273    2.2  2.73   2.80
 105.05  1329    5.32  0.353  0.247    2.5  2.70   2.84
 105.75  1283    6.74  0.423  0.257    2.7  2.80   2.85
 105.45  1620    5.98  0.462  0.283    2.2  2.75   2.80
 106.10  1579    7.63  0.389  0.258    3.3  2.86   2.90
 106.75  1579    4.98  0.360  0.253    2.3  2.67   2.82
- ?

 106.90  1679    5.25  0.062  0.211   14.2  2.69   3.37
 107.55  1065    8.46  0.141  0.215   10.0  2.90   3.24
 108.20  1024    8.94  0.129  0.212   11.6  2.92   3.29
 108.85  1064    6.92  0.118  0.212    9.8  2.81   3.23
 110.50   852    7.71  0.136  0.212    9.5  2.86   3.22
 111.05  1092    7.36  0.141  0.212    8.8  2.84   3.19
 111.70  1092    6.74  0.097  0.206   11.6  2.80   3.29
 112.70  1534    7.74  0.107  0.209   12.1  2.86   3.31
 119.50     2   10.05> 0.469  0.341    3.6  2.98   2.92
 120.15     2   14.90> 0.329  0.285    7.6  3.15   3.15
 119.50   658   19.40> 0.287  0.255   11.3  3.26   3.28
 120.05   699   25.70> 0.386  0.294   11.1  3.38   3.28
 120.70   699   20.36  0.362  0.421    9.4  3.28   3.22
 122.45   329   11.45  0.278  0.887    6.8  3.03   3.11
 121.50  1826   14.58  0.593  0.815    4.1  3.14   2.96
 119.95  1400   17.22  0.600  0.783    4.8  3.21   3.00

DETECTION
[ 1 ] 35.60 N   82.87 E ( 126.10 109.90 119.25 143.45 119.30 s)
  119.25   841   35.18> 1.084 0.872    5.4  3.52   3.04

  SIDE LOBE :
[ 2 ] 32.00 N   86.87 E ( 126.10 109.85 120.65 143.30 117.55 s)
  120.65   464   26.78  0.791 0.945    5.7  3.40   3.05

DETECTION
[ 1 ] 35.60 N   82.87 E ( 126.75 110.55 119.90 144.10 119.95 s)
  119.90   841   46.67> 1.041 0.956    7.5  3.64   3.14

  SIDE LOBE :
[ 3 ] 32.00 N   86.87 E ( 126.75 110.50 121.30 143.95 118.20 s)
  121.30   464   42.32  0.888 0.969    8.0  3.60   3.16

  SIDE LOBE :
[ 5 ] 31.60 N   77.87 E ( 126.75 111.95 119.75 142.85 121.50 s)
  119.75   441   27.15  0.764 0.804    5.9  3.41   3.07

  SIDE LOBE :
[ 6 ] 30.80 N   77.87 E ( 126.75 112.05 119.90 142.70 121.45 s)
  119.90   359   25.24  0.751 0.798    5.6  3.38   3.05
- ?
```

TABLE III-9
(Continuation)

The columns:

1. Time (seconds).
2. Index of the beam having largest coherent power.
3. The largest coherent power (Z-statistic) threshold 10.
4. Signal coherence (r') on the list beam, threshold 0.75.
5. Power semblance on the listed beam, threshold 0.75.
6. Total power on the listed beam (Z-statistic), threshold 1.
7. Logarithm of absolute coherent power on the listed beam.
8. Logarithm of absolute total power on the listed beam.

For each detection and side-lobe the coordinates of the beam target and the arrival times on channels are listed.

target region. The coherence measures excluded most of the side-lobes, passing only two (three-four and five-six in the Figure) situated north of the event.

The side-lobe pattern of coherent energy from event five at the time of arrival of signal is plotted three-dimensionally to Figure III-12. X and Y coordinates are the geographical position of the beam target point, and the vertical coordinate is the beam coherent power. A similar plot was done for the total input power observed on the beams at the time of signal arrival. It is shown in Figure III-13. It is essentially the quantity on which incoherent beamforming is based.

An essential part of coherent beamforming of an regional-size array is to accurately determine relative station time corrections to align the P-wave signals. These time corrections were determined for the source region of this experiment, in Central Asia, utilizing large master events. Since extensive regions of the earth's surface will have to be calibrated, the optimum spacing of the master events is of vital interest. Also, in regions of only moderate seismicity, masters are sparse and the time corrections may have to be interpolated. Other investigators have published estimates on how accurately station time residuals measured from one event can predict the station residuals of another event. The time prediction error S was defined in Section III - E. We made measurements of S from earthquakes in Central Asia. We observed that when event-to-event distance is less than 1000 km the maximum prediction errors was in all cases less than 0.5 seconds. For a distance less than 550 km (five degrees) we can with reasonable confidence state that the prediction errors do not exceed 0.5 seconds. We conclude that a spacing of master events of seven degrees is sufficient. Our r.m.s. S-values are approximately similar to those measured by Engdahl (1977) who observed Fiji-Tonga earthquakes using Alaskan stations. This lends further credence to our results. We also verified a consistent station amplitude pattern for events from our selected source region. This makes possible signal amplitude equalization before beamforming which improves detection and location of small events. Amplitude equalizing also allows us to measure how closely the relative power levels among channels agree with the predicted power levels. when a detection is declared by a rise in coherent power. This statistic (power semblance), mentioned above, helps to eliminate false alarms.

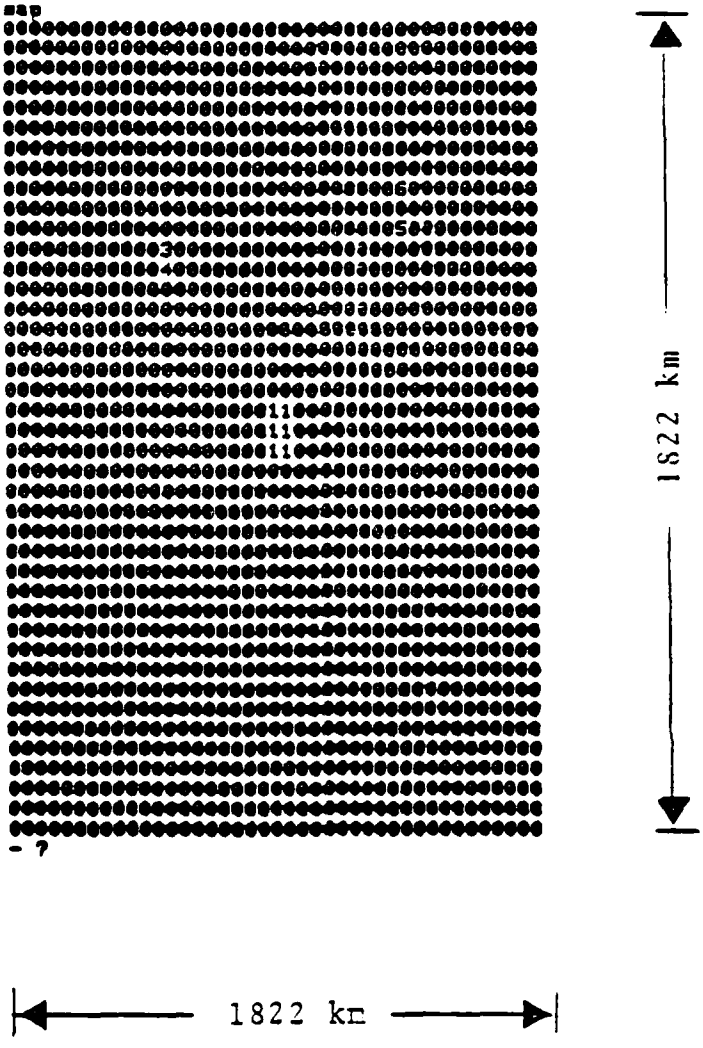

FIGURE III-11

THE PATTERN OF COHERENT SIDE-LOBES (3 TO 6)

AND CORRECT ALIGNMENT (1)

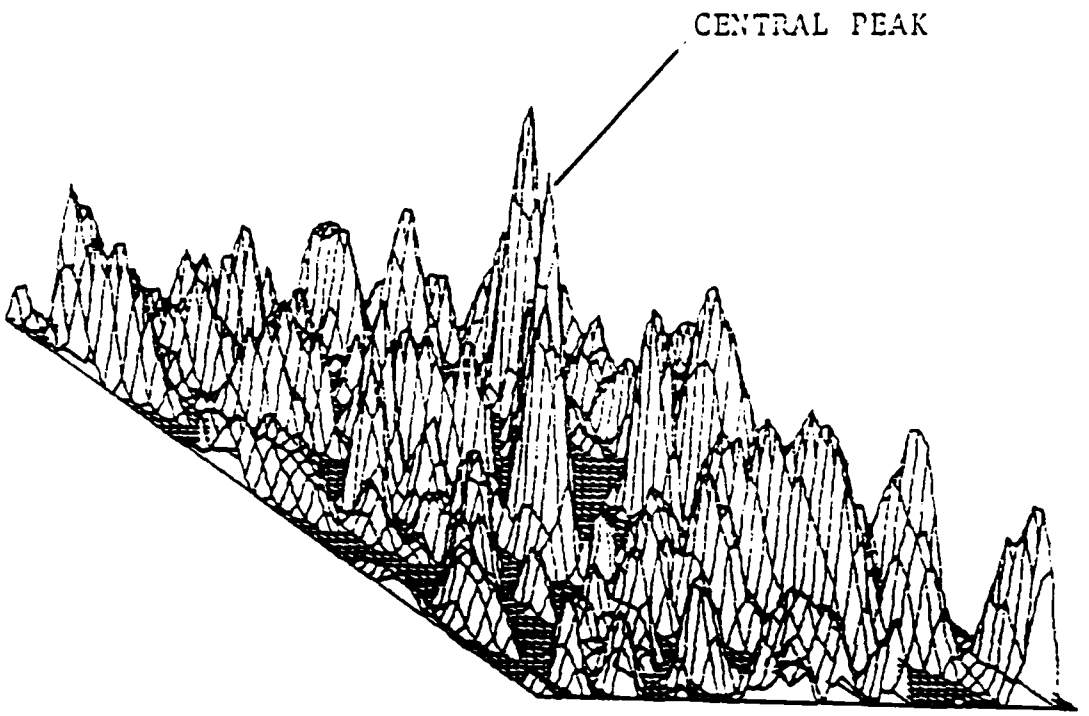

The pattern of coherent power on 61 x 61 beams at the time of arrival of P-wave from event 5. The multitude of side-lobes visible here were excluded by the coherence measures. The area covered is a square with side 2700 km. The epicenter is in the center of the area.

FIGURE III-12
THREE-DIMENSIONAL PLOT OF COHERENT POWER

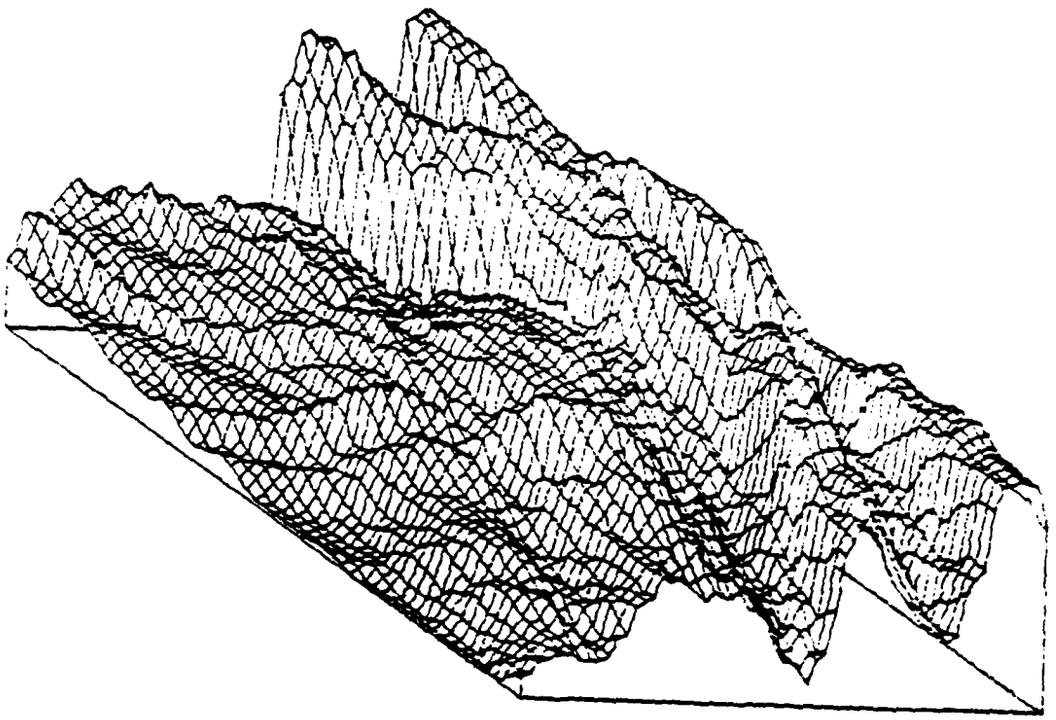

The pattern on total input power on 61 x 61 beams covering a square target area with side 2700 km, at the time of arrival of signal from event five. The epicenter is in the center of the plot. Note erratic maxima and low resolution.

FIGURE III-13
THREE-DIMENSIONAL PLOT OF TOTAL POWER

G. CONCLUSIONS OF THE SECTION

We have found several conditions which have to be true for coherent beamforming of station networks when used to locate teleseismic events, relative to master events:

- The correlation of signal waveforms between stations decrease with increasing station separation, falling to zero (in average) of separations larger than 20 degrees. This observation is dependent on region, but suggests that network apertures should be less than 20 degrees.

- The distance between the master event and the true epicenter of the event to be located must be less than 500 km for accurate location, using a station network with aperture 100 km. The distance limit is probably dependent on the tectonic setting of the station network, which in our case was in Alaska.

In addition to the usual choices of no detection, detection and false alarm, we have in case of monitoring a source region also the choice of mislocated detection (i.e. our detection corresponds to a true event which occurred outside the monitored region). We attempted first to improve the detection capability (without increasing the false alarm rate) beyond that provided by delay-and-sum beamforming and frequency filtering. The problem of mislocated detections was given less attention. We observed that improvements in detectability could be achieved by adaptive beamforming combined with band-pass filtering. Improvement could also be done by computing the semblance of the input traces and use it as gain control of the output beams. These improvements are not offset by a rise in false alarm rate. The main conclusions are summarized below.

- Even in case of noise which is uncorrelated among the input channels, adaptive beamforming combined with band-pass filtering provides a better detectability of weak signals than conventional beamforming. The amount of improvement was about 1.5 to 6 dB (the amplitude ratio of signal to the largest noise amplitude observed on a 30 seconds long section of noise.) Measuring the improvement by Z-statistics, we observed in one experiment no improvement, in another case an improvement equal to 1.4 standard deviations (σ) of noise.

- The improvement mentioned above stems from the whitening of noise by the adaptive multichannel filter. Levin's constraint on the multichannel filter does not allow the spectrum of a

signal arriving from the look-direction to be whitened. Signal-to-noise ratio is thus improved in certain frequency bands. Significantly, we did not observe an improvement in detectability using adaptive beamformer without band-pass filtering. Pre-filtering the input traces seemed to give better detectabilities than post-filtering of output beams. It worsens the location capability, however, and can not be used.

- Multiplication of the output beams with the semblance of the input traces improved signal detectability (signal/maximum noise amplitude) by 2 to 8 dB. Improvement (-0.3 to 0.8 σ) was largest when no filtering was done. The improvement is at least partly additive to the improvement obtained by the adaptive beamformer. Combinations of the two procedures gave 3 to 9 dB (-0.3 to 1.6 σ).

- Computation of coherent power (beam power minus input power) seems to give at least as large improvement of Z-statistic over conventional beamforming as the above methods. In one example, the Z-value of 44.1 σ (barely detectable) was improved to 5.7 σ (well detectable).

After making a detection, there is still uncertainty on whether the event is situated on the target region covered with beams. Use of coherent power instead of beam power tends to suppress randomly aligned signal energy, but it is still necessary to use criteria to suppress detections from off-region events. For that purpose, we use the ratio of coherent input power to total input power and another criteria measuring the relative power levels of input channels.

- By using suitable input coherence criteria, we developed procedures to remove false alarms which cause erroneous locations and occur due to a chance alignment of peaks and troughs of the record. We have now reached a point where even large off-region events virtually never trigger a false location due to a chance alignment.

- The results suggest that events within about five degrees from a master event can be located to within 45 km from the epicenter reported by N.E.I.S. Using conventional Joint Epicenter location, where the onsets are timed separately, such an accuracy can be achieved only at very high signal-to-noise ratios. Simulation showed that coherent beamforming can achieve this accuracy down to the level where signals are undetectable on individual channels. Due to the sparsity of the master events this could not be demonstrated with an actual example.

SECTION IV
REFERENCES

Berteussen K. A., A. Christoffersson, E. S. Husebye and S. Dahle, Wave Scattering Theory in Analysis of P-Wave Anomalies at NORSAR and LASA, Geophys. J. R. Astr. Soc. (1975) 42, pp. 403-417.

Der, Z. A. and T. W. McElfresh: The Relationship Between Anelastic Attenuation and Regional Amplitude Anomalies of Short-Period P Waves in North America., Bull. Seism. Soc. Am., Vol. 67, No. 5, pp. 1303-1317, October 1977.

Dewey J. W., Seismicity and Tectonics of Western Venezuela, Bull. Seism. Soc. Am., Vol 62, No. 6, pp. 1711-1751, December 1972.

Engdahl E. R., JGR, Interpretation of Relative Teleseismic P Wave Residuals, Vol 82, No. 36, pp. 5671-5682.

Frost O. L., IEEE, An Algorithm for Linearly Constrained Adaptive Array Processing, Vol. 60, No. 8, August 1972.

Neidell N. S. and M. T. Taner, Semblance and Other Coherency Measures for Multichannel Data, Geophysics, Vol. 36, No. 3, pp. 482-497, June 1971.

Noponen, I., Bull. Seism. Soc. Am., Seismic ray Direction Anomalies Caused by Deep Structure in Fennoscandia, Vol 64, No. 6, pp. 1931-1941, December 1974.

Noponen, I., Jour. of Physics of the Earth, Use of Particle Motion in Detecting and Identifying Crustal Phases from Near Events, Vol 16, No. 2, 1968.

Sax, R. L., and Staff, Event Identification-Application to Area of Interest Events, TR No. 20, ALEX(01)-TR-78-08, 13 November 78.

Shen W., Geophysics, A Constrained Minimum Power Adaptive Beamformer with Time-Varying Adaptation Rate, Vol. 44, No. 6, pp. 1088-1096, 6 June 1979.

Sutton G. H., Short Period Seismic Energy Radiation Patterns From Underground Nuclear Explosions and Small Magnitude Earthquakes, Bull. Seism. Soc. Am., Vol. 57, No. 2, pp. 249-267, April, 1967.

Swindell W. H. and Snell N. S., Station Processor Automatic Signal Detection System, Phase I: Final Report, ALEX(01)-FR-77-01, 15 March 1977, Texas Instruments.

Unger R., Automatic Detection, Timing and Preliminary Discrimination of Seismic Signals with the Instantaneous Amplitude, Phase and Frequency, ALEX(01)-TR-77-04, 27 March 1978, Texas Instruments.

APPENDIX A

The input and a part of the output of the beamforming experiments described in Section III, Chapter C are collected in this Appendix (Experiments I to VII). Signal and noise have been mixed with various noise amplifications, and band-pass filters have been applied. In each figure, the stations from top are in the order DR-CO, KM-CL, KN-UT, LC-NM and MN-NV. The signals are from the Kuriles Input data to coherent power-forming experiments described in Section III, Chapter F are also shown in the Appendix (Events 1 to 11).

EXPERIMENT I

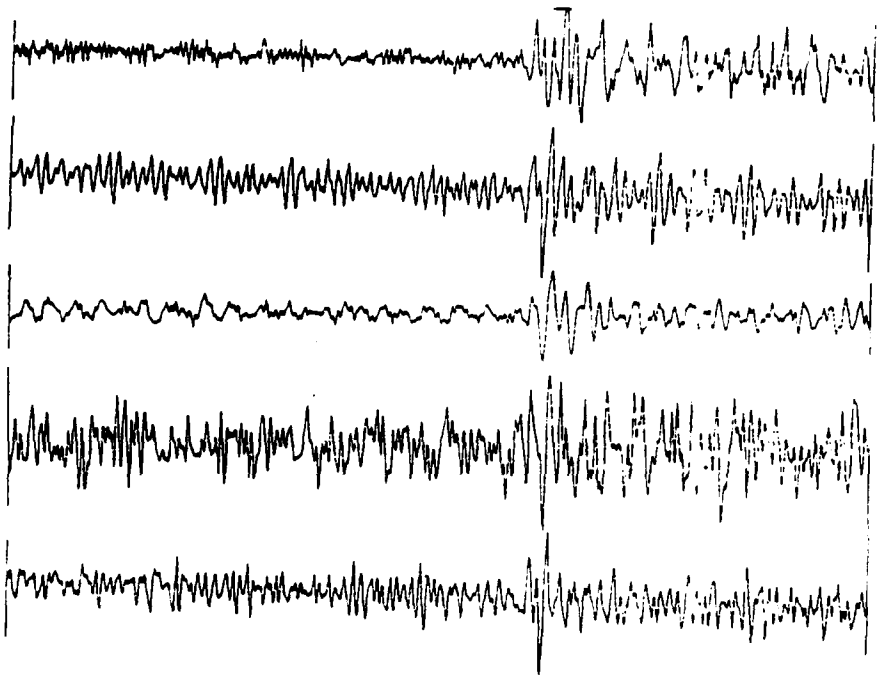

EXPERIMENT II

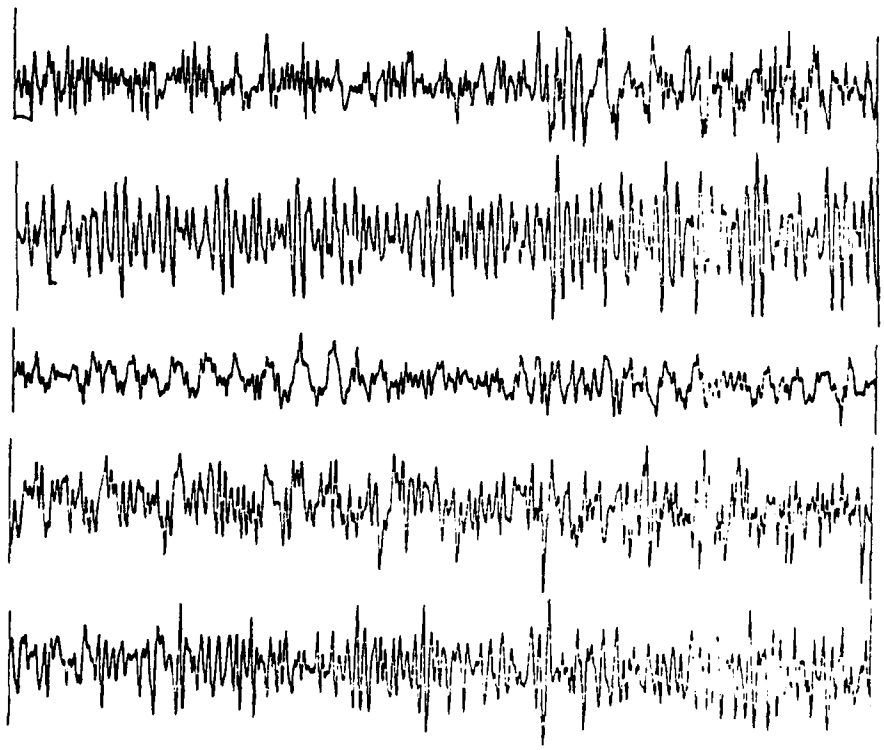

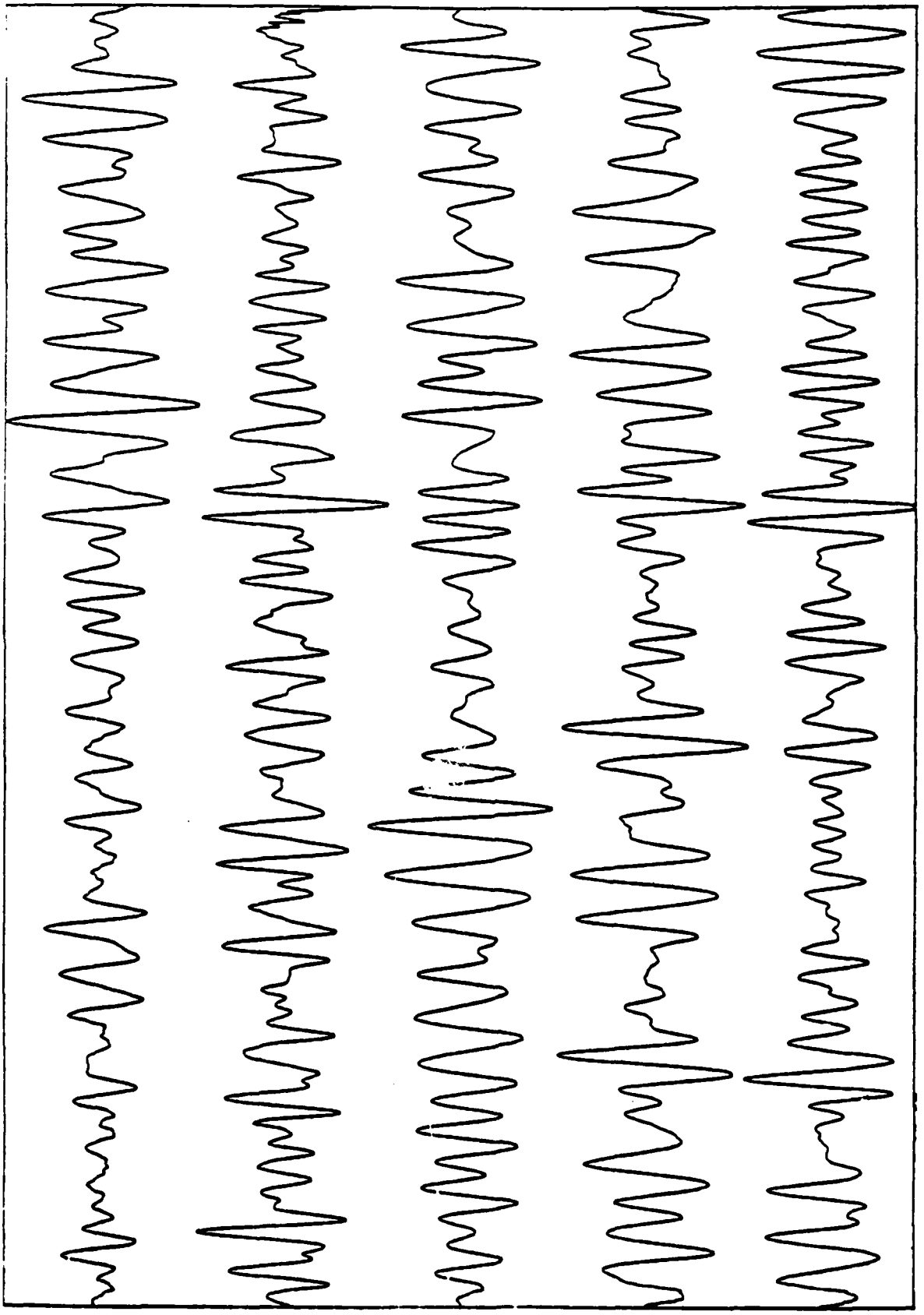

EXPERIMENT III

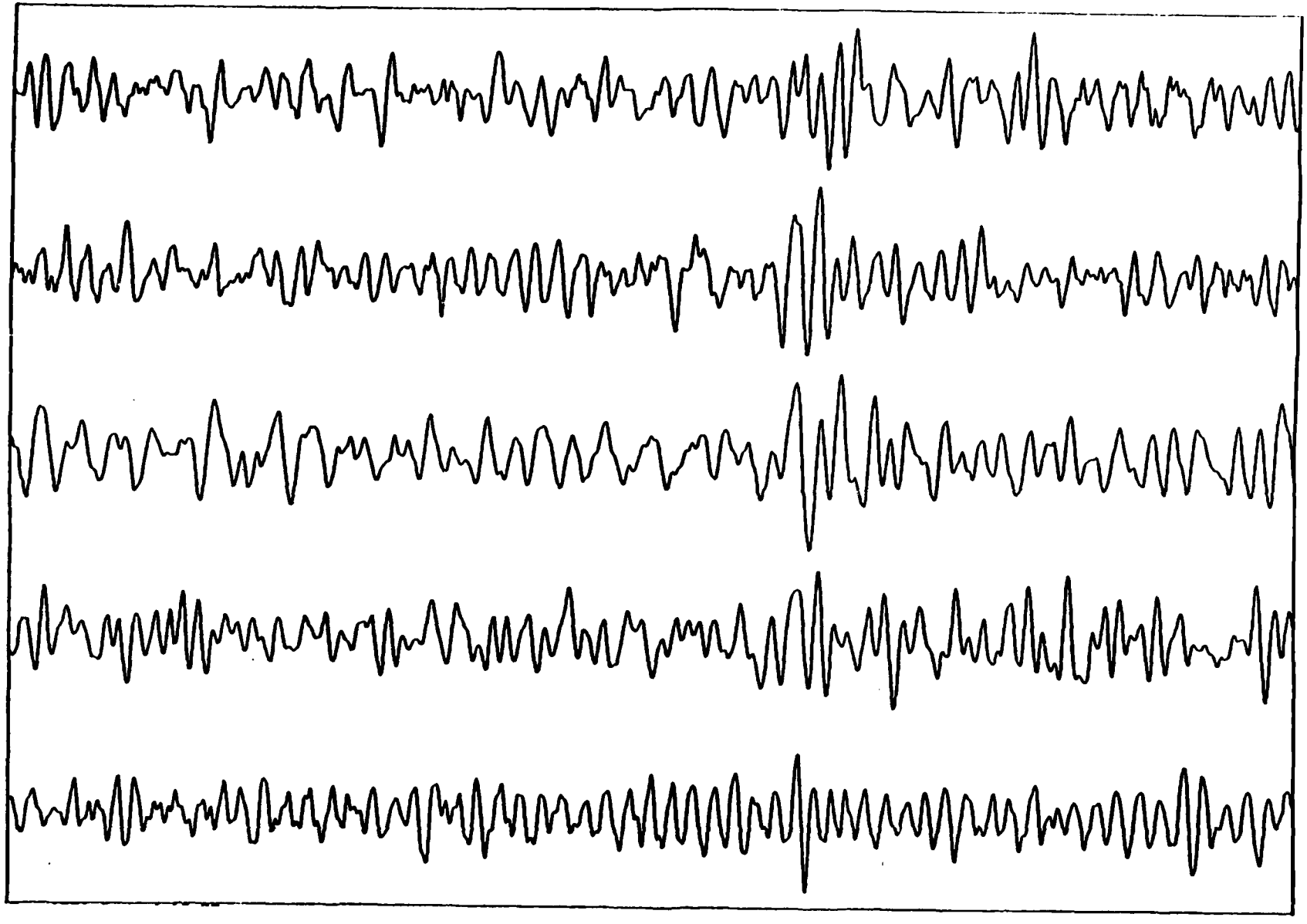

EXPERIMENT IV (a)

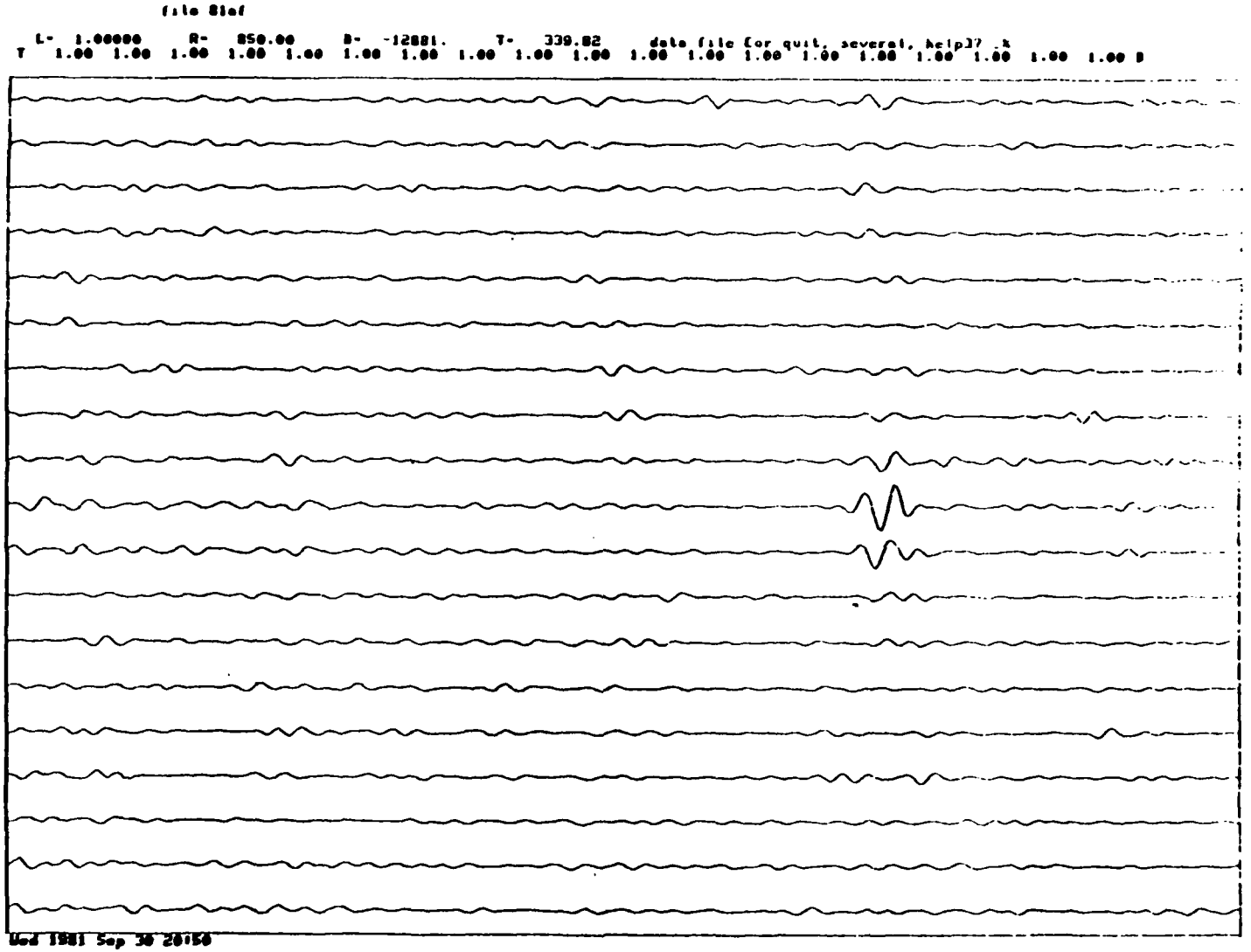

EXPERIMENT IV

ABF X CONVENTIONAL $\mu = 2.0$ FILTERED. (OUTPUT)

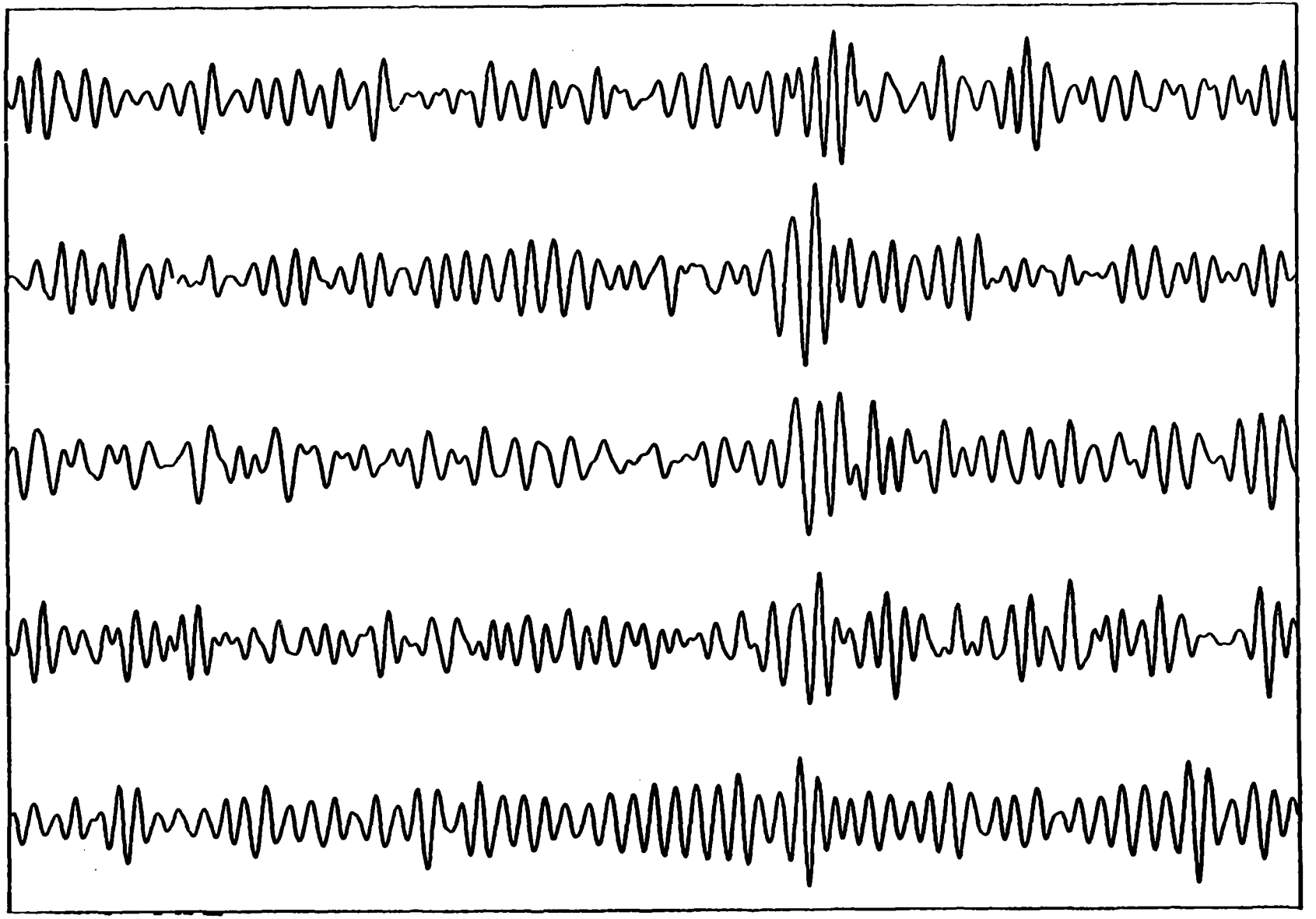

EXPERIMENT V

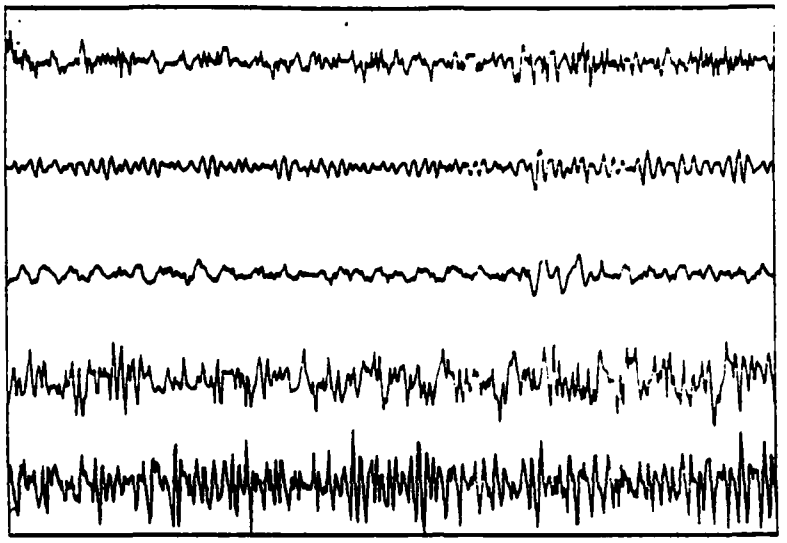

EXPERIMENT VI

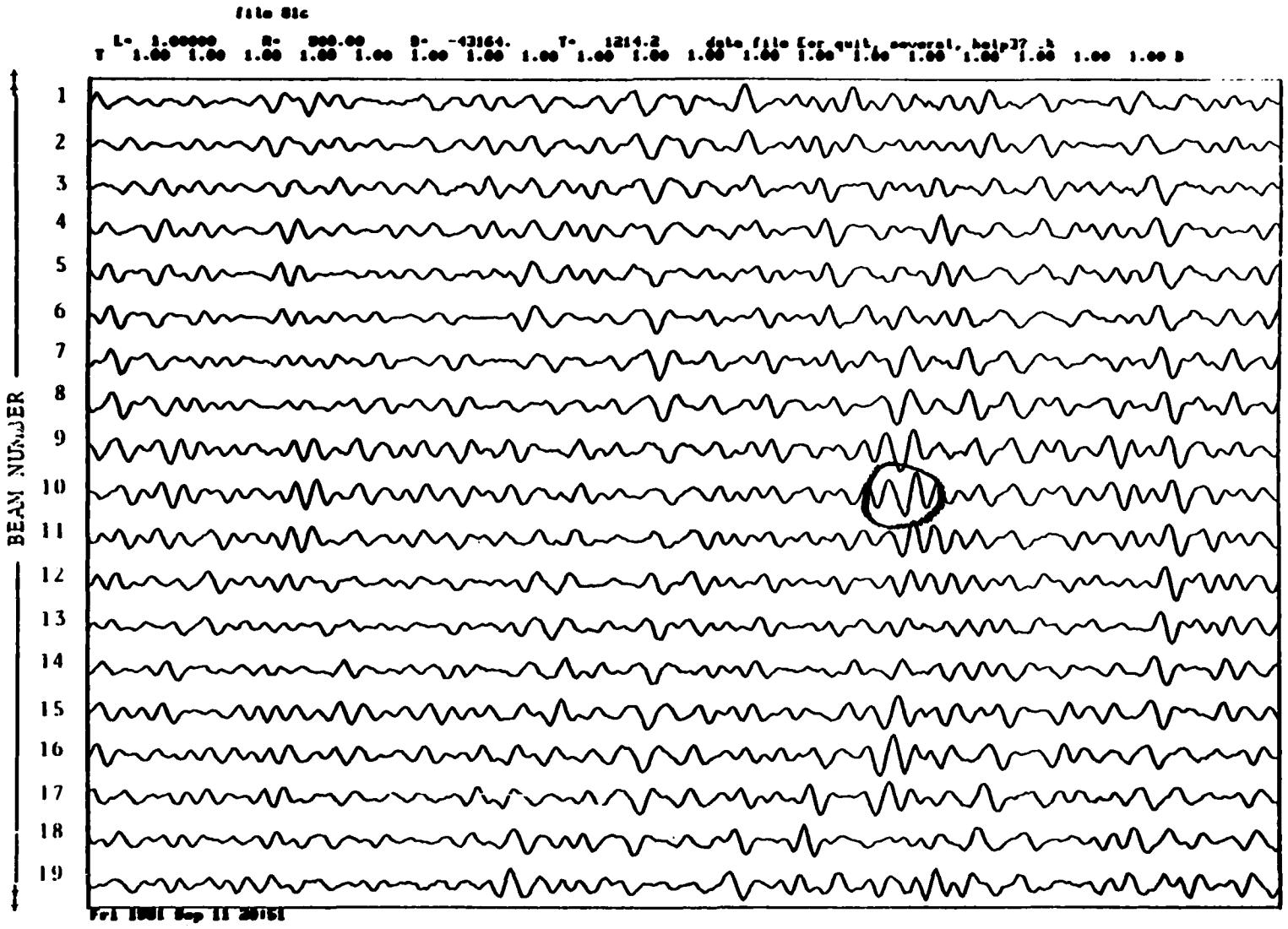

FILTERED CONVENTIONAL BEAMS

OUTPUT a

EXPERIMENT VI

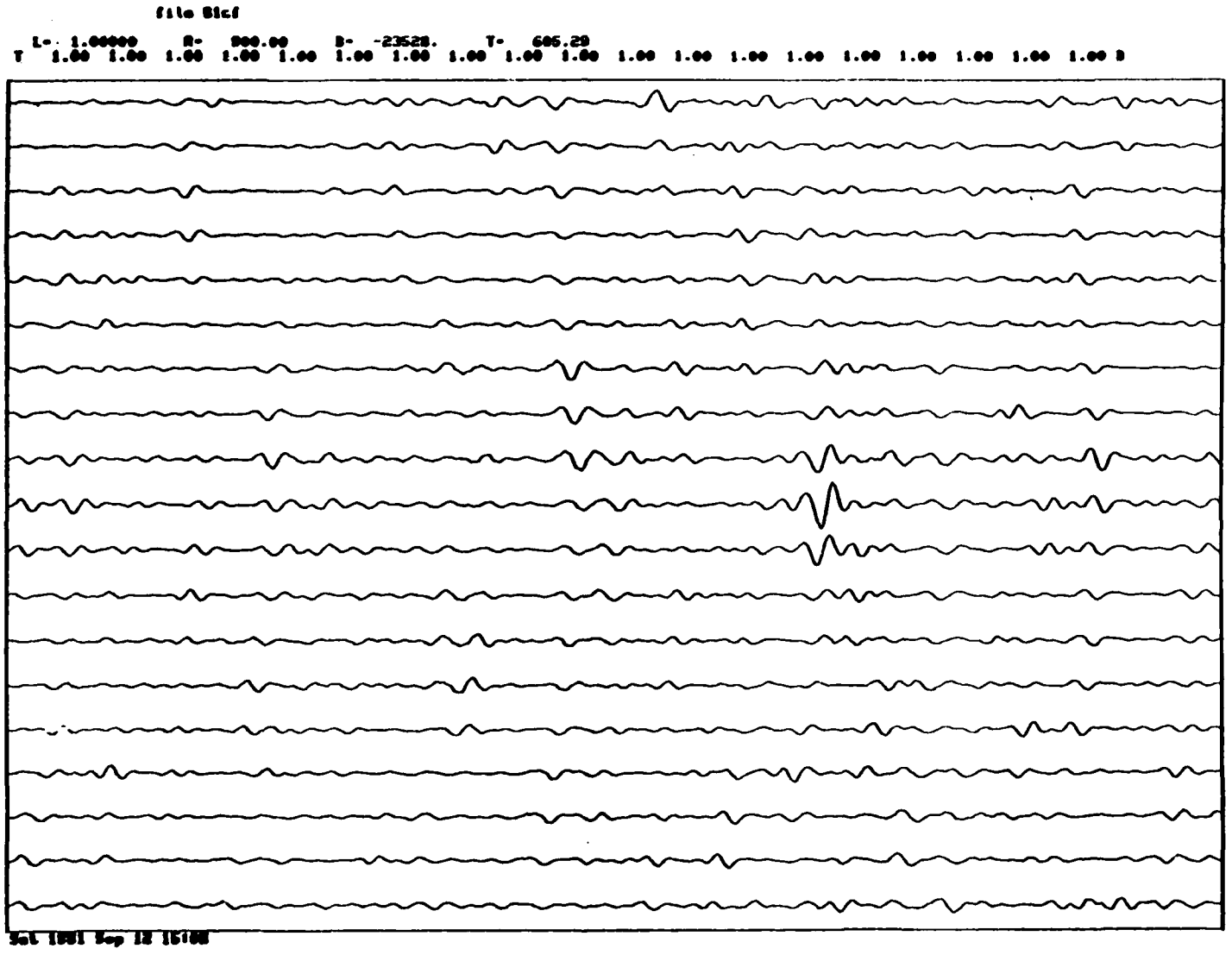

EXPERIMENT VI

SEMBLANCE BEAM BAND PASS FILTERED. (OUTPUT)

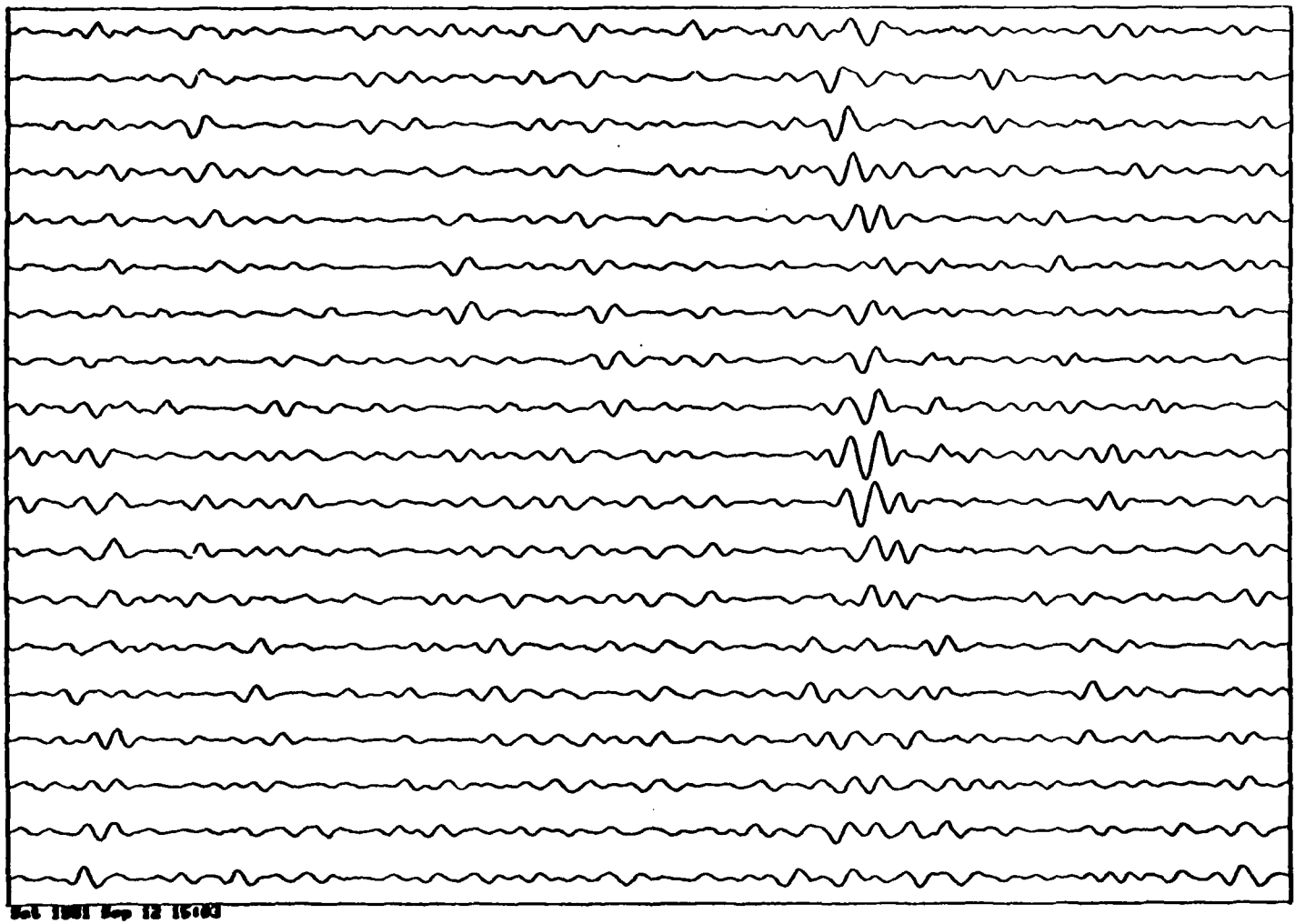

(Output c). Adapt output bp filtered, μ_2 0.6.

EXPERIMENT VI

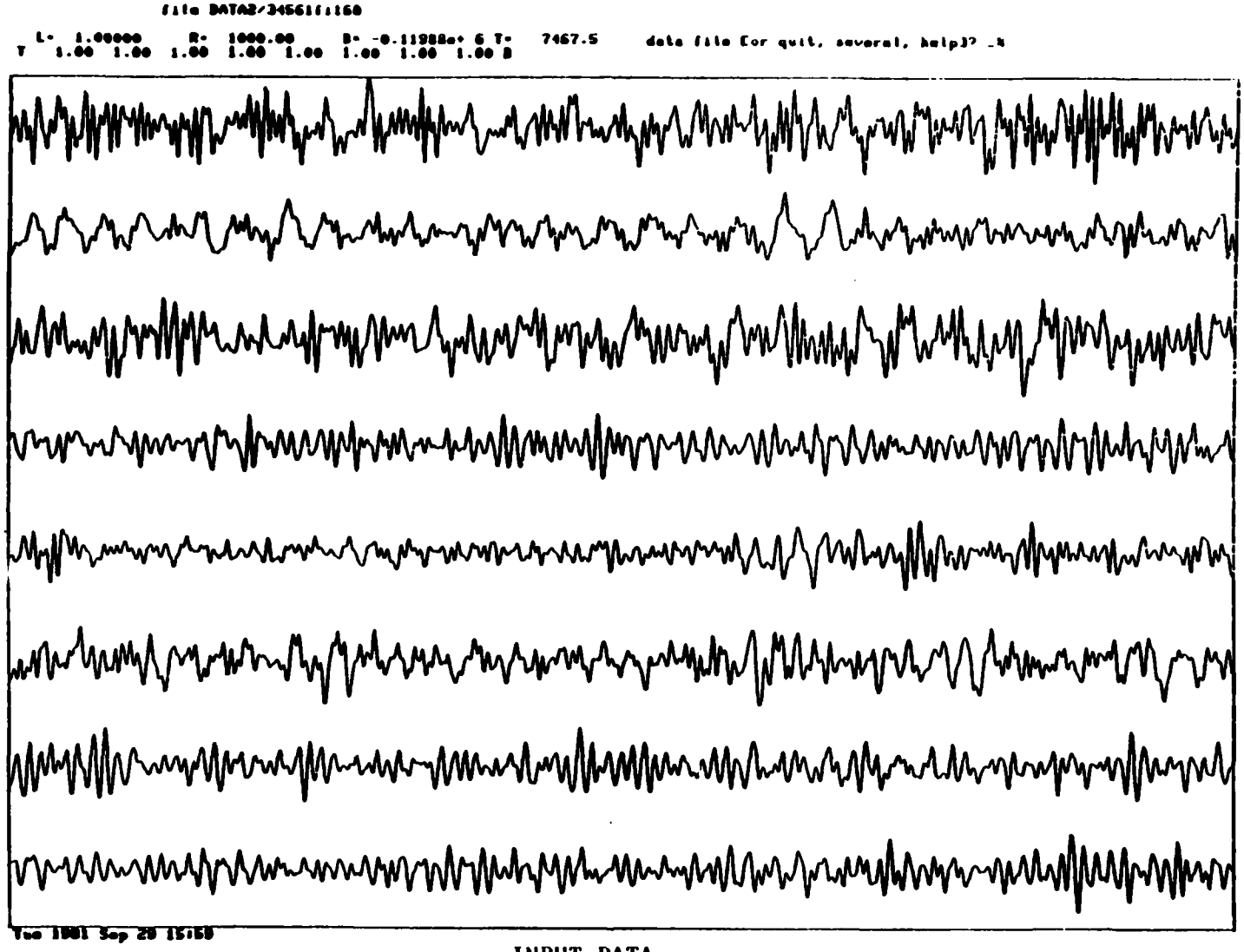

INPUT DATA
EXPERIMENT VII

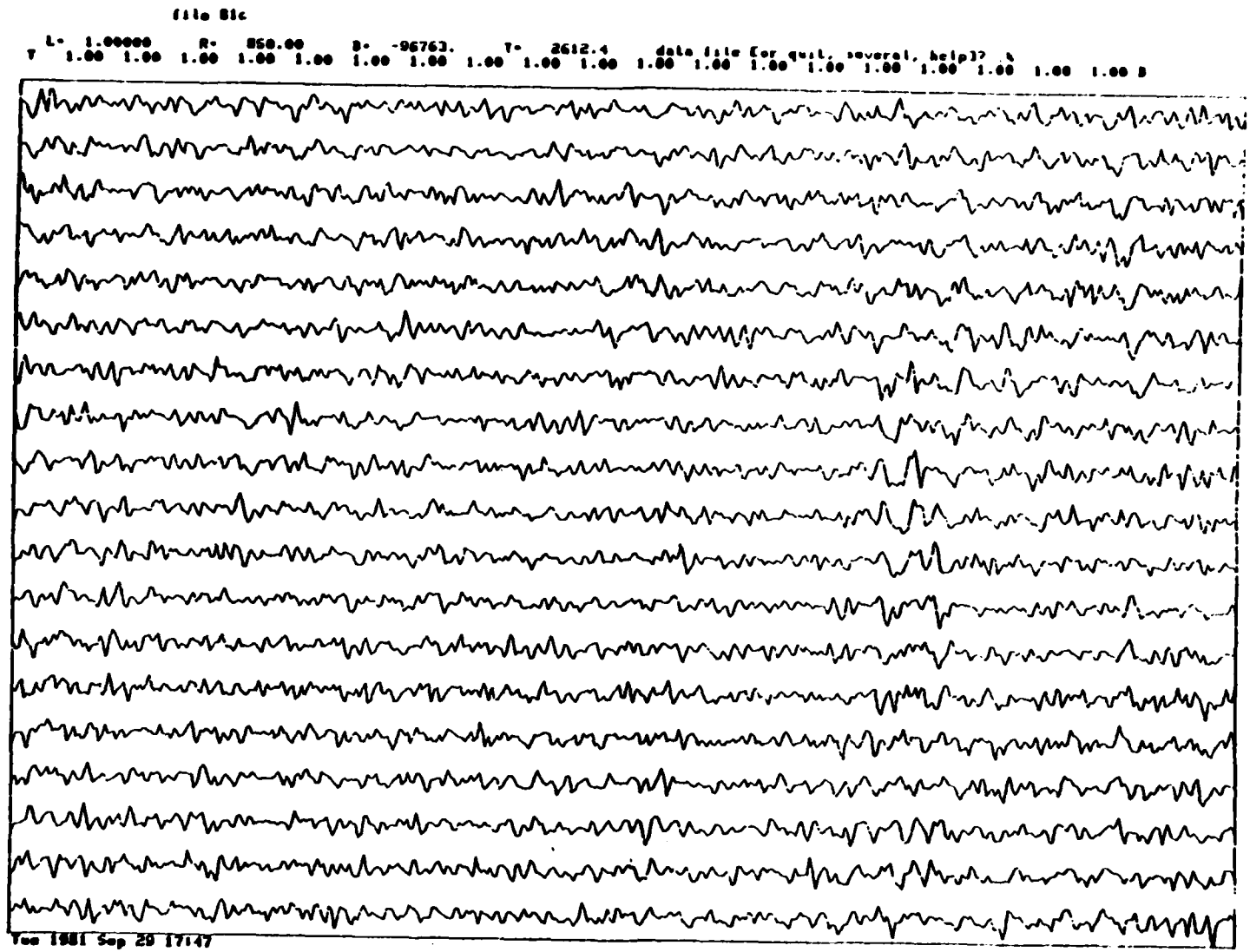

CONVENTIONAL BEAMS
OUTPUT
EXPERIMENT VII

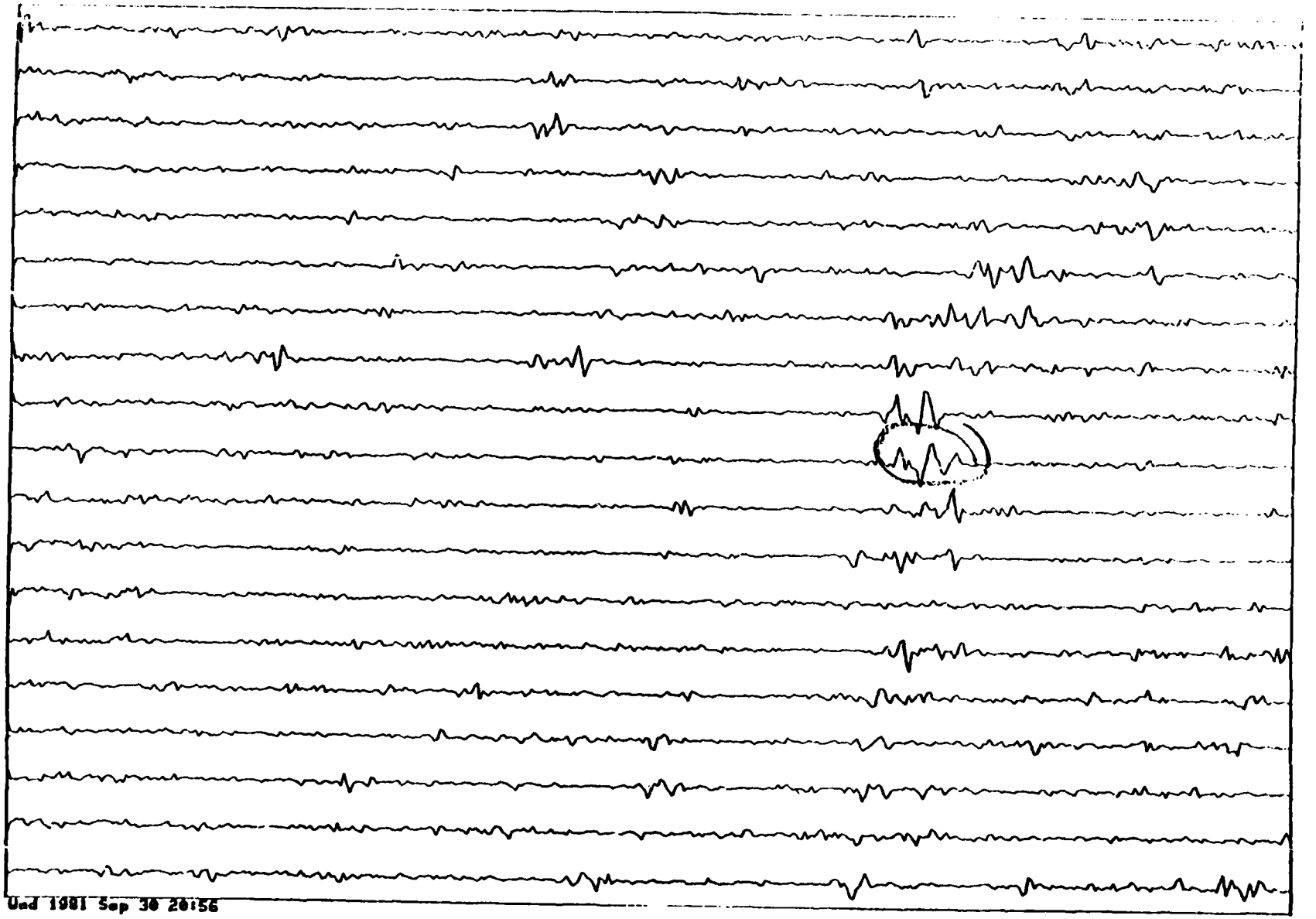

EXPERIMENT VII

OUTPUT DATA: ADAPTIVE BEAMS MULTIPLIED WITH SEMBLANCE

```
21    279001.co1 L=   2000 R=   3499 B= -0.425E+01 T=  0.355E+01
22    279001.co2 L=   2000 R=   3499 B= -0.165E+01 T=  0.163E+01
23    279001.co3 L=   2000 R=   3498 B= -0.682E+00 T=  0.921E+00
24    279001.co4 L=   2000 R=   3499 B= -0.264E+02 T=  0.208E+02
25    279001.co5 L=   2000 R=   3498 B= -0.453E+01 T=  0.343E+01

THE SAMPLE RATE IS  20.0 POINTS PER SECOND
```

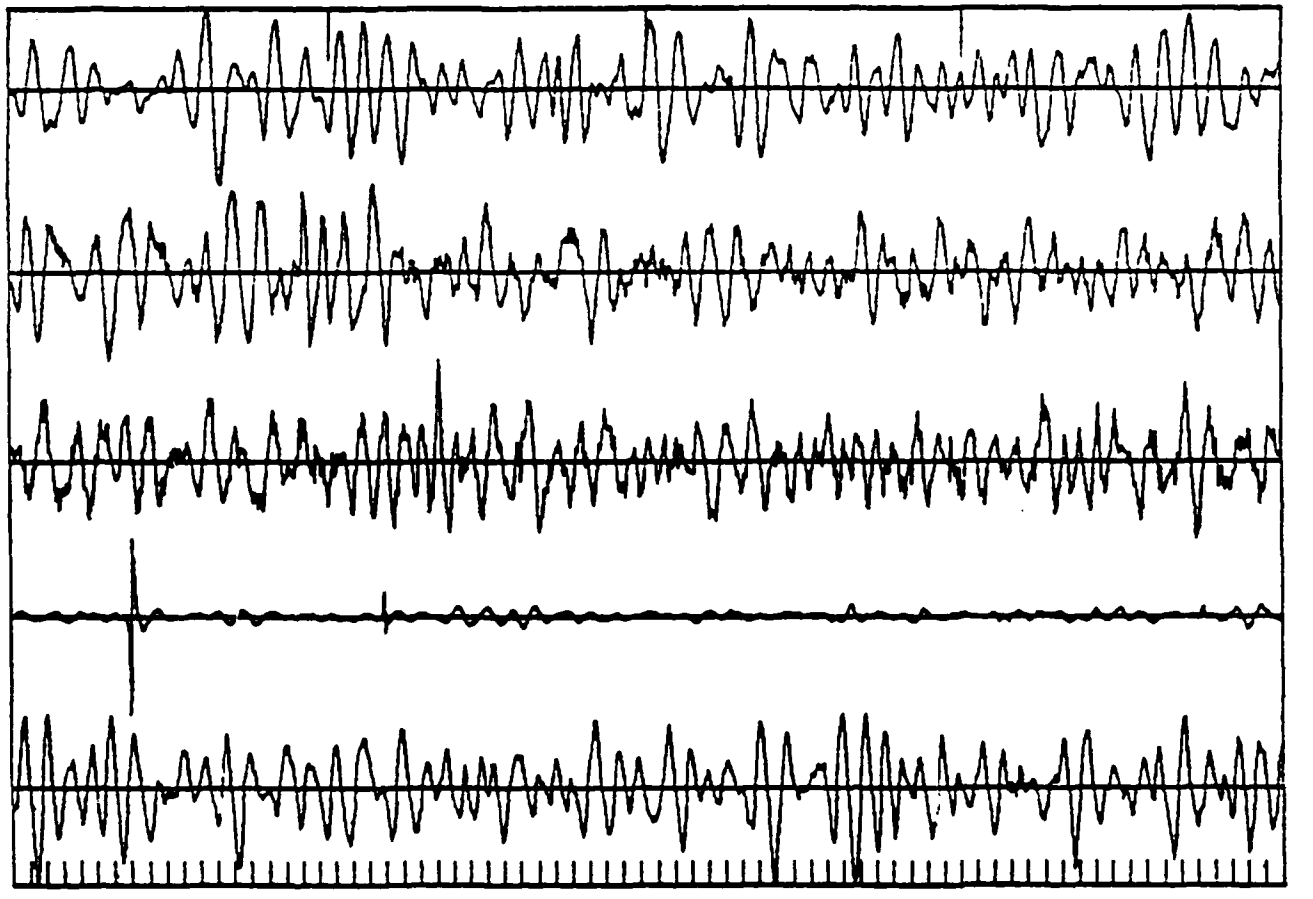


```
FORTRAN STOP
$

25-NOV-81     11:24:19
```

EVENT 1

```
21    280401.co1 L=   2000 R=   3499 B= -0.870E+01 T=  0.959E+01
22    280401.co2 L=   2000 R=   3499 B= -0.546E+01 T=  0.355E+01
23    280401.co3 L=   2000 R=   3499 B= -0.228E+01 T=  0.245E+01
24    280401.co4 L=   2000 R=   3499 B= -0.643E+01 T=  0.565E+01
25    280401.co5 L=   2000 R=   3499 B= -0.698E+01 T=  0.712E+01
```

THE SAMPLE RATE IS 20.0 POINTS PER SECOND

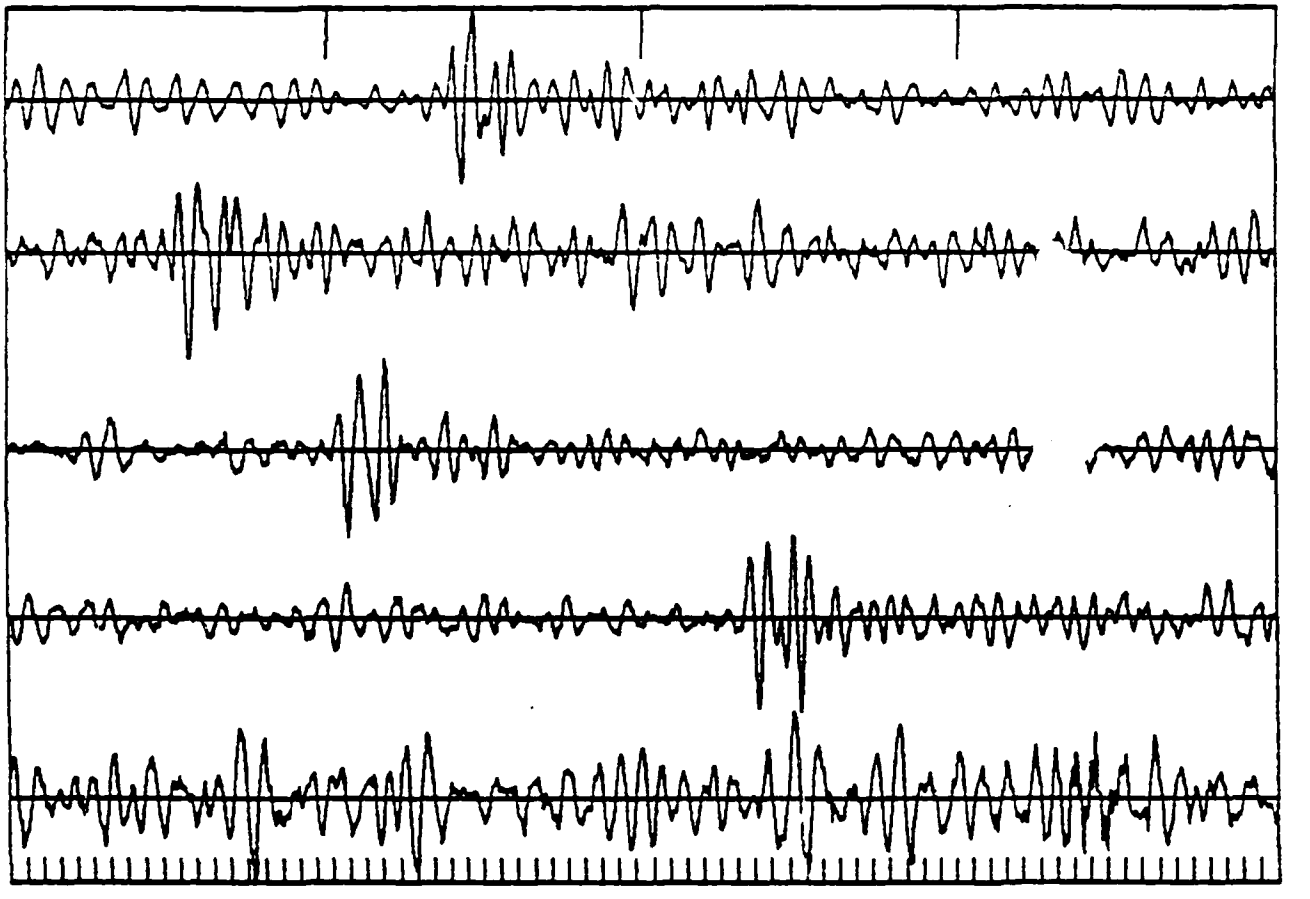

FORTRAN STOP

25-NOV-81 11:39:54

EVENT 2

```
21    281003.co1 L=   1500 R=   3499 B= -0.985E+01 T=  0.103E+02
22    281003.co2 L=   1500 R=   3499 B= -0.551E+01 T=  0.385E+01
23    281003.co3 L=   1500 R=   3499 B= -0.239E+01 T=  0.219E+01
24    281003.co4 L=   1500 R=   3499 B= -0.728E+01 T=  0.539E+01
25    281003.co5 L=   1500 R=   3499 B= -0.557E+01 T=  0.523E+01

THE SAMPLE RATE IS  20.0 POINTS PER SECOND
```

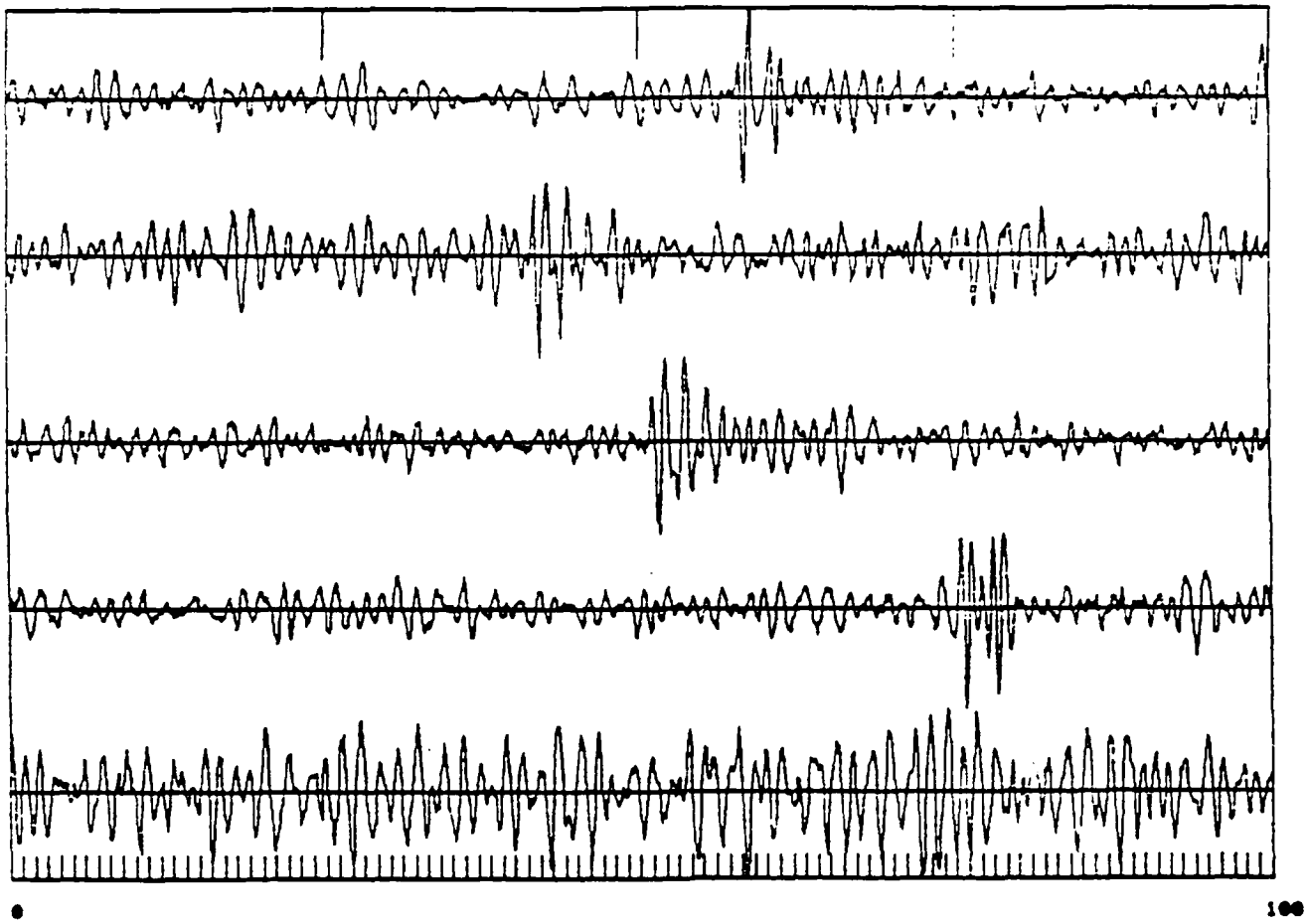


```
FORTRAN STOP
$

25-NOV-81     13:20:05
```

EVENT 5

21	281004.co1	L=	1500	R=	3499	B=	-0.359E+01	T= 0.369E+01
22	281004.co2	L=	1500	R=	3499	B=	-0.259E+01	T= 0.233E+01
23	281004.co3	L=	1500	R=	3499	B=	-0.823E+00	T= 0.827E+00
24	281004.co4	L=	1500	R=	3499	B=	-0.788E+02	T= 0.126E+03
25	281004.co5	L=	1500	R=	3499	B=	-0.458E+01	T= 0.556E+01

THE SAMPLE RATE IS 20.0 POINTS PER SECOND

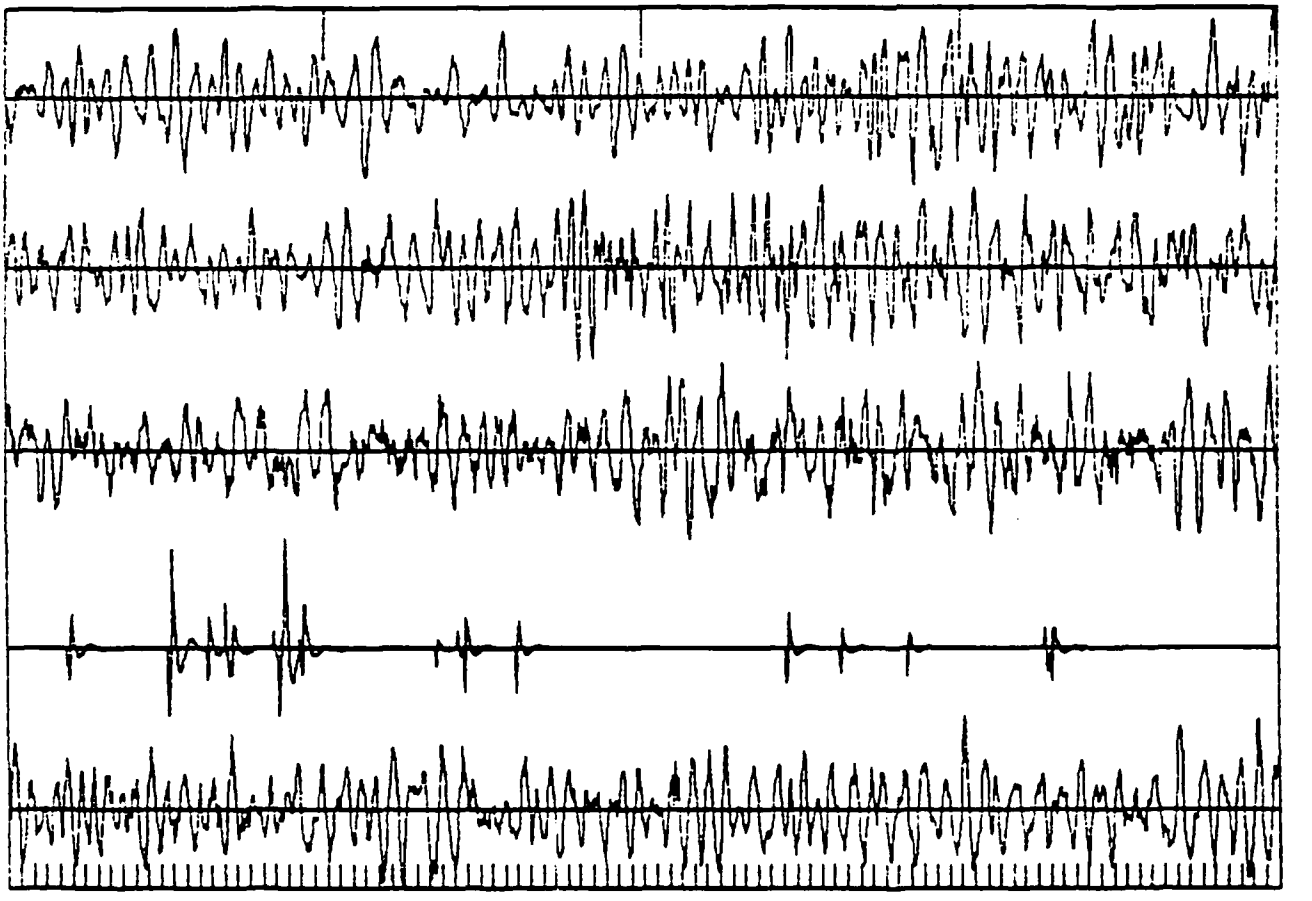

FORTRAN STOP
$

25-NOV-81 17:49:14

EVENT 6

```
22    282002.co1 L=   2000 R=   3499 B= -0.114E+02 T=  0.195E+02
23    282002.co2 L=   2000 R=   3499 B= -0.884E+01 T=  0.182E+02
24    282002.co3 L=   2000 R=   3499 B= -0.305E+01 T=  0.330E+01
25    282002.co4 L=   2000 R=   3499 B= -0.6  7+01 T=  0.489E+01
26    282002.co5 L=   2000 R=   3499 B= -0.62 E+01 T=  0.817E+01
```

DO YOU WISH TO PLOT EXISTING DATA AGAIN (Y/N) ?

THE SAMPLE RATE IS 20.0 POINTS PER SECOND

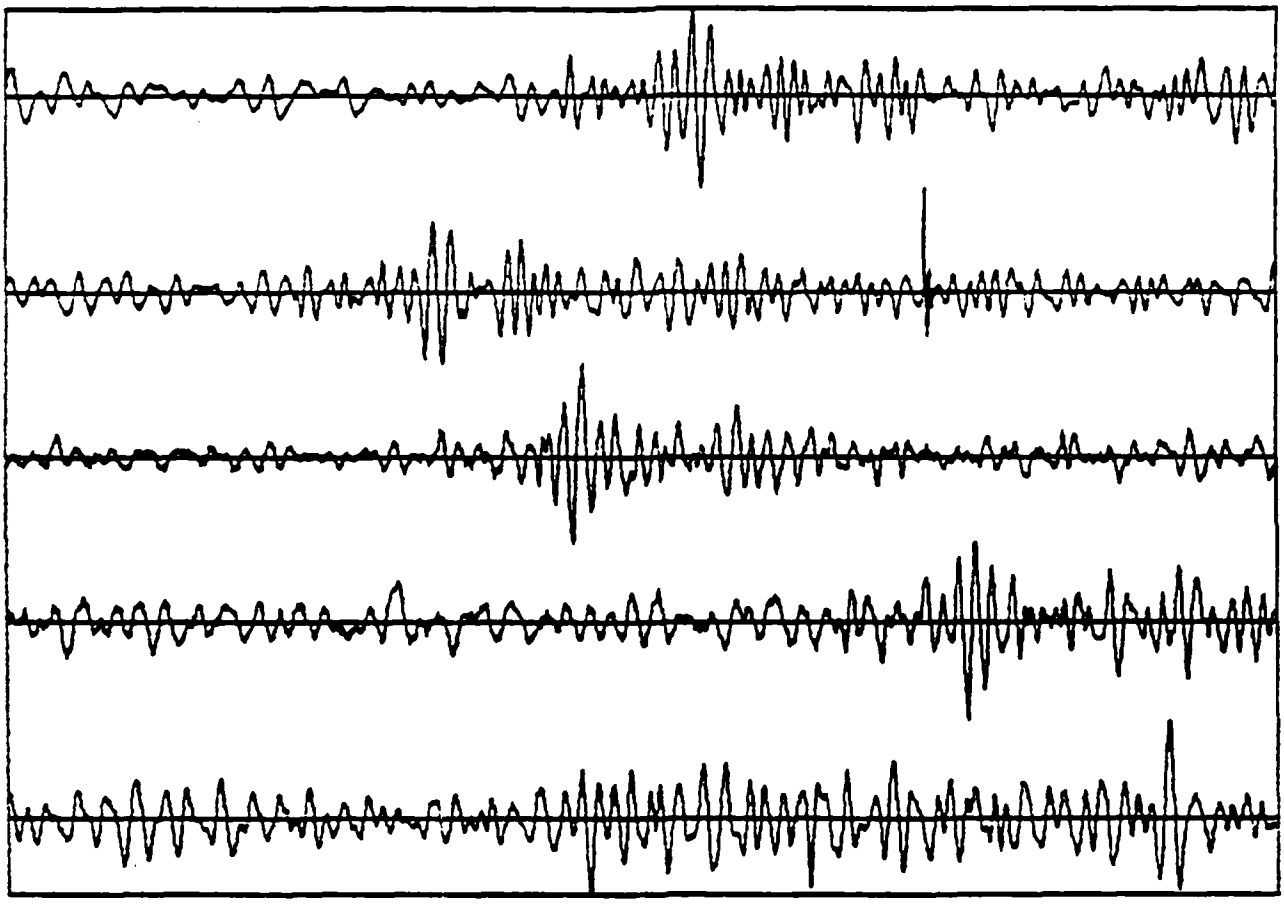

25-NOV-81 08:24:33

EVENT 8

```
21    284001.co1 L=    1500 R=    3499 B= -0.476E+01 T=  0.479E+01
22    284001.co2 L=    1500 R=    3499 B= -0.967E+01 T=  0.916E+01
23    284001.co3 L=    1500 R=    3499 B= -0.115E+01 T=  0.137E+01
24    284001.co4 L=    1500 R=    3499 B= -0.503E+01 T=  0.451E+01
25    284001.co5 L=    1500 R=    3499 B= -0.500E+01 T=  0.522E+01
```

DO YOU WISH TO PLOT EXISTING DATA AGAIN (Y/N) ?

THE SAMPLE RATE IS 20.0 POINTS PER SECOND
DASHED LINES ARE AT 10 SECOND INTERVALS

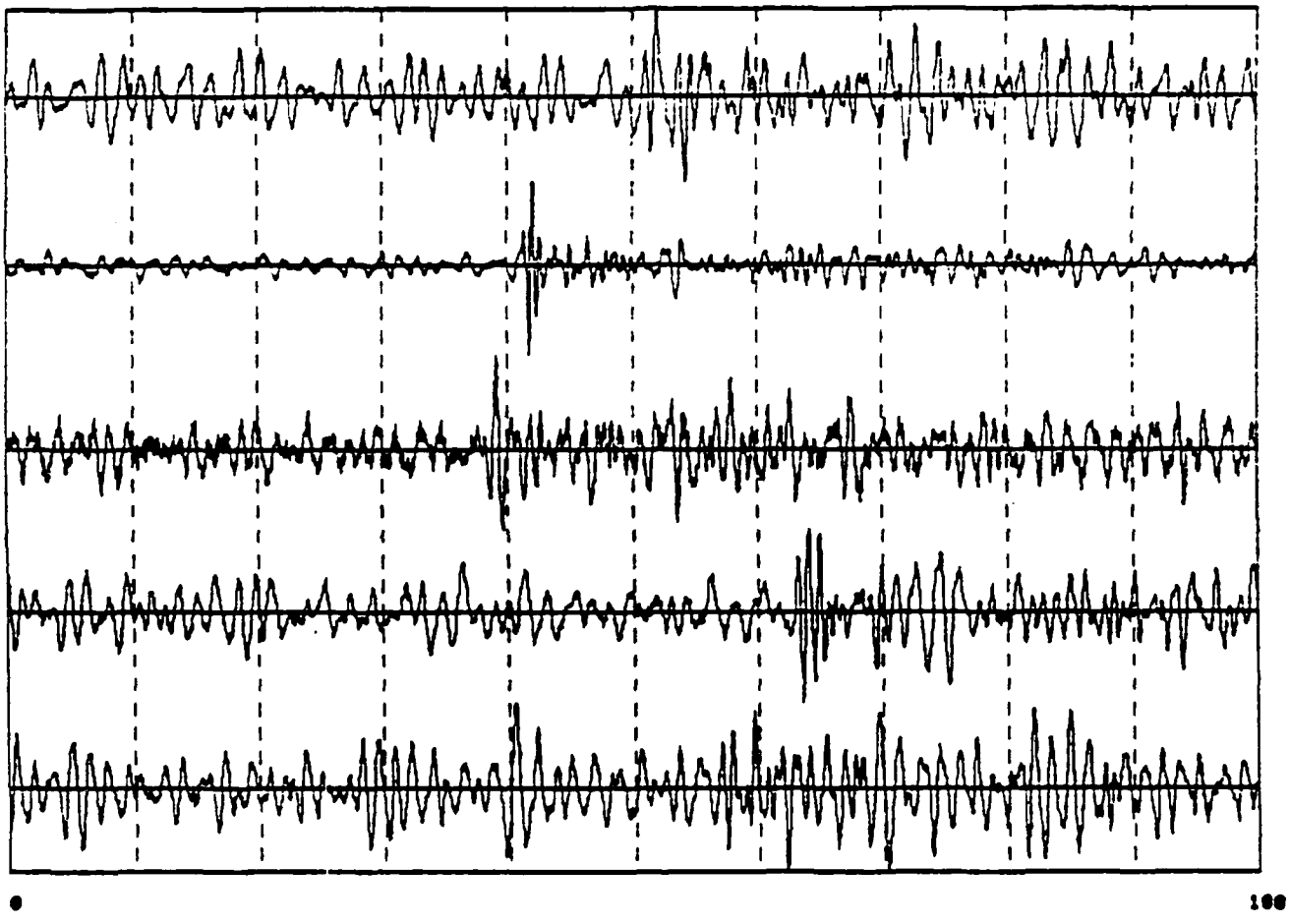

28-NOV-81 11:21:17

EVENT 11